NCOA7 Deficiency Reprograms Lysosomal Behavior and Sterol Metabolism to Promote Endothelial Dysfunction and Pulmonary Arterial Hypertension

by

Lloyd David Harvey

Bachelor of Science, University of Pittsburgh, 2015

Submitted to the Graduate Faculty of the

School of Medicine in partial fulfillment

of the requirements for the degree of

Doctor of Philosophy

University of Pittsburgh

2021

UNIVERSITY OF PITTSBURGH

SCHOOL OF MEDICINE

This dissertation was presented

by

Lloyd David Harvey

It was defended on

August 2, 2021

and approved by

Imad Al Ghouleh, Ph.D., Assistant Professor, Department of Medicine

Donald B. DeFranco, Ph.D., Professor, Department of Pharmacology & Chemical Biology

Michael J. Jurczak, Ph.D., Assistant Professor, Department of Medicine

Stacy G. Wendell, Ph.D., Research Associate Professor, Department of Pharmacology & Chemical Biology

Dissertation Director: Stephen Y. Chan, M.D., Ph.D., Professor, Department of Medicine

NCOA7 Deficiency Reprograms Lysosomal Behavior and Sterol Metabolism to Promote Endothelial Dysfunction and Pulmonary Arterial Hypertension

Lloyd David Harvey, Ph.D.

University of Pittsburgh, 2021

Pulmonary arterial hypertension (PAH) is an enigmatic vascular disorder characterized by complex pulmonary vessel remodeling. Barriers to effective therapies have included a relatively low disease prevalence and pathogenic, multisystem mechanisms whose pathways remain incompletely defined. To better understand the molecular origins of PAH, we and our colleagues performed the largest, unbiased metabolomics screen of more than 2,000 PAH patients and identified a cluster of oxysterols and bile acids that had strong associations to clinical parameters of disease. A mechanistic role, however, for oxysterols and bile acids in the pathogenesis of PAH has never been established. Recently, lysosomes have been implicated as central mediators of sterol homeostasis within the cell. Accordingly, we identified the nuclear receptor co-activator 7 (NCOA7) as a molecule of interest, as previous literature has documented a role in endolysosomal trafficking. As such, we leveraged parallel metabolomics and orthogonal genomics data from The FINRISK Study of nearly 8,000 people to discover that candidate metabolites were negatively associated with an allelic variant at SNP rs11154337 in *NCOA7*. We then confirmed that proinflammatory stimuli integrate onto NF-κB to control the expression of *NCOA7* in an allele-specific manner. Knockdown of NCOA7 resulted in lysosomal dysfunction and sterol accumulation, thereby resulting in the production of oxysterol species through cholesterol 25-hydroxylase (CH25H). Production of oxidized sterol species immunoactivated the endothelium as noted by increased vascular cell adhesion molecule 1 (VCAM1) and immune cell attachment. In

support of this mechanism, we confirmed in an angioproliferative mouse model that the loss of NCOA7 worsened hemodynamic indices of disease. Furthermore, we found activation of the CH25H pathway by vessel staining and subsequent VCAM1 upregulation and immune infiltration, which was also supported by the elevation of downstream oxidized sterols in the serum of these animals. Overall, the totality of our work serves as one of the first successful examples of multi-omics integration in the identification of a causal variant, maps the first mechanistic explanation of sterol aberrations in PAH, and implicates oxidized lipid species and NCOA7 as potential targets for biomarker development and therapeutic targeting.

Table of Contents

List of Tables

List of Figures

Preface

The Choice

The intellect of man is forced to choose

perfection of the life, or of the work,

And if it take the second must refuse

A heavenly mansion, raging in the dark.

When all that story's finished, what's the news?

In luck or out the toil has left its mark:

That old perplexity an empty purse,

Or the day's vanity, the night's remorse.

William Butler Yeats

The Winding Star and Other Poems, 1933

1.0 Introduction

This work was adapted from a manuscript in submission:

Lloyd D. Harvey, Sanya Arshad, Mona Alotaibi, Anna Kirillova, Wei Sun, Neha Hafeez, Adam Handen, Yi-Yin Tai, Ying Tang, Chen-Shan C. Woodcock, Jingsi Zhao, Annie M. Watson, Yassmin Al Aaraj, Callen T. Wallace, Claudette M. St. Croix, Donna B. Stolz, Gang Li, Jeffrey McDonald, Haodi Wu, Thomas Bertero, Mohit Jain, and Stephen Y. Chan. NCOA7 Deficiency Coordinates Lysosomal Dysfunction and Sterol Metabolism to Promote Endothelial Dysfunction and Pulmonary Arterial Hypertension. *In submission*.

In addition, there are some influences from previous, published manuscripts in this chapter:

Harvey LD, Chan SY. Evolving Systems Biology Approaches to Understanding Non-Coding RNAs in Pulmonary Hypertension. J Physiol. 2019;597(4):1199-1208.

Ranchoux B, Harvey LD, Ayon RJ, et al. Endothelial Dysfunction in Pulmonary Arterial Hypertension: An Evolving Landscape (2017 Grover Conference Series). Pulm Circ. 2018;8(1):2045893217752912.

Harvey LD, Chan SY. Emerging Metabolic Therapies in Pulmonary Arterial Hypertension. J Clin Med. 2017;6(4).

1.1 Pulmonary Hypertension

Pulmonary hypertension (PH) is a historically neglected and devastating vascular disorder with no cure. As a disease, PH is characterized by complex pulmonary vascular remodeling, an increase in pulmonary vascular resistance, subsequent right ventricular hypertrophy, and eventual failure of the right ventricle.

1.1.1 Clinical Characteristics

1.1.1.1 Classification

In response to an epidemic of pulmonary vascular disease associated with use of the anorectic stimulant Aminorex across Europe, the World Health Organization (WHO) organized the first World Symposium on Pulmonary Hypertension (WSPH) in October of 1973 (Gurtner, 1972; Luthy, 1975). Over the next half century, five more symposia would be held to review and organize clinical and scientific findings to improve the identification and treatment of patients living with this devastating and deadly disease.

As an umbrella term, PH serves to encompass a clinical presentation of pulmonary vascular disease that may be due to a multitude of varied and seemingly disparate triggers. In response to such diversity, the WSPH has organized PH into a classification schema based on five major groupings (Table 1). Group I comprises an especially severe form of this disease that has idiopathic, heritable, and comorbid etiologies (*e.g.*, connective tissue disorders, HIV infection, schistosomiasis, *etc*.), termed pulmonary arterial hypertension (PAH) (Simonneau et al., 2019). Common to etiologies falling under the Group I classification is the involvement and obliteration

of the pulmonary arterioles, which culminates as the pathognomonic plexiform lesion (Tuder et al., 2007). Groups II, III, IV, and V represent a wide variety of conditions that can cause PH, such as left heart disease, lung diseases and/or hypoxia, thromboembolic diseases, and unclear multifactorial mechanisms, respectively (Simonneau et al., 2019).

Table 1. Classification Schema for Pulmonary Hypertension

I.	**PAH**
I.i	Idiopathic PAH
I.ii	Heritable PAH
I.iii	Drug- and Toxin-induced PAH
I.iv	PAH associated with:
I.iv.i	Connective tissue disease
I.iv.ii	HIV infection
I.iv.iii	Portal hypertension
I.iv.iv	Congenital heart disease
I.iv.v	Schistosomiasis
I.v	PAH long-term responders to calcium channel blockers
I.vi	PAH with overt features of venous/capillaries (PVOD/PCH) involvement
I.vii	Persistent PH of the newborn
II.	**PH due to Left Heart Disease**
II.i	PH due to heart failure with preserved LVEF
II.ii	PH due to heart failure with reduced LVEF
II.iii	Valvular heart disease
II.iv	Congenital/acquired cardiovascular conditions leading to post-capillary PH
III.	**PH due to Lung Diseases and/or Hypoxia**
III.i	Obstructive lung disease
III.ii	Restrictive lung disease
III.iii	Other lung diseases with mixed restrictive/obstructive pattern
III.iv	Hypoxia without lung disease
III.v	Developmental lung disorders
IV.	**PH due to Pulmonary Artery Obstructions**
IV.i	Chronic thromboembolic PH
IV.ii	Other pulmonary artery obstructions
V.	**PH with Unclear and/or Multifactorial Mechanisms**
V.i	Hematologic disorders
V.ii	Systemic and metabolic disorders
V.iii	Others
V.iv	Complex congenital heart disease

1.1.1.2 Epidemiology

From an epidemiological perspective, PAH is considered a rare disease with 15 to 50 affected persons per million in the United States and Europe (Beshay et al., 2020). The National Institutes of Health (NIH) organized one of the earliest registries that collected data on patients living with PAH from 1981 to 1985 (Rich et al., 1987). The basic demographics of this registry found that in 187 patients, there was a female and Caucasian predominance and a mean age of presentation of 36 years old. As specific interventions did not exist at this time, the registry found that survival rates of PAH without treatment are grim: with 68%, 48%, and 34% alive at 1, 3, and 5 years, respectively (D'Alonzo et al., 1991; Rich et al., 1987).

In 2006, a multicenter, observational registry was established to collect demographics and clinical data on PAH patients in the United States, known as the Registry to Evaluate Early and Long-Term PAH Disease Management (REVEAL) (Benza et al., 2012a; McGoon et al., 2008; McGoon and Miller, 2012) Notably, this registry reported that 79.5% of individuals were female, translating to a 4.8 to 1 female-to-male ratio (Frost et al., 2011); paradoxically, it has been noted that female sex simultaneously confers a survival benefit through undefined mechanisms (Shapiro et al., 2012). In addition, the registry noted that 46% of patients in the Group I classification are labeled as idiopathic PAH, meaning that they are never given an explanation to the origin of disease. Moreover, this lack of definitive etiology underscores the need to further study this disease, as the underlying sequence of molecular events are still poorly defined. Lastly, REVEAL has demonstrated an uptick in patient survival with 85%, 68%, and 49% alive at 3, 5, and 7 years after diagnosis, respectively (Benza et al., 2012b). The notable increase in survival is likely due to a variety of factors, such as the development of PAH-specific therapies and a better ability to

diagnosis and manage disease, thereby altering the fundamental composition of the PAH patient cohort over time (Levine, 2021).

1.1.1.3 Presentation & Diagnosis

The clinical picture of a patient with pulmonary vascular disease is relatively non-specific. In fact, the diagnosis of PH is often delayed due the non-specificity of the most common symptoms—exertional dyspnea, lethargy, and fatigue (Braganza et al., 2019; Peacock, 1999; Runo and Loyd, 2003). Estimates attempting to quantify the delay from initial symptom onset to an official diagnosis report a period longer than two years (Brown et al., 2011). As pulmonary vessels remodel and ultimately occlude, there is an increased pulmonary vascular resistance in the pulmonary vascular bed. This increase in pulmonary vessel resistance ultimately forces the right ventricle, which normally operates under low resistance and thus pressure, to compensate and subsequently hypertrophy. As disease progresses and ultimately worsens, patients can develop symptoms of right ventricular failure, such as exertional chest pain secondary to poor perfusion of myocardial tissue, exertional syncope, and peripheral edema. Because of the increased workload on the right ventricle, the driving cause of mortality in this patient population is failure of the right ventricle.

Although a diagnosis of PH can technically be made from a constellation of clinical findings and non-invasive testing, the most assured way requires direct hemodynamic interrogation through right heart catheterization (RHC). Since the first WSPH in 1973, PH has been defined as a mean pulmonary arterial pressure (mPAP) ≥ 25 mmHg in the supine position and at rest (Hatano and Strasser, 1975). This original definition was somewhat arbitrary in its delineation as a marker of abnormal mPAP. However, in 2009, an analysis of 1187 subjects across

47 studies determined that mPAP at rest was 14.0±3.3 mmHg, meaning that two standard deviations from the mean would equate an mPAP ≥ 20 mmHg as being abnormal (Kovacs et al., 2009).

To address this, the sixth WSPH in 2019 lowered the mPAP required for diagnosis from ≥ 25 mmHg to ≥ 20 mmHg (Simonneau et al., 2019); however, it must be noted that mPAP cannot be used in isolation in the classification of PH, as the elevation of PAP can occur secondary to various different causes, such as cardiac shunts, increased cardiac output (CO), elevated pulmonary arterial wedge pressure (PAWP) in left heart disease, or hyperviscosity. Invasive hemodynamic measurements can thus be interpretated to better define potential anatomical locations of disease etiology (*i.e.*, pre-capillary involvement suggesting origins in the pulmonary arterioles and post-capillary involvement suggesting origins in venous beds or even at the left ventricle). In the most recent schema, pre-capillary PH is thought of with Groups I, III, IV, and V and post-capillary PH with Groups II and V.

Critical in the classification and diagnosis of pre-capillary PH requires a calculation of pulmonary vascular resistance (PVR), which is based on the principles of Ohm's Law and defined as the following:

$$PVR = \frac{mPAP - PAWP}{CO}$$

PVR is defined in Wood Units (WU) as the difference between pressure at the right ventricle/in the pulmonary artery (*i.e.*, mPAP) minus the pressure beyond the pulmonary venous bed/at the left ventricle (*i.e.*, PAWP) divided by CO. As such, pre-capillary PH requires—in addition to an mPAP ≥ 20 mmHg—a PVR ≥ 3 WU and a PAWP ≤ 15 mmHg, whereas post-capillary PH requires the converse with a PVR < 3 WU and a PAWP > 15 mmHg (Badesch et al., 2009; Barst et al., 2004; Hoeper et al., 2013; Simonneau et al., 2019). Ultimately, the issue with

attempts to stratify patients into classification schema is complicated by the fact that many patients fit various descriptions due to multiple comorbidities (*e.g.*, HIV infection in the setting of chronic obstructive pulmonary disease) or their disease changes overtime to reflect pre- and post-capillary involvement (*e.g.*, the development of left heart disease as one ages).

Table 2. Hemodynamic Classification of Pre- & Post-Capillary PH

Capillary Classification	Hemodynamics	Clinical Classification
Pre-Capillary PH	mPAP ≥ 20 mmHg PAWP ≤ 15 mmHg PVR ≥ 3 WU	I III IV V
Post-Capillary PH	mPAP ≥ 20 mmHg PAWP > 15 mmHg PVR < 3 WU	II V
Combined Pre- & Post-Capillary PH	mPAP ≥ 20 mmHg PAWP > 15 mmHg PVR ≥ 3 WU	II V

1.1.1.4 Therapeutic Interventions

Despite advances in our understanding of pulmonary vascular disease over the last few decades, significant barriers and challenges still exist in the treatment of patients afflicted by this devastating disease. Current clinical therapies operate to primarily alleviate symptoms and manage disease with no appreciable effect on disease progression or reversal. For this reason, there is a dire and significant need to advance new therapies. The regimen for therapeutic intervention in PH is primarily designed for Group I PAH and target various aspects underlying the regulation of vasomotor tone within pulmonary vessels through three major mechanisms: endothelin-1 (ET-1), nitric oxide (NO), and prostacyclin pathways (Lau et al., 2017).

ET-1 acts as a potent vasoconstrictor through its action at the G-protein coupled receptors ET_A and ET_B, which are differentially expressed by cell type and thus causes cell-type specific signaling cascades. For instance, ET_A is expressed predominantly in smooth muscle cells, where its activation causes vasoconstriction, proliferation, and fibrosis. ET_B, however, is expressed predominantly in ECs, where its activation triggers anti-proliferative pathways and vasodilatory effects (Davie et al., 2002). As such, endothelin receptor antagonists (ERAs), which either target ET_A alone (*e.g.*, Ambrisentan) or both ET_A and ET_B (*e.g.*, Bosentan and Macitentan), have exhibited improvement in functional outcomes for patients living with PAH (Liu et al., 2021).

The second mechanism through which current therapies act is through modulation of NO signaling. Endothelial nitric oxide synthase (eNOS) produces the vasodilatory molecule NO, which binds to soluble guanylyl cyclase (sGC). Activated sGC converts guanosine triphosphate (GTP) into the signaling molecule cyclic guanosine monophosphate (cGMP), which in turn activates a protein kinase to cause smooth muscle cell relaxation. This signaling cascade is subsequently terminated by phosphodiesterases that regulate cGMP concentrations in the cell (Schermuly et al., 2008). Thus, drugs in this class function by either stimulating sGC production (*e.g.*, Riociquat) or through inhibition of phosphodiesterase type 5 (*e.g.*, Sildenafil, Tadalafil, and Vardenafil) to primarily promote smooth muscle cell relaxation (Barnes et al., 2019).

Finally, prostacyclin is a prostanoid generated by the endothelium that binds to prostaglandin I2 (PGI2) receptors on smooth muscle cells to induce vasodilation through a similar mechanism to NO signaling (*i.e.*, generation of a secondary messenger to activate a vasodilatory kinase) (Gomberg-Maitland and Olschewski, 2008). Traditionally, the prostanoid analogue Epoprostenol was administered via continuous infusion to improve disease in patients; fortunately,

the latest formulations do not require continuous infusion (*e.g.*, Iloprost, Treprostinil, and Selexipag) (Sitbon et al., 2015).

Overall, the current mainstay of PH treatment involves repurposed drugs that do more to support and preserve right ventricular function than to halt or reverse disease pathology (Humbert et al., 2004). The lack of therapeutic agents capable of preventing and/or reversing structural alterations within the pulmonary vasculature and right ventricle warrants the discovery of novel drug targets through preclinical studies. Unfortunately, challenges in the identification of novel drug targets are inherent to the disease process of PH. As a relatively rare disease with multifactorial mechanisms of pathogenesis, identification of potential targets is variable based on the underlying disease-inciting stimulus. The elucidation of novel metabolic targets—when coupled with our recent understanding of genetic polymorphisms and their role in PH—becomes highly specific to subpopulations of patients, which further reduces an already limited population for clinical testing of new interventions.

1.1.2 Cellular & Molecular Pathology

1.1.2.1 A Brief History

Tracing the historical arc of PH research reveals a foundational basis of understanding rooted in pathological manifestations within the pulmonary arterioles (Dresdale et al., 1951). Early investigations focused on hypoxia and the vasoconstrictive effects on pulmonary vasculature. Under normal conditions, hypoxic pulmonary vasoconstriction is a physiologically protective response that optimizes ventilation-perfusion matching by diverting blood flow away from alveoli with poor ventilation (Ward and McMurtry, 2009). The early idea of PH being mediated through

hypoxia-mediated vasoconstriction served as an impetus for therapeutic intervention with the development and use of selective vasodilatory agents, as previously discussed. The paradigm has shifted, however, over time toward the notion that the origin of PH is founded instead in myriad molecular aberrations that manifest as a remodeling of the pulmonary vasculature characterized by pathological hyperproliferation and a resistance to apoptosis (Archer et al., 2010).

1.1.2.2 The Endothelium

The innermost layer of blood vessels—or the endothelium—is a highly dynamic and sentient organ, existing as the interface between circulating factors and the vascular bed of surrounding parenchymal tissue. For this reason, the endothelium is characterized by significant intrapopulation heterogeneity, where ultrastructure and thus function is based on anatomical location and the surrounding vessel microenvironment (Evans et al., 2021). In the pulmonary vasculature, the function of the endothelium has critical roles in the regulation of vasomotor tone, immune cell trafficking, cellular homeostasis (*i.e.*, transport of vital molecules for tissue function), transmural signaling cascades into surrounding tissue, and, perhaps most obviously, acting as a physical barrier (Budhiraja et al., 2004).

There is a belief that the activation of the endothelium and its subsequent dysfunction occurs in response to an inciting stimulus, whether it be a genetic predisposition (*i.e.*, heritable PAH), infection (*i.e.*, HIV-associated or *Schistosoma mansoni*-associated PAH), environmental (*i.e.*, drug- or toxin-induced PAH), or idiopathic. Broadly, endothelium destabilization triggers an acute cascade of molecular events that result in hyperproliferation of endothelial cells (*i.e.*, intimal hyperplasia and neointima formation), smooth muscle cells (*i.e.*, medial hypertrophy or muscularization of the arteriole), and fibroblasts (*i.e.*, adventitial expansion) (Chan and Loscalzo,

2008). The culminating histological lesion is pathognomonically referred to as the plexiform lesion. Beyond the obvious expansion of the vessel layers, the plexiform lesion demonstrates marked perivascular infiltration of inflammatory cells and *in situ* thromboses, occasionally showing occlusion of the vessel lumen (Humbert et al., 2019).

1.1.2.3 The Diseased Endothelium in Pulmonary Arterial Hypertension

Pulmonary arterial endothelial cell dysfunction is central to understanding the pulmonary vascular disease. For example, transgenic mice with Fas-induced endothelial apoptosis develop abnormal hemodynamics with disease-consistent pulmonary vessel lesions—evidence that endothelial apoptosis can induce PH (Goldthorpe et al., 2015). In patients with advanced PAH, there have been a multitude of observations in support of an apoptosis-resistant, hyperproliferative clonal endothelial population involved in the plexiform lesion (Lee et al., 1998; Masri et al., 2007). The *in vitro* propagation of endothelial cells isolated from idiopathic PAH patients further supports this with the maintenance of the apoptosis-resistant, hyperproliferative phenotype (Taraseviciene-Stewart et al., 2006; Tu et al., 2011). As such, the emerging paradigm posits that early molecular events result in an acute, apoptotic phenotype, which eventually selects for a clonal, apoptosis-resistant, hyperproliferative, and immune-activated endothelial population over time (Lee et al., 1998; Masri et al., 2007; Sakao et al., 2005).

In addition, there has been a growing appreciation for the immune system and how its dysregulation may contribute to pulmonary vascular disease. Early histological examinations revealed the presence of macrophages and lymphocytes in vessel lesions (Caslin et al., 1990; Tuder et al., 1994). And, more recently, studies have identified the elevation of various inflammatory markers in the serum of PAH patients that correlate with disease severity or mortality, such as

interleukin (IL)-1beta, IL-2, IL-6, IL-8, IL-10, IL-12, IL-18, and tumor necrosis factor-α (Soon et al., 2010). Furthermore, the degree of perivascular immune infiltration has been correlated with the degree of intimal and medial thickening in pulmonary vessels—a direct implication of immune dysregulation and vessel remodeling (Hu et al., 2020). As such, efforts to establish a central and unifying hypothesis to explain such observations have put forth a central role for mitochondrial metabolism and its reprogramming as a potential mechanism (Paulin and Michelakis, 2014).

The basis of this metabolic theory is founded in several molecular and cellular processes observed in both PH and cancer that rely upon the mitochondrion as the epicenter of metabolic control and regulation. Mammalian cells under hypoxic conditions demonstrate a metabolic shift away from oxidative phosphorylation toward glycolysis and lactic acid fermentation to sustain ATP production and facilitate acute survival—known as the Pasteur effect. This metabolic shift toward glycolysis—first described by Otto Warburg in cancer cells under normal oxygen tension—serves to sustain uncontrolled, neoplastic growth (Warburg, 1956). Similarly, the hyperproliferative, antiapoptotic, and glycolytic phenotype of the vasculature in PH has drawn comparisons to the cellular phenotype observed in cancer, collectively contributing to proliferation and resistance to apoptosis (Archer et al., 2010; Tuder et al., 2012).

1.1.2.4 Identification of Bile Acids in Pulmonary Arterial Hypertension

Although noble in its attempt, the metabolic theory of PH has failed to comprehensively link discordant aspects of the underlying pathophysiology, such as genetic predisposition, metabolic derangements beyond mitochondrial reprogramming, and immune dysregulation. In an attempt to better understand and perhaps link the molecular origins of PAH, we and our colleagues Alotaibi et al. have performed the largest, unbiased metabolomics screen of PAH patients to date

with a subsequent genomic association of identified metabolites (unpublished)—utilizing over 2,000 samples from the PAH Biobank at Cincinnati Children's Hospital Medical Center under Dr. William Nichols, the University of Pittsburgh Medical Center under Dr. Stephen Chan, and the Vanderbilt University Medical Center under Dr. Anne Hemnes.

Existing as an interface between the genome and the environment, the metabolome of pulmonary vascular disease is undefined. As such, Alotaibi et al. set out on the task to map the metabolome from the serum of PAH patients. To do so, they utilized directed, non-targeted liquid chromatography-mass spectrometry (LC-MS) as a tool for the high-depth profiling of metabolites. This unbiased approach allowed for the detection of both polar and non-polar species. Previous studies have attempted to identify biomarkers in PAH patients, yet these studies were often too small to make any definitive conclusions (Bujak et al., 2016; Lewis, 2014; Rhodes et al., 2017; Zhao et al., 2015). Despite the limitations of previous work, Alotaibi et al. hypothesized that unbiased, metabolomics on a cohort of over 2,000 patients would produce a distinct, metabolomic signature identifying bioactive species that would be associated to clinical parameters and mortality of PAH.

Partitioning the cohort for discovery of a metabolomic signature revealed greater than 500 metabolites that reached a metabolome-wide threshold for significance (*i.e.*, $P = 1 \times 10^{-5}$) and a hazard ratio above 1.2. Validation of these metabolites in the remaining cohort was narrowed down to roughly 100 metabolites that were also associated with patient mortality (Figure 1A). Chemical networking was then utilized to agnostically identify novel metabolites, where molecules were fragmented into smaller product ions to create fingerprints. The ion spectra for a given metabolite was then analyzed in a way to allow for clustering of similar signatures. This approach produced a highly ranked group of 51 metabolites that shared a common fingerprint that grouped them as an

oxidized form of cholesterol (*i.e.*, oxysterols and downstream bile acids). To determine if the identified 51 metabolites had clinical utility in predicting progression of disease, they were compared against traditional clinical measures, such as age, sex, body mass index, pulmonary vascular resistance, functional class, six-minute walk distance, mean right atrial pressure, and cardiac index. Notably, the totality of these clinical features only had a predictive area under the ROC curve (AUC) for mortality of 68.6% (95% confidence interval, 62.9% to 74.3%), whereas the identified 51 metabolites had an AUC of 78.5% (95% confidence interval, 73.8% to 83.1%). In combination, however, there is no appreciable enhancement in prediction of disease progression (AUC 79.7%; 95% confidence interval, 75.0% to 84.3%), indicating that the relevant information for disease severity is embedded into the identified metabolites (Figure 1B). Further analysis of patients based on the degree of metabolite levels revealed a stratification of patients based on probability of survival and a relative metric of metabolite expression (Figure 1C).

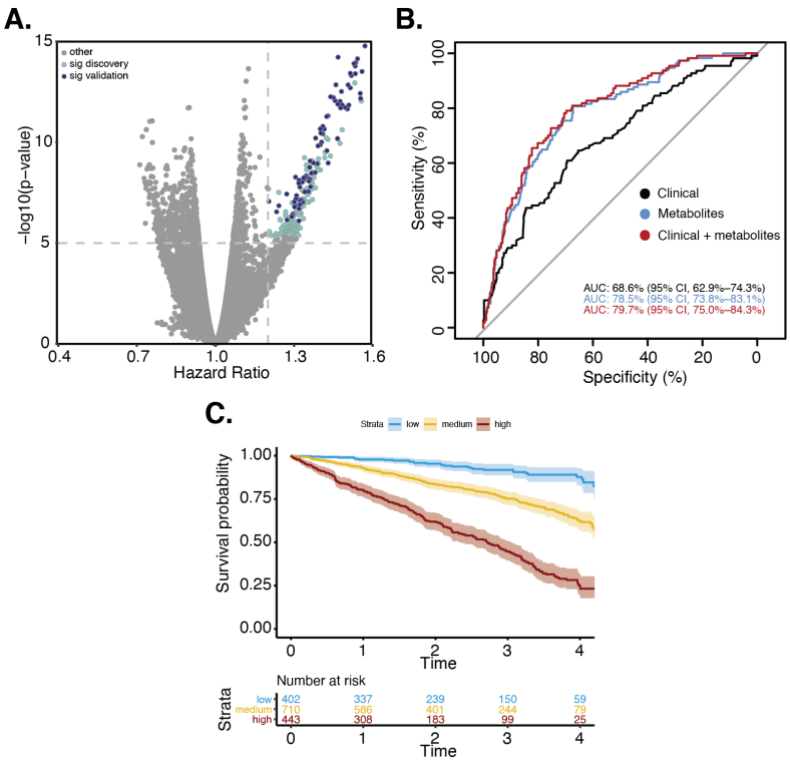

Figure 1. Serum Metabolites Predict Disease Progression in PAH

A. Volcano plot of unbiased, metabolomics-identified of serum metabolites in a discovery cohort (teal) and subsequently verified in a validation cohort (navy) determined by a metabolome-wide significance of a *P*-value less than 1 x 10^{-5} (gray dashed-line) and a hazard ratio significance arbitrarily defined as 1.2 (gray dashed-line). **B.** Predictive capacity of mortality for clinical features (black), the top cluster of 51 similar metabolites (blue), or both features combined (red). **C.** Kaplan-Meier curve depicting stratification of top metabolites based on relative expression and its effect on patient survival probability over time.

Ultimately, the work completed by Alotaibi et al. identified that a metabolomic signature undergirds PAH and that this metabolome has predictive capacity and clinical utility in patient prognosis. The top 51 metabolites identified as a cluster through chemical networking are oxidized forms of cholesterol—also known as oxysterols and their downstream bile acid derivatives. A mechanistic role, however, for oxysterols and bile acids in the pathogenesis of pulmonary vascular disease has never been established. With the efforts of Alotaibi et al., an unbiased, population-

scale metabolomics study has provided the foundational substrate from which mechanistic studies can now propagate.

1.1.2.5 Sterol Metabolism in Pulmonary Arterial Hypertension

Bile acids are soluble derivatives of highly insoluble cholesterol that are synthesized through a series of oxidative steps. The oxidation of cholesterol can occur via various pathways with the first reaction generating what are known as oxysterols, which are further oxidized into bile acids. With each successive oxidative step, the solubility of the cholesterol-derivatives increases, meaning that these molecules can be more easily transported out of the cell—an important distinction when considering aberrations in cholesterol homeostasis. In addition, previous work has shown that the three major bile acids found in circulation can induce immune-activation of the endothelium, as noted by ICAM1 and VCAM1 upregulation—cellular adhesion molecules that allow for immune-cell attachment and recruitment (Qin et al., 2006). Notably, there exist a series of studies demonstrating the production of bile acids in endothelial cells, which focus predominantly on the activation of the 27-hydroxylation pathway.

In bovine aortic endothelial cells, there are high levels of sterol 27-hydroxylase (*CYP27A1*) activity, resulting in the accumulation of the oxysterol 27-hydroxycholesterol (27-HC) and downstream bile acid 3β -hydroxy-5-cholestanoic acid (3-HCOA) (Reiss et al., 1994). Similarly, human umbilical vein endothelial cells (HUVECs) can be loaded with cholesterol *in vitro* to increase both the synthesis and excretion of 27-HC and 3-HCOA (Bjorkhem et al., 1994; Lund et al., 1996), and human studies have documented a direct correlation between circulating cholesterol and 27-HC (Babiker et al., 2005). Because the total of mass of endothelial cells throughout the body is large, it has been posited that perhaps a significant portion of circulating 27-HC actually

derives from the endothelium and more specifically the lung (Babiker et al., 1997; Javitt, 1994). In support of this, human patients undergoing pulmectomy for a chronic condition demonstrated a nearly 50% reduction in circulating levels of 3-HCOA after removal—implicating the lung as the major source of extrahepatic 27-HC and downstream metabolites (Babiker et al., 1999).

The role of sterol homeostasis in regulating endothelial behavior and PAH is only just developing. Clinical studies have indicated that systemic markers of cholesterol metabolism may possess prognostic relevance in PAH but are somewhat contradictory (Al-Naamani et al., 2016; Jonas et al., 2018; Kopec et al., 2017; Larsen et al., 2016). Initial work on the use of statins in preclinical models has suggested potential therapeutic benefit, such as through the inhibition of fibroblast proliferation (Carlin et al., 2012; Zhu et al., 2018b). However, the use of statins fails to address aberrations in intermediates downstream of its target and the effects of accumulating intermediates. In endothelial cells, there has been limited work on how altered sterol metabolism results in endothelial dysfunction (Goveia et al., 2014). The perturbation of cholesterol homeostasis has been shown to alter processes like angiogenesis (Fang et al., 2013), immune activation (Whetzel et al., 2010), nitric oxide synthesis (Boger et al., 2000; Ivashchenko et al., 2010), and cell growth regulatory pathways (*i.e.*, mammalian target of rapamycin [mTOR] signaling) (Xu et al., 2010) in endothelial cells, suggesting relevance in regulating cellular behavior. In the context of PAH, studies have emerged suggesting a role for enhanced membrane fluidity (*i.e.*, decreased membrane cholesterol) in exerting control over the vasodilatory effects of calcium-dependent, nitric oxide signaling in endothelial cells (Zhang et al., 2017, 2018). Yet, a definitive role for sterol metabolism in endothelial behavior is not firmly established.

1.1.2.6 Lysosomal Control of Sterol Metabolism

Recently, lysosomes have surfaced as having a principal role in sterol metabolism. As highly acidic organelles, lysosomes contain numerous pH-sensitive, hydrolytic enzymes responsible for the breakdown of both endogenous and exogenous cargo—as their primary function is to serve as the endpoint for autophagic, endocytic, and phagocytic pathways. Central to the maintenance of lysosomal enzyme function is proper acidification of the luminal space, which is mediated by the vacuolar H^+ ATPase (V-ATPase) family. Loss of the hydrolytic capacity or transport ability of the lysosome results in a class of diseases known as lysosomal storage disorders, where cellular studies demonstrate the lysosomal accumulation of macromolecules and, in particular, lipid species, such as oxysterols (de Araujo et al., 2020). As such, the observation of increased bile acids in the serum and lungs of PAH patients poses the question of whether there is an observable dysregulation of cholesterol homeostasis at the level of the endothelium, and if this dysregulation is due in part to failure of proper endolysosomal trafficking.

To address this question, we identified the nuclear receptor co-activator 7 (*NCOA7*) as a potential molecule of interest, as previous literature has documented a role in endolysosomal trafficking. Namely, homologues of *NCOA7* identified in *Drosophila* were found to have protective effects in preventing bacterial pathogen entry via the endocytic pathway (Wang et al., 2012). And, most recently, NCOA7 was further confirmed to regulate endolysosomal physiology through direct binding and modulation of V-ATPase activity (Castroflorio et al., 2021; Doyle et al., 2018), insinuating that perhaps NCOA7 can modulate sterol metabolism. Accordingly, we set out to discover if NCOA7 has a central role in regulating sterol homeostasis at the endothelium to promote oxysterol and bile acid synthesis and subsequent pulmonary vascular disease.

2.0 NCOA7 is Upregulated in Pulmonary Vascular Endothelial Cells

This work was adapted from a manuscript in submission:

Lloyd D. Harvey, Sanya Arshad, Mona Alotaibi, Anna Kirillova, Wei Sun, Neha Hafeez, Adam Handen, Yi-Yin Tai, Ying Tang, Chen-Shan C. Woodcock, Jingsi Zhao, Annie M. Watson, Yassmin Al Aaraj, Callen T. Wallace, Claudette M. St. Croix, Donna B. Stolz, Gang Li, Jeffrey McDonald, Haodi Wu, Thomas Bertero, Mohit Jain, and Stephen Y. Chan. NCOA7 Deficiency Coordinates Lysosomal Dysfunction and Sterol Metabolism to Promote Endothelial Dysfunction and Pulmonary Arterial Hypertension. *In submission*.

2.1 Introduction

NCOA7 was originally identified and characterized in a screen for estrogen receptor (ER) α interacting proteins, where it was formerly known as the 140 kDa estrogen receptor associated protein or ERAP140 (Shao et al., 2002). Shortly thereafter, it was noted that the sequence of *NCOA7* is highly like the oxidation resistance gene 1 (*OXR1*)—a gene product that belongs to a conserved family of eukaryotic proteins involved in oxidation resistance. Genomic analyses have demonstrated marked similarity in gene structure that includes exon boundary retention, which suggests a common evolutionary origin likely from a gene duplication event (Durand et al., 2007). Ensuing work identified a unique and highly truncated isoform of *NCOA7*, previously referred to as *Ncoa7B* or as *NCOA7* alternative start (*NCOA7-AS*), that was markedly upregulated in response

to interferon stimulation (Shkolnik et al., 2008; Yu et al., 2015) (Figure 2). Due to its interferon-mediated upregulation, it was posited that perhaps this unique isoform functioned as a cellular defense mechanism against pathogens through either innate and/or adaptive immune responses.

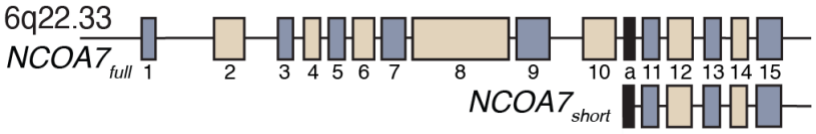

Figure 2. Gene Structure of NCOA7

Structure of the full-length and short-length isoforms of *NCOA7* located at 6q22.33. Exons are denoted by rectangles. The black rectangle denotes the first exon of the short-length isoform.

Subsequently, orthologues of *NCOA7* identified in *Drosophila* were found to have protective effects in preventing bacterial pathogen entry via the endocytic pathway (Wang et al., 2012). And, most recently, NCOA7 was further confirmed to regulate endolysosomal physiology through the direct binding and modulation of V-ATPase subunits to modulate viral infection through lysosomal acidification (Doyle et al., 2018). Beyond immune regulatory capacities, a role for NCOA7 acting at the lysosome has been further confirmed by proteomic construction of a V-ATPase interactome (Merkulova et al., 2015) and neuronal studies showing that loss of NCOA7 caused defective lysosomal formation and function (Castroflorio et al., 2021). Moreover, confirmation of direct human relevance has been validated in families that have bi-allelic, loss-of-function variants in the *NCOA7* homologue *OXR1*, where affected proband demonstrate dysfunctional lysosomes by electron microscopy in comparison to unaffected kin (Wang et al., 2019).

In addition to the limited mechanistic work, there have been few –*omics*-based studies that have recognized NCOA7 in other disease processes. Interestingly, these studies demonstrate a possible role for NCOA7 in female specific cancers, thereby implying that its functional activity may modulate estrogen and thus sterol metabolism. For example, a meta-analysis on three genome-wide association studies for endometrial cancer implicated a risk locus near *NCOA7* (Cheng et al., 2016). Moreover, a sequence of reports have provided somewhat contradicting evidence for NCOA7 involvement in breast cancer (Gao et al., 2019; Higginbotham et al., 2011; Sullner et al., 2012). When coupling these –*omics*-based association studies in estrogen-related cancers with the female predominance of PAH (*i.e.*, 4.8 to 1), NCOA7 is further implicated as molecule of interest.

Thus, the limited literature on NCOA7 documenting its role as an endolysosomal modulatory factor may suggest an as-of-yet undiscovered function in oxysterol and bile acid regulation. If so, such a mechanism may then correspond—and even underlie—our joint observation with Alotaibi et al. of the association of serum bile acids with mortality in PAH. As such, we set out to first investigate whether NCOA7 was dynamically altered in various models of PH, and, if so, how this molecule may be induced or activated under triggers of pulmonary vascular disease.

2.2 Materials & Methods

2.2.1 Cell Culture

Primary human pulmonary arterial endothelial cells (PAECs; Lonza) were plated on collagen-coated plasticware with EGM™-2 Endothelial Cell Growth Medium-2 BulletKit™

(Lonza; CC-3162). Growth media contained 5% fetal bovine serum (FBS), Gentamicin, Amphotericin B, and Plasmocin prophylaxis. Growth media was changed every two days. Experiments were performed between passages three and seven. For experimentation, serum media was reduced to 0.1% FBS and all antibiotics were removed. Routine *Mycoplasma* testing was performed. All cells were kept in standard conditions (*i.e.*, 20% O_2, 5% CO_2, with N_2 balance at 37°C) unless otherwise noted. Exposure to recombinant human IL-1β (1 ng/mL; PeproTech; 200-01B) or recombinant human IL-6/IL-6Rα protein chimera (10 ng/mL; R&D Systems; 8954-SR) was done for 24 hours. Exposure to hypoxia was done in a modular hypoxia chamber (*i.e.*, 0.2% O_2, 5% CO_2, with N_2 balance at 37°C) for 24 hours.

Inducible pluripotent stem cells (iPSCs) were kept on BD Matrigel™ hESC-qualified Matrix-coated plasticware (BD Biosciences; 354277) and passaged in Essential 8™ medium (ThermoFisher; A1517001) without antibiotics and with daily media changes. After differentiation into iPSC-derived endothelial cells (iPSC-ECs), cells were plated on 0.2% Gelatin-coated (Sigma-Aldrich; G1393) plasticware and switched to the EGM™-2 Endothelial Cell Growth Medium-2 BulletKit™.

2.2.2 RNA Extraction & Quantitative Polymerase Chain Reaction

Cells were lysed in QIAzol Lysis Reagent (Qiagen; 79306), and RNA was extracted using the Rnaeasy Kit (Qiagen; 74004). Complementary DNA was synthesized using the High-Capacity cDNA Reverse Transcription Kit (ThermoFisher; 4368813). Quantitative real-time PCR (RT-qPCR) was performed on an Applied Biosystems QuantStudio 6 Flex Real-Time PCR instrument. Target gene expression was normalized to a housekeeping gene (*i.e.*, *ACTB*) and fold change was calculated using the $2^{-\Delta\Delta Ct}$ method. TaqMan™ Universal PCR Master Mix (ThermoFisher;

4305719) was used with TaqMan primers. PowerUp™ SYBR™ Green Master Mix (ThermoFisher; A25742) was used with custom designed primers.

2.2.3 Immunofluorescent Staining of Lung Tissue

OCT-embedded lung tissue was sliced using a cryostat at thickness of 5 to 7 microns and were subsequently mounted onto gelatin-coated histological slides. Sections were rehydrated with PBS for five minutes, fixed in 2% PFA for 30 minutes, permeabilized in 0.1% Triton X-100 for 15 minutes, and blocked in 5% donkey serum and 2% BSA in PBS for one hour at room temperature. Primary antibodies were diluted in 2% BSA and incubated overnight at 4°C. AlexaFluor conjugated secondary antibodies were used (ThermoFisher) at a dilution of 1:1000 in 2% BSA for one hour at room temperature. Sections were then counterstained with Hoescht for one minute at room temperature and then mounted. Small pulmonary vessels (30 to 100 microns in diameter) not associated with a bronchial airway were selected for imaging.

2.2.4 Single-Cell Transcriptomics

Single cell RNA sequencing was performed on lungs of healthy controls and idiopathic PAH patients (N=3 per group). Expression matrices were derived using CellRanger (Zheng et al., 2017). Subsequent batch correction, scaling, and normalization were all performed using SCTransform in Seurat v3 (Butler et al., 2018; Hafemeister and Satija, 2019; Stuart et al., 2019). Cell types were determined with SingleR (Aran et al., 2019) using the Blueprint ENCODE reference (Consortium, 2012). Cells were identified as positively expressing *NCOA7* if the

transformed expression value was greater than 0. Cells expressing *NCOA7* were identified as having a transformed expression value greater than 0.2.

2.2.5 Generation of iPSCs and CRISPR-Cas9 Gene-Editing

To generate the isogenic lines, we introduced the G allele for SNP rs11154337 into control iPSCs with pSpCas9(BB)-2A-GFP (PX458; Addgene; 48138) as the vector for genome editing. For the site-specific CRISPR-Cas9 and guide RNA sequence construction, two reverse complementary guide oligos were annealed and then ligated to the linearized PX458 vector. The single-stranded oligodeoxynucleotide (ssODN) template with mutation/correction sites was designed as previously described (Ran et al., 2013). Control iPSCs were dispersed as single cells the day before transfection at 40 to 50% confluency. The next day, CRISPR-Cas9 and ssODN templates were transfected into the iPSCs using GeneJammer reagent according to the manufacturer's protocol (Agilent Technologies 204132). After 36 hours following transfection, GFP positive cells were sorted out using FACS and were seeded at a density of 2,000 cells per well in a 6-well plate. After expansion for about one-week, single cell-derived colonies were observed and picked for genotype characterization and subsequent expansion. DNA was extracted from collected cells using QuickExtract solution (Epicenter). PrimeSTAR® GXL DNA Polymerase (Clontech) was used for PCR amplification and genotyping of the edited region. The sequence of primers used for identifying the targeted sequences are specified in Table 5.

2.2.6 Differentiation of iPSCs into Endothelial Cells

The creation of iPSC-ECs was done using a chemical differentiation protocol with three major steps: mesoderm induction, endothelial specification, and iPSC-EC purification (Gu, 2018). Briefly, mesoderm induction was done through Wnt signaling activation using the glycogen synthase kinase-3β inhibitor CHIR99021 (Selleckchem; S2924) in RPMI medium (Life Technologies; 11875-093) with B-27 minus insulin (Life Technologies; A18956-01) supplementation. The use of insulin-free B27 is believed to improve differentiation efficiency, as insulin negatively affects mesoderm induction (Lian et al., 2013). Next, endothelial lineage specification was done using supplemented growth factors like vascular endothelial growth factor (VEGF; 50 ng/mL; Gemini; 300196P) and fibroblast growth factor (FGF; 25 ng/mL; Gemini; 300113P) in EGM™-2 Endothelial Cell Growth Medium-2 BulletKit™. To increase yield, the transforming growth factor β (TGFβ) inhibitor SB431542 (10 μM; Selleckchem; S1067) was also added, as it promotes EC generation and inhibits smooth muscle cell differentiation from endothelial progenitors (James et al., 2010). Lastly, iPSC-EC purification was done using magnetic-activated cell sorting (MACS) against the mature EC surface marker vascular endothelial (VE)-cadherin, also known as CD144. Mature iPSC-ECs were labeled with magnetic CD144 MicroBeads (Miltenyi Biotech; 130-097-857), captured by a column in a magnetic field, and then separated from the unlabeled cells. Purified iPSC-ECs were maintained in EGM™-2 Endothelial Cell Growth Medium-2 BulletKit™.

2.2.7 Characterization of iPSC-ECs by Flow Cytometry

Cells before and after $CD144^+$ purification were analyzed using flow cytometry against endothelial surface markers. Specifically, expression of the mature endothelial progenitor marker CD34 (FITC Anti-CD34 Clone 581; BD Pharmingen™; 555821) (Cheng et al., 2013), the mature endothelial marker VE-cadherin/CD144 (APC Anti-CD144 Clone Bv9; BioLegend; 348508) (Giannotta et al., 2013), and the vascular endothelial growth factor receptor 2 (VEGFR2, or CD309; PE Anti-CD309 Clone 89106; BD Pharmingen™; 560872) (Yang et al., 2008) were assessed. Samples were run on the BD LSRFortesssa™ Flow Cytometer (BD Biosciences) at the Unified Flow Core at the University of Pittsburgh.

2.2.8 Characterization of iPSC-ECs by Immunofluorescent Staining

After $CD144^+$ purification, iPSC-ECs were further characterized by immunofluorescent staining of cell surface markers. Briefly, cells were fixed with 4% paraformaldehyde (PFA) for 15 minutes at room temperature, and then blocked in 5% bovine serum albumin (BSA) for one hour at room temperature. Cells were stained with Anti-VE-cadherin/CD144 antibody (1:100; abcam; ab33168) or Anti-CD31 (also known as platelet and endothelial cell adhesion molecule-1; PECAM-1; 1:100; abcam; ab24590) overnight at 4°C. After rinsing with PBS, cells were incubated with appropriate secondary antibodies (1:1000) in 5% BSA for one hour at room temperature. Cells were rinsed with PBS and mounted with ProLong™ Gold Antifade Mountant with DAPI (ThermoFisher; P36935). Images were acquired on a Nikon A1 Confocal Microscope at the Center for Biologic Imaging at the University of Pittsburgh.

2.2.9 Characterization of iPSC-ECs by in vitro Tube Formation

To confirm an endothelial phenotype, a capillary-like tube formation assay was performed using the *in vitro* Angiogenesis Assay (R&D Systems; 3470-096-K) (DeCicco-Skinner et al., 2014). A basement membrane extract with reduced growth factors was plated onto a 96-well plate and allowed to solidify for 30 minutes at 37°C. iPSC-ECs were then plated (20,000 cells per well) into the well with cell-type specific media deficient for growth factors and serum. After six hours, capillary-like structures were imaged with the EVOS^{TM} XL Core Imaging System (ThermoFisher) at 10x magnification.

2.3 Primary Data

2.3.1 NCOA7 is Upregulated in Response to Various Triggers

To determine a role for NCOA7 in pulmonary vascular disease, primary human pulmonary vascular cells were exposed to various triggers of PAH. A common feature shared among patients living with a Group I diagnosis of PAH is the elevation of proinflammatory cytokines (*e.g.*, IL-1β and IL-6) in their serum (Rabinovitch et al., 2014). To model this, IL-1β (1 ng/mL) was applied to human pulmonary arterial endothelial cells (PAECs) and was noted to induce a marked and preferential upregulation of an alternative-start, short-length version of *NCOA7* (*NCOA7*$_{short}$) in comparison to the canonical, full-length isoform (*NCOA7*$_{full}$) (Figure 3A & B). Similarly, the application of IL6/IL6Rα (10 ng/mL) to human PAECs resulted in preferential induction of *NCOA7*$_{short}$ over its full-length isoform, although not to the same degree (Figure 3C & D). Hypoxia,

or low oxygen tension, is a well-established driver of Groups I and III PH and trigger of molecular pathways implicated in disease pathogenesis (Simonneau et al., 2019; Stenmark et al., 2006). Human PAECs exposed to hypoxia (0.2% O_2) demonstrated preferential upregulation of *NCOA7*$_{short}$ compared to its full-length isoform (Figure 3E & F). Taken together, these data indicate a potential role for this unique, alternative-start isoform in response to triggers associated with PH.

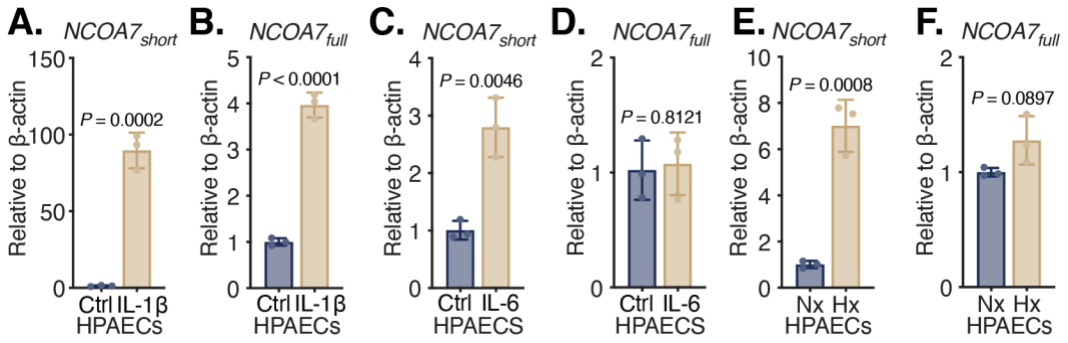

Figure 3. NCOA7 is Upregulated in Response to Various Triggers

A & B. *NCOA7* expression via RT-qPCR in human PAECs subjected to IL-1β (1 ng/mL) for 24 hours. N=3 per group; Student's *t*-test. **C & D.** *NCOA7* expression via RT-qPCR in human PAECs subjected to IL-6/IL-6Rα (10 ng/mL) for 24 hours. N=3 per group; Student's *t*-test. **E & F.** *NCOA7* expression via RT-qPCR in human PAECs subjected to hypoxia (<1% O_2) for 24 hours. N=3 per group; Student's *t*-test. All data are presented as mean ± standard deviation.

Using a severe inflammatory rodent model of PH, transgenic mice under constitutive IL-6 overexpression and chronic hypoxia demonstrated elevated *Ncoa7* expression in $CD31^+$ endothelial cells isolated from lung tissue (Figure 4A & B).

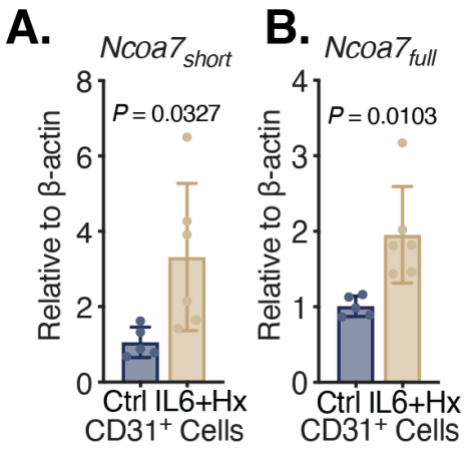

Figure 4. A Proinflammatory Rodent Model of PH Induces Ncoa7 in Endothelial Cells

A & B. *Ncoa7* expression via RT-qPCR in CD31+ isolated cells from total lung of IL-6 transgenic mice under chronic hypoxia (10% O_2 for three weeks). N=5-7 per group; Student's *t*-test. All data are presented as mean ± standard deviation.

Examining the *in situ* localization of NCOA7 in various rodent models of PH, we found that NCOA7 was markedly upregulated. In the chronic hypoxia mouse model, the *Il6* transgenic mouse model, and the monocrotaline-injected rat model NCOA7 was globally upregulated in pulmonary vessels (Figure 5). Notably, this upregulation appears to colocalize within both the intimal (or endothelial) and medial (or smooth muscle) layers of the vessel, signifying a role for NCOA7 function beyond the endothelium.

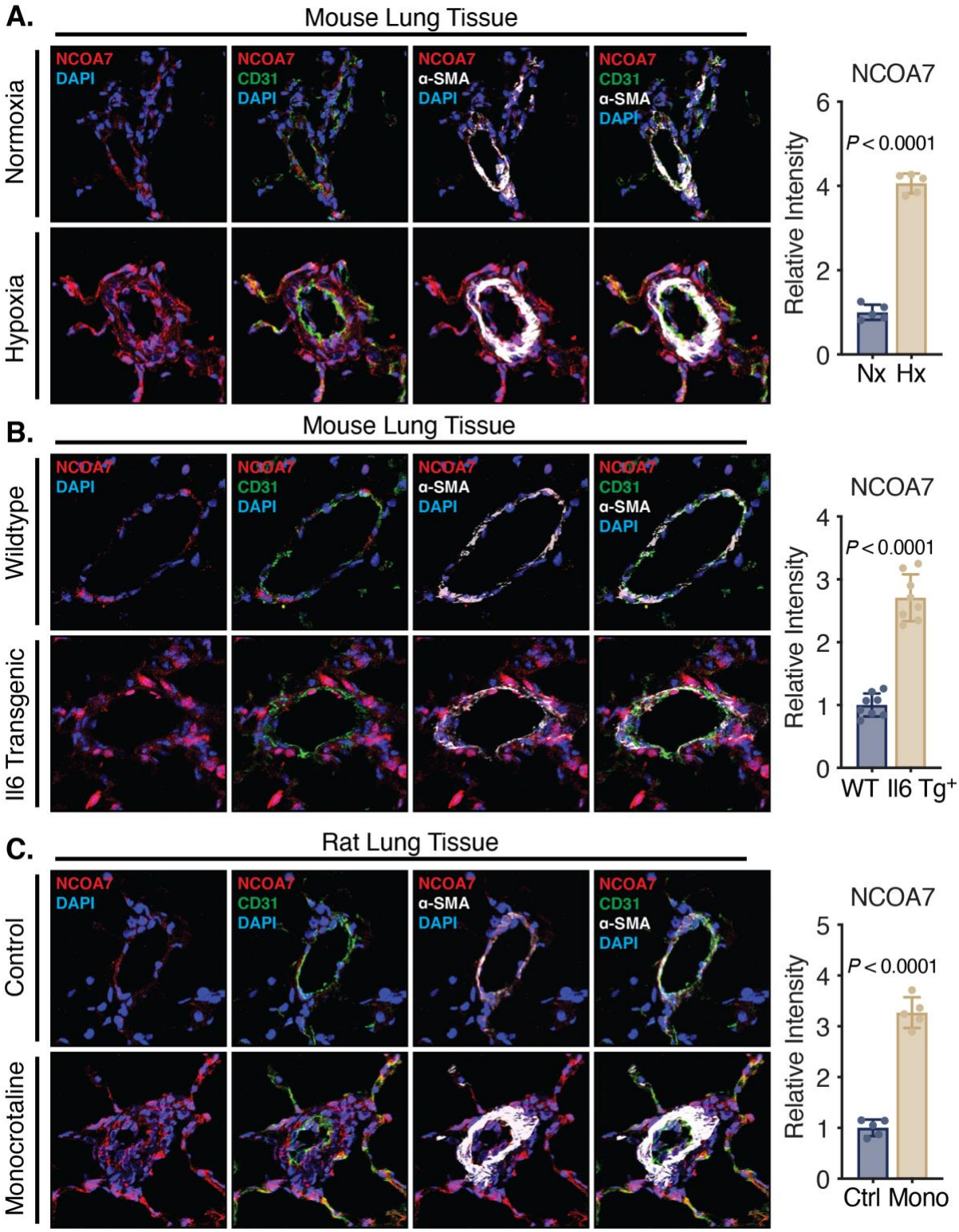

Figure 5. NCOA7 is Upregulated in Lungs of Rodent PH Models

A. Pulmonary vessels from normoxic or hypoxia mice stained for NCOA7 (red), CD31 (endothelial cells; green), α-SMA (smooth muscle cells; white), and DAPI (blue). Quantification of relative intensity. N=5 per group; Student's *t*-test. **B.** Pulmonary vessels from wildtype or *Il6* transgenic mice stained for NCOA7 (red), CD31 (green), α-SMA (white), and DAPI (blue). Quantification of relative intensity. N=8 per group; Student's *t*-test. **C.** Pulmonary vessels from control or monocrotaline-injected rats stained for NCOA7 (red), CD31 (green), α-SMA (white), and DAPI (blue). Quantification of relative intensity. N=5 per group; Student's *t*-test. All data are presented as mean ± standard deviation.

In addition, human lung tissue from healthy controls or patients diagnosed with Group I PH also had demonstrable elevations in NCOA7 expression within pulmonary vessels (Figure 6).

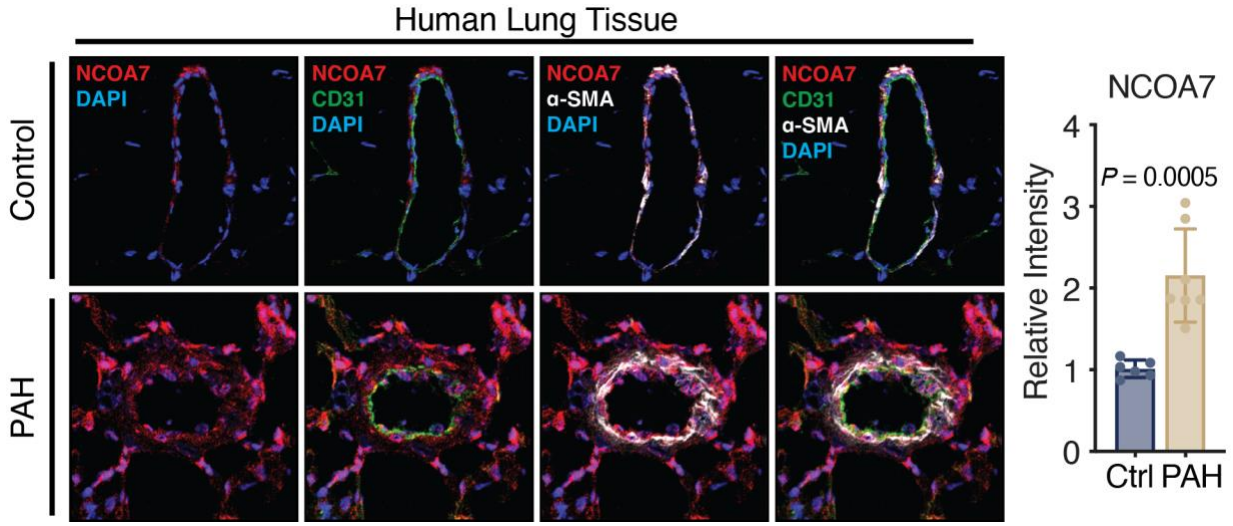

Figure 6. NCOA7 is Upregulated in PAH Lungs

Pulmonary vessels from healthy control or patients with PAH stained for NCOA7 (red), CD31 (endothelial cells; green), α-SMA (smooth muscle cells; white), and DAPI (blue). Quantification of relative intensity. N=6-7 patients per group with the average intensity of 4-7 vessels per patient plotted; Student's *t*-test. All data are presented as mean ± standard deviation.

Single-cell RNA sequencing performed on lungs from healthy and idiopathic PAH patients revealed an increased number of endothelial cells expressing *NCOA7* (22.58% versus 29.66%) (Figure 7A). Further analysis of this endothelial population revealed that *NCOA7* expression was significantly upregulated in PAH patients (Figure 7B). When taken together, these data demonstrate that various proinflammatory models are similarly integrating onto the upregulation of *NCOA7* within the pulmonary vessel.

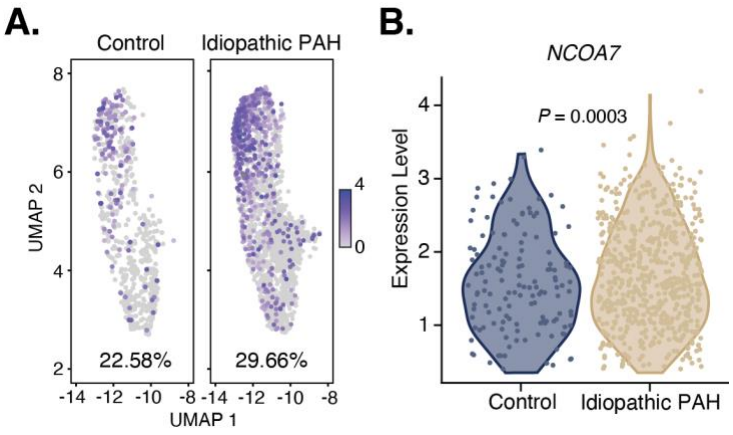

Figure 7. Single Cell Transcriptomic Analysis Reveals Elevated NCOA7 in PAH

A. Feature plot of endothelial cells (Seurat cluster #4) expressing *NCOA7* identified via single-cell RNA sequencing on lungs from control or idiopathic PAH patients. Of 620 endothelial cells identified in control lungs, 140 or 22.58% express *NCOA7*. Of 2013 endothelial cells identified in idiopathic PAH lungs, 597 or 29.66% express *NCOA7*. Cells were identified as expressing *NCOA7* if the transformed expression value was greater than 0. N=3 per group. **B.** Violin plot of *NCOA7* expression only in expressing endothelial cells identified via single-cell RNA sequencing. Plotted cells were identified if the transformed expression value of *NCOA7* was greater than 0.2. N=3 per group.

2.3.2 NCOA7 is Under Transcriptional Control of NF-κB

To investigate upstream transcriptional control of *NCOA7*, the UCSC Genome Browser was accessed to examine predicted binding sites in the canonical and non-canonical promoter regions. Notably, a component of the well-established inflammatory transcription factor complex—the RelA/p65 (*RELA*) subunit of NF-κB—was predicted to bind at each promoter region, perhaps explaining its induction under proinflammatory stress (Kent et al., 2002). In support of this idea, the genetic knockdown of *RELA* in human PAECs completely abrogated the IL-1β-mediated upregulation of both *NCOA7* isoforms, demonstrating its requirement for transcription (Figure 8A & B). To confirm direct promoter-transcription factor binding, a chromatin immunoprecipitation coupled with quantitative PCR (ChIP-qPCR) was performed, which revealed a significant enrichment of p65/RelA at DNA sequences of both the canonical (*i.e.*, full-length) and non-canonical (*i.e.*, short-length) promoters (Figure 8C).

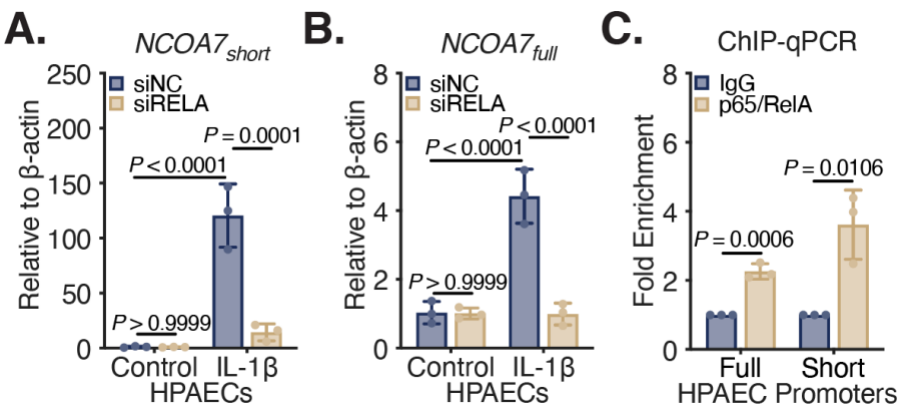

Figure 8. NCOA7 Expression is Regulated by p65/RelA

A & B. Expression of *NCOA7* via RT-qPCR in human PAECs subjected to RNAi against *RELA* under control or IL-1β conditions for 24 hours. N=3 per group; Two-way ANOVA. **C.** Chromatin immunoprecipitation-qPCR of sheared chromatin from human PAECs incubated with Anti-IgG or Anti-p65/RelA. qPCR was performed using primers against the canonical (*i.e.*, full-length) and non-canonical (*i.e.*, short-length) promoters. ChIP-qPCR is presented as fold enrichment, where Anti-p65/RelA is relative to the negative Anti-IgG sample. N=3 per group; Student's *t*-test. All data are presented as mean ± standard deviation.

2.3.3 The Identification of a Functional Single Nucleotide Polymorphism

In seeking whether the specialized genomic architecture of NCOA7 may control gene expression, we surveyed annotated single nucleotide polymorphisms (SNPs) based on their proximity to the non-canonical promoter region and their predicted ability for long-range interactions that may allow for a positional backfolding onto the canonical promoter. In doing so, we identified a candidate SNP—rs11154337—located near an intronic region proximal to the non-canonical promoter of *NCOA7* with potential regulatory function, as noted by an enrichment for histone modifications (Kent et al., 2002). To discern potential regulatory function at the canonical promoter, we utilized publicly available high-throughput chromatin conformation capture on human umbilical vein endothelial cells (GEO IDs GSM3438650 and GSM3438651) from the 3D-

genome Interaction Viewer & database (3DIV; http://3div.kr). Analysis of three-dimensional interactions revealed that SNP rs11154337 has long-range interactions greater than 120 kilobases with the canonical promoter region of *NCOA7* (Figure 9A). Furthermore, positional weight matrix analysis of the SNP containing region identified Krüppel-like factor 4 (KLF4) as possessing the highest difference in log-odds score (4.93065) of transcription factors based on the presence of the C or G allele with high preference for the G allele. KLF4 has proven direct binding capacity to p65/RelA in endothelial cells to reduce inflammation (Yoshida and Hayashi, 2014), and the deletion of KLF4 in rodent models of PH worsened disease by hemodynamic and histologic indices (Shatat et al., 2014). Chromatin immunoprecipitation against p65/RelA revealed a significant enrichment for the SNP containing region, denoting the presence of a potential p65/RelA-KLF4 complex (Figure 9B).

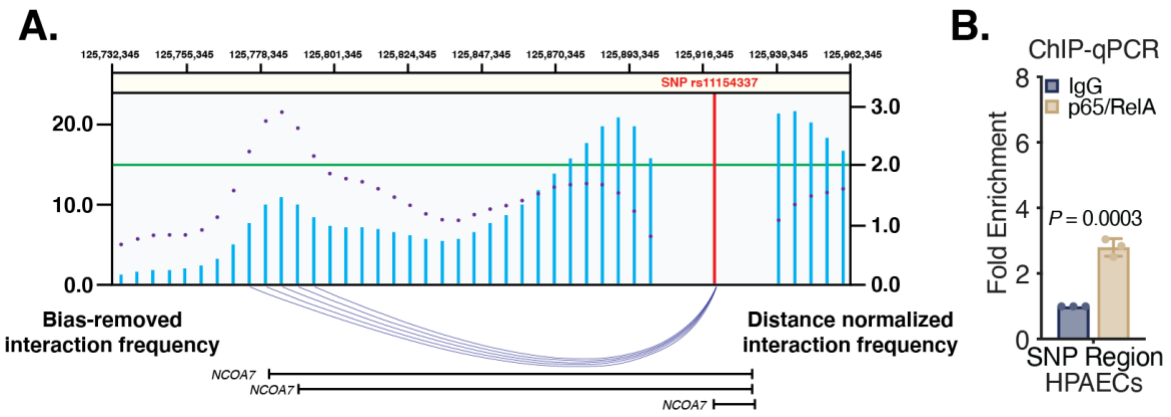

Figure 9. Identification of a Functional SNP in NCOA7

A. High-throughput chromatin conformation capture on human umbilical vein endothelial cells (GEO IDs GSM3438650 and GSM3438651). Blue bars represent the bias-removed chromatin interaction frequency, and the purple dots represent the distance-normalized interaction frequency. The arcs, depicted in indigo, represent the identified interactions of SNP rs11154337 in red defined by the threshold line in green. Data were obtained from the 3D-genome Interaction Viewer & database (3DIV; http://3div.kr). Gene map of NCOA7 isoforms depicted below. **B.** Chromatin immunoprecipitation-qPCR (ChIP-qPCR) of sheared chromatin from human PAECs incubated with Anti-IgG or Anti-p65/RelA. qPCR was performed using primers against the region containing SNP rs11154337. ChIP-qPCR is presented as fold enrichment, where Anti-p65/RelA is relative to the negative Anti-IgG sample. N=3 per group; Student's *t*-test. All data are presented as mean ± standard deviation.

To directly study the cellular and biological activity of this polymorphism, we sought to generate a set of genetically matched, isogenic inducible pluripotent stem cell (iPSC) lines with the allelic variants of SNP rs11154337. The creation of SNP-edited, isogenic lines allows for the reliable identification of potential functional effects of a single polymorphism by excluding potential disparities in genetic background or epiphenomena from various human cell lines (Shi et al., 2017).

Accordingly, we performed CRISPR-Cas9-gene editing in iPSCs that were homozygous for the C allele (*i.e.*, C/C) to produce an isogenic, SNP-edited, heterozygous iPSC line (*i.e.*, C/G)

(Ran et al., 2013) (Figure 10A). The iPSCs were then differentiated into endothelial cells (iPSC-ECs) and purified through a vascular endothelial cadherin (VE-Cadherin; also known as CD144)-based magnetic separation (Gu, 2018) (Figure 10B). Purified iPSC-ECs exhibited marked enrichment of the endothelial cell markers CD34, CD144, and CD309, and immunofluorescent staining of iPSC-ECs against CD144 and CD31 revealed a patterning consistent with the endothelium. Moreover, iPSC-ECs displayed angiogenic potential, as noted by vessel formation in growth factor-depleted Matrigel (Figure 10C & D). In sum, these data support that iPSC-ECs can serve as surrogate models for the direct study of primary endothelial cells.

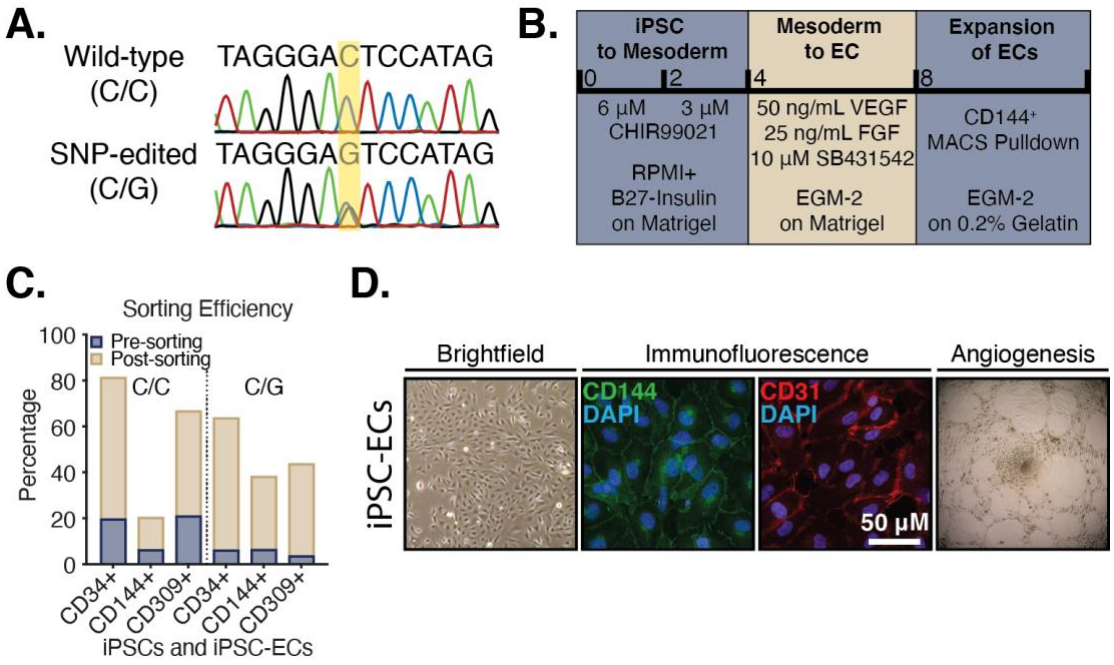

Figure 10. The Generation of Isogenic, SNP-Edited iPSC-Derived Endothelial Cells

A. DNA sequencing of iPSCs demonstrating a wild-type homozygous C/C line and its isogenic, CRISPR-Cas9, SNP-edited heterzygous C/G line. The site of SNP-editing is highlighted in yellow. **B.** Overview of the chemical induction protocol used to produce iPSC-derived endothelial cells (Gu, 2018). **C.** Flow cytometric analysis of pre- and post-sorted cells demonstrating that CD144^{+} magnetic activated cell sorting enriches for an endothelial population using lineage specific markers (*i.e.*, CD34, CD144, and CD309). **D.** Brightfield imaging demonstrating the cobblestone morphology associated with endothelial cells. Immunofluorescent staining demonstrating the membrane expression of endothelial specific markers CD144 (green) and CD31 (red). Functional angiogenesis assay demonstrating the ability of derived cells to form tubes (*i.e.*, vessels) in culture.

Utilizing isogenic, SNP-edited iPSC-ECs, we observed that C/G iPSC-ECs have markedly higher expression of *NCOA7* isoforms when compared to the C/C line, confirming that the G allele does in fact alter transcription of *NCOA7* (Figure 11). These expression data are consistent with the chromatin capture data indicating SNP rs11154337 interaction at the canonical promoter in

human umbilical vein endothelial cells and the computational prediction of enhanced KLF4 binding to the G allele, which would presumably enhance *NCOA7* transcription.

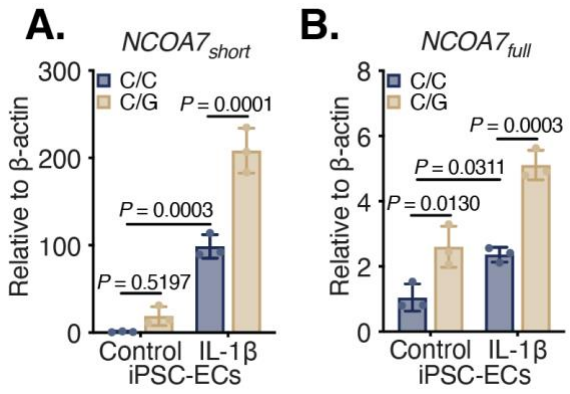

Figure 11. NCOA7 Expression is SNP-Dependent

A & B. Expression of *NCOA7* isoforms via RT-qPCR in isogenic, SNP-edited iPSC-ECs under control or IL-1β conditions for 24 hours. N=3 per group; Two-way ANOVA. All data are presented as mean ± standard deviation.

2.3.4 A Functional Genomic & Metabolomic Association

Given the allele-specific role of SNP rs11154337 in controlling NCOA7, and when coupled with the potential importance of this gene in endolysosomal trafficking and sterol handling, we hypothesized that this SNP may control oxysterol and bile acid production and thus associate with the key metabolites identified as predictive of human PAH mortality by unbiased plasma metabolomic analysis described above. Yet, one of the greatest challenges in the post-genomic era has been linking a statistical association between trait and disease to biological function. Accordingly, we set out to not only assess whether SNP rs11154337 within *NCOA7* is associated to the metabolites identified by Alotaibi et al. but also if this polymorphism could functionally affect the production of bile acid metabolites through the direct biological activity of NCOA7. As

such, this would be among the first examples in any cardiovascular disease of defining a genomic and metabolomic statistical association derived from large population-based sequencing and subsequently linking that association to causative biological activity and clinical prognostic utility.

Utilizing the top 51 clustered metabolites, Alotaibi et al. found that 30 of these metabolites were validated in their association to mortality from data collected in the Vanderbilt University Medical Center cohort. Out of these 30 metabolites, a subset of 18 were validated in association to six-minute walk distance among all three cohorts—a clinical measure of disease severity. As such, we then examined whether these 18 candidate metabolites were associated to SNP rs11154337 by utilizing a *P*-value cutoff of 0.003 (defined by an α of 0.05 divided by 18 candidate metabolites). To do so, we and Alotaibi et al. leveraged The FINRISK Study of nearly 8,000 patients—where participants in this cohort had not only DNA sequencing performed via SNP arrays but also were subject to unbiased, serum metabolomics analysis performed by the same LC/MS method (Borodulin et al., 2018). We discovered that two metabolites were negatively associated with the G allele of SNP rs11154337—metabolite 665110 ($P = 0.008$) and metabolite 667200 ($P = 0.001$). Examining our candidate metabolite further, we and Alotaibi et al. found that metabolite 667200 was significantly associated to six-minute walk distance ($P = 1.74 \times 10^{-5}$; effect size -16.07 with 95% confidence interval of -23.37 to -8.77) and mean right atrial pressure (mRAP; a hemodynamic surrogate of morbidity; $P = 2.61 \times 10^{-16}$; effect size 0.88 with 95% confidence interval of 0.67 to 1.08).

In summary, these data demonstrate that various proinflammatory stimuli integrate onto the p65/RelA subunit of NF-κB to control the expression of *NCOA7* in an allele-specific manner—noted by the presence of the G allele at SNP rs11154337 and elevated *NCOA7* expression. In addition, we and Alotaibi et al. show that a metabolite with *positive* correlations to clinical severity

and mortality in PAH is simultaneously *negatively* associated with the G allele of SNP 11154337. Thus, this rare combination of mechanistic evidence coupled with broad human population-based genomic-metabolomic associations implicating NCOA7, oxysterols, and bile acids to PAH pathogenesis, we postulated that a failure to upregulate (*i.e.*, lack a G allele) or a deficiency of NCOA7 drives the production of oxysterols and downstream serum bile acids to promote endothelial dysfunction and the development of PAH.

2.4 Discussion

2.4.1 NCOA7 is an Immune-Responsive Element

The early work on NCOA7 and its unique alterative start, highly truncated isoform have reported its immune-responsive induction under interferon stimulation (Shkolnik et al., 2008; Yu et al., 2015). This observation led to the hypothesis that perhaps NCOA7—as an interferon-responsive element—functioned as a cellular defense mechanism against invasive pathogens. In support of this notion, two studies have demonstrated that *NCOA7* homologues in *Drosophila* prevent bacterial pathogen entry via the endocytic pathway (Wang et al., 2012) and that NCOA7 can inhibit viral infection through enhanced modulation of V-ATPases (Doyle et al., 2018).

There is an increasing appreciation of immune dysregulation as a robust component of panvascular remodeling and how this dysregulation serves as an insult to the endothelium—a conditional player and sentinel of the immune system (Mai et al., 2013). In accordance with previous observations, we demonstrated that NCOA7 is induced under other proinflammatory triggers, such as through IL-1β and IL-6 application *in vitro*. In addition, we found significant

upregulation of *Ncoa7* in $CD31^+$ endothelial cells isolated from the lungs of a severe inflammatory rodent model of PH. In humans, we performed single-cell RNA sequencing on lungs from healthy controls or PAH patients and found that in identified endothelial cells there was a higher rate of cells positive for *NCOA7* expression and that overall transcript expression was higher as well. Taken together, these data provide compelling evidence of the immune responsive nature of NCOA7—an important observation given the systemic, proinflammatory state observed in PAH patients.

2.4.2 Regulation of NCOA7, SNP rs11154337, & Chromatin Architecture

Our work has made considerable advancements in the transcriptional regulation of *NCOA7*. We have demonstrated a necessary and critical role for the p65/RelA subunit of NF-κB in the IL-1β-mediated upregulation of both isoforms, as genetic silencing of *RELA* completely abrogates induction of *NCOA7*. Notably, the addition of IL-1β and thus NF-κB involvement to previous observations of NCOA7 as an interferon-responsive element suggestions a functional cooperation between two antimicrobial host defense pathways: (1) initial detection at the plasma membrane via Toll-like receptors and activation of the NF-κB pathway and (2) potential endosomal pathogen escape that triggers an interferon-mediated response and STAT1/2 activation via Janus tyrosine kinases (JAK) (Wienerroither et al., 2015). Moreover, these data add to the observation that p65/RelA of NF-κB is upregulated in the PAECs of patients living with PAH (Price et al., 2013) by implicating *NCOA7* as a novel molecule in disease pathogenesis.

Furthermore, our work confirmed the direct binding of the p65/RelA subunit of NF-κB to both the canonical and non-canonical promoters of *NCOA7* via chromatin immunoprecipitation-qPCR. Most excitingly, we showcased the biological function of SNP rs11154337 in regulating

the expression of short- and full-length *NCOA7* isoforms in isogenic, SNP-edited, iPSC-ECs and further confirmed that p65/RelA binds to the regulatory region containing SNP rs11154337. Despite this finding, computational analysis of this region suggests that p65/RelA is not capable of direct DNA binding based on its positional weight matrix; however, we discovered on further analysis that the positional weight matrix of Krüppel-like factor 4 (KLF4) has the highest difference in log-odds score (4.93065) of transcription factors based on the presence of the C or G allele with high preference for the G allele. Notably, KLF4 is known to directly bind to p65/RelA in endothelial cells to reduce inflammation (Yoshida and Hayashi, 2014), indicating that the isolated DNA fragments isolated from the pulldown of p65/RelA were likely complexed with KLF4 as the direct binding partner to the SNP region. To confirm this, a direct ChIP against KLF4 must be performed. Moreover, the expression of KLF4 has demonstrated protective effects in rodent models of PH with its deletion worsening right ventricular hypertrophy, right ventricular systolic pressure, and pulmonary arteriole muscularization (Shatat et al., 2014). Thus, the presence of the G allele may confer a computationally predicted affinity for KLF4 binding, thus directly interacting with p65/RelA to increase the expression of *NCOA7* and thus exert anti-inflammatory properties within the endothelium. Future work should be pursued to determine if the genetic knockdown of *KLF4* prevents *NCOA7* expression and whether chromatin immunoprecipitation-qPCR can demonstrate higher enrichment in isogenic, SNP-edited, iPSC-ECs with the G allele.

In addition, we unexpectedly observed that the presence of the G allele in our iPSC-ECs similarly prevented the upregulation of the full-length isoform. To investigate this further, we accessed publicly available high-throughput chromatin conformation capture on human umbilical vein endothelial cells (GEO IDs GSM3438650 and GSM3438651) from the 3D-genome Interaction Viewer & database (3DIV; http://3div.kr). We found that SNP rs11154337 has long-

range interactions (greater than 120 kilobases) with the canonical promoter region of *NCOA7*, raising the question of whether this SNP regulates full-length expression through a long-range interaction (Krietenstein et al., 2020). To confirm this, we are in the process of performing chromatin conformation capture (3C) on human PAECs and our isogenic, SNP-edited iPSC-ECs to determine if there is an intragenic interaction between SNP rs11154337 and the canonical promoter of *NCOA7*.

2.4.3 Moving Beyond Association: A Functional –Omics Era

Over the last decade, a series of scientific developments has allowed for the application of high-throughput, data-gatherinng technologies in the interrogation of cellular behavior to incredible detail. Beyond mapping the genomic landscape via the Human Genome Project, the advent of innovative –*omics*-based platforms (*i.e.*, metabolomic, proteomic, and transcriptomic approaches) has made multi-dimensional, molecular profiling of biological samples more accessible. The application of these technologies to rare disease, such as PAH, has been particularly difficult, for not only is there a numerical power limitation but also an inability to study human tissue until either patient death or lung transplanation. For this reason, clinicians and scientists are forced to study the pathogenesis of pulmonvary vascular disease from a single snapshot in time that fails to adequately address the spatio-temporal complexity of disease (Harvey and Chan, 2019).

Despite these barriers in the –*omics*-based application of high-throughput technologies to rare diseases, the advent of sequencing technologies and metabolomics profiling has revolutionized our understanding of the complex genetic inheritance underlying PAH and has lent insight into metabolomic signatures of disease. In fact, every gene that is currently implicated or

associated in the pathogenesis of PAH has been identified using these technologies: the discovery of *BMPR2* using familial linkage analyses and Sanger sequencing (Deng et al., 2000; International et al., 2000; Thomson et al., 2000), the identification of *ACRVL1/ALK1* and *ENG* in families with segregating hereditary hemorhagic telangiectasia (HHT; a subtype of Group I PH) (Chaouat et al., 2004; Harrison et al., 2005; Trembath et al., 2001), the detection of *BMPR2* signaling intermediates *SMAD1*, *SMAD4*, and *SMAD9* through DNA sequencing (Nasim et al., 2011; Shintani et al., 2009), the uncovering of *CAV1*, *EIF2AK4*, *KCNK3*, and *TBX4* using whole exome sequencing (Austin et al., 2012; Best et al., 2014; Eyries et al., 2014; Kerstjens-Frederikse et al., 2013; Levy et al., 2016; Ma et al., 2013; Zhu et al., 2018a), and, most recently, the association of *HLA-DPA1/DPB1* and *SOX17* in the largest genome-wide association study (GWAS) on PAH patients to date (*i.e.*, greater than 2,000 patients) (Rhodes et al., 2019). In addition, pharmacogenomics data have demonstrated a role for a genetic variant in the efficacy of endothelin-1 receptor antagonist therapy (Benza et al., 2015). Simultaneously, metabolomics profiling has unearthed metabolism-specific aberrations and implicated biomarkers with correlative capacity in disease severity and patient outcomes in PH (Fessel et al., 2012; Rhodes et al., 2017; Zhao et al., 2014a).

As has been made abundantly clear in the aforementioned section, these newfound data-gathering technologies have fundamentally advanced our understanding of disease in the betterment of patient care by providing insight into the underlying genetic architecture of disease (*i.e.*, disease-causing variants), clinical prognostics (*i.e.*, biomarkers), and personalized medicine (*i.e.*, pharmacogenomics). Yet, at the same time, some of these observations have failed to directly translate into clinical utility. For example, the vast majority of metabolomics profiling has provided observational data with limited clinical meaning. In addition, limited GWAS analyses on PAH patients—in part due to linkage disequilibrium, SNP genotyping methodologies, and a

paucity of patient tissue—have made it difficult to precisely locate causal variants. This challenge is further compounded by the fact that most associations are in non-coding regions, thereby making biological interpretation inherently more difficult.

Despite these barriers, we believe that our work—in conjunction with Alotaibi et al.—will be unique in integrating both genomics and metabolomics datasets in the identification of a functional nucleotide variant with direct, mechanistic underpinnings in the synthesis of a metabolite with demonstrable, disease-inciting activity and clinical utility in the progression and management of human disease.

Our collective data therefore indicate that the heightened proinflammatory state observed in PAH integrates onto the p65/RelA subunit of NF-κB to augment the expression of *NCOA7* in an allele-specific manner—noted by the presence of the G allele at SNP rs11154337. In addition, we and Alotaibi et al. show that a metabolite with *positive* correlations to clinical severity and mortality in PAH is simultaneously *negatively* associated with the G allele of SNP 11154337. Accordingly, we postulated that a failure to upregulate (*i.e.*, lack a G allele) or a deficiency of NCOA7 will result in an elevation of serum bile acids to promote endothelial dysfunction and the development of PAH.

3.0 Loss of NCOA7 Results in Lysosomal Dysfunction & Lipid Accumulation

The work was adapted from a manuscript in submission:

Lloyd D. Harvey, Sanya Arshad, Mona Alotaibi, Anna Kirillova, Wei Sun, Neha Hafeez, Adam Handen, Yi-Yin Tai, Ying Tang, Chen-Shan C. Woodcock, Jingsi Zhao, Annie M. Watson, Yassmin Al Aaraj, Callen T. Wallace, Claudette M. St. Croix, Donna B. Stolz, Gang Li, Jeffrey McDonald, Haodi Wu, Thomas Bertero, Mohit Jain, and Stephen Y. Chan. NCOA7 Deficiency Coordinates Lysosomal Dysfunction and Sterol Metabolism to Promote Endothelial Dysfunction and Pulmonary Arterial Hypertension. *In submission*.

3.1 Introduction

Previous and limited work has identified a potential role for NCOA7 as an endolysosomal regulatory factor, noting its ability to acidify the lysosome in the context of preventing pathogen entry via an endolysosomal route. In the context of PH, there has been a paucity of work related to the lysosome that has primarily focused on autophagic pathways dependent upon downstream lysosomal function in the degradation of cellular content, often examining the roles of lysosomal adaptor molecules (Chichger et al., 2019; Sehgal and Lee, 2011). A definitive role for autophagy has not been established in PH with the most recent consensus positing that the extent of autophagic pathway activation may either be beneficial or harmful in disease progression (Chen et al., 2018).

One of the more notable studies has previously revealed that inhibition of autophagy and lysosomal activity using chloroquine or hydroxychloroquine prevented the development of experimental PH; however, the benefit of autophagy inhibition was observed at the level of pulmonary arterial smooth muscle cells with no effect on the endothelium (Long et al., 2013). Moreover, the proposed mechanism was that inhibition of autophagic and lysosomal pathways prevented the degradation of the bone morphogenetic protein type II receptor (*BMPR2*)—a key molecule that when functionally lost underlies the vast majority of heritable PAH diagnoses (International et al., 2000). Conversely, a case report of a patient with severe PAH secondary to an inborn error of lysosomal enzyme activity noted elevated levels of pro-endothelin-1 and endothelin-1 in the patient's serum, implying that failure of lysosomal hydrolase activity prevented the degradation of this potent vasoconstrictor (Recla et al., 2015). Ultimately, these limited studies demonstrate that focusing on a single molecule secondary to lysosomal dysfunction may be too reductionistic, for the lysosome acts as a critical metabolic, regulatory hub in overall cellular function and health.

Given that recent and compelling evidence further places the lysosome as a critical regulator of sterol metabolism, we aimed to investigate (1) if NCOA7 functioned at the lysosome within the endothelium, (2) the extent to which NCOA7 modulated lysosomal behavior to govern sterol metabolism, and (3) if manipulation of NCOA7 could produce alterations in sterol metabolism consistent with our joint metabolomic correlations in the largest metabolomics cohort of PAH patients, thereby providing a mechanistic explanation.

3.2 Materials & Methods

The following methods are in addition to those discussed in section 2.2.

3.2.1 Transfection of Cells for RNA Silencing

Human PAECs were transfected at approximately 70 to 80% confluency using negative control (siNC) or target gene (siGene) silencing RNA (siRNA) at 20 nM. Lipofectamine® 2000 (ThermoFisher; 11668019) was mixed with siRNA per manufacturer's protocol. Lipofectamine®:siRNA mixture was incubated with human PAECs in Opti-MEM™ reduced serum media for 4 to 6 hours (ThermoFisher; 31985062). After incubation, transfection media was removed and replaced with full serum, cell-specific growth media. Experiments were performed 48 hours post-transfection.

3.2.2 Construction of Lentiviral Plasmids & Particles

The cDNA sequences encoding full-length NCOA7 (mRNA transcript variant 1, NM_181782.5) and short-length NCOA7 (mRNA transcript 6, NM_001199622.2) were amplified by PCR with HindIII and NheI linkers. The PCR products were directly cloned downstream of Myc-tagged green fluorescent protein (mGFP) open reading frame in the pmGFP-ADAR1-p110 vector (Addgene; 117928). The cDNA sequences encoding mGFP fused full- and short-length *NCOA7* were further subcloned into the pCDH-CMV-MCS-EF1α-Puro lentiviral expression vector (Systems Biosciences; CD510B-1). Cloned plasmids were verified by DNA sequencing at the Genomics Research Core at the University of Pittsburgh.

HEK293T cells were maintained in Dulbecco's Modified Eagle Medium (DMEM) with 10% FBS. HEK293T cells were transfected using Lipofectamine® 2000 (ThermoFisher; 11668019) with lentiviral plasmids containing the target gene (or an empty vector for control virus) and packaging plasmids from the ViraPower™ Lentiviral Packaging Mix (ThermoFisher; K497500). Viral particles were harvested 48 hours after transfection, pelleted, and then filtered.

3.2.3 Transduction of Cells for Lentiviral Vector Delivery

Human PAECs were transduced by direct application of media with polybrene (8 μg/mL) containing viral particles with an empty, control vector expressing GFP or with the target gene. Transduction efficiency was assessed via GFP expression and direct measures of transcript and protein expression. Experiments were performed 72 hours after transduction.

3.2.4 Protein Extraction & Immunoblotting

Cells were rinsed two times with PBS before collection in RIPA buffer containing protease and phosphatase inhibitors. Protein concentration was determined using the Pierce™ BCA Protein Assay Kit (ThermoFisher; 23225). Protein lysates were separated using 4–15% Mini-PROTEAN® TGX™ Precast Protein Gels (Bio-Rad Laboratories; 4561086) and subsequently transferred onto a PVDF membrane. Membranes were blocked with 5% BSA in Tris-buffered saline with 0.1% Tween 20 (TBST) for one hour at room temperature. Primary antibodies were subsequently added and incubated at 4°C overnight (Table 8). The next day blots were washed three times for 10 minutes each with TBST. Blots were then incubated with the appropriate secondary antibody coupled to HRP for one hour at room temperature. After another round of TBST washing, blots

were visualized using Pierce ECL reagents and images were captured using the BioRad ChemiDoc XRS+.

3.2.5 Transcriptomic Analysis of NCOA7-Deficient Human PAECs

Microarray data were obtained using the Affymetrix Clariom D Human Array at the Genomics Research Core at the University of Pittsburgh. The microarray chip was performed on four groups in triplicate for a total of 12 samples. Human PAECs were subjected to either knockdown control or of the gene *NCOA7*. Additionally, groups were then either left in control conditions or further challenged with the proinflammatory cytokine IL-1β for 24 hours. Raw data were processed using Bioconductor packages in the language R to produce a list of differentially expressed genes that were selected using a Benjamini-Hochberg corrected p-value less than 0.05 in order to minimize the false discovery rate (FDR).

The following add-on packages were utilized: oligo, limma, affycore tools, gplots, pd.clariom.d.human for the analysis of this microarray data. Very broadly, the flow of this program serves to take raw microarray data in .CEL format into a list of differentially expressed genes. The workflow included loading the raw data into R, filtering and normalizing the raw data, plotting to demonstrate uniformity among the samples, adding annotations (*i.e.*, Entrez IDs, Gene Symbols, and Gene Names), setting up a comparison matrix to run statistical analyses among the groups, generating a list of differentially expressed genes, filtering said list, constructing a heat map to depict generalized trends, and to overlap the produced list of genes with our PH Network.

Gene-set enrichment analyses (GSEA) of identified differentially expressed genes were then created using Gene Ontology (Ashburner et al., 2000; The Gene Ontology, 2017),

REACTOME (Croft et al., 2014; Fabregat et al., 2017), KEGG (Kanehisa et al., 2017), and BioCarta (Nishimura, 2001).

3.2.6 Proximity Ligation Assay

Direct interaction of NCOA7 with the V-ATPase subunit ATP6V1B2 was assessed using the Duolink® Proximity Ligation Assay (Millipore Sigma; DUO92102). Human PAECs were plated in a Nunc™ Lab-Tek™ II Chamber Slide™ System (20,000 per well; ThermoFisher; 154453) and then fixed with 4% paraformaldehyde for 15 minutes. After permeabilization and blocking per the manufacturer's protocol, wells were incubated with either mouse anti-NCOA7 antibody (Santa Cruz Biotechnology; sc-393427), rabbit anti-ATP6V1B2 antibody (abcam; ab73404), both antibodies, or neither antibodies overnight at 4°C. Cells were then incubated with the PLUS and MINUS probes for one hour, ligated for 30 minutes, and amplified for 100 minutes at 37°C. Slides were then mounted with ProLong™ Gold Antifade Mountant with DAPI (ThermoFisher; P36935). Images were acquired on a Nikon A1 Confocal Microscope at the Center for Biologic Imaging at the University of Pittsburgh.

3.2.7 Transmission Electron Microscopy & Lysosomal Hypertrophy

Human PAECs grown on tissue culture plasticware were fixed in 2.5% glutaraldehyde in 100 mM PBS (8 gram/L NaCl, 0.2 gram/L KCl, 1.15 gram/L $Na_2HPO_4 \cdot 7H_2O$, 0.2 gram/L KH_2PO_4, pH 7.4) overnight at 4°C. Monolayers were washed in PBS three times and then post-fixed in aqueous 1% osmium tetroxide, 1% Fe_6CN_3 for one hour. Cells were washed three times in PBS and then dehydrated through a 30-100% ethanol series with several changes of Poly/Bed® 812

embedding resin (Polysciences). Cultures were embedded by inverting Poly/Bed® 812-filled BEEM® capsules on top of the cells. Blocks were cured overnight at 37ºC, and then cured for two days at 65ºC. Monolayers were pulled off the coverslips and re-embedded for cross sectioning. Ultrathin cross sections (60 nm) of the cells were obtained on a Riechert/Leica UltraCut E ultramicrotome, post-stained in 4% uranyl acetate for 10 minutes and then 1% lead citrate for seven minutes. Sections were viewed on a JEOL JEM-1400Flash transmission electron microscope at 80 kV. Images were taken using a bottom mount AMT digital camera. Acquired micrographs were analyzed manually in a blinded manner. Lysosomal area was quantified using Fiji.

3.2.8 Assessment of Lysosomal Hydrolase Activity

Lysosomal activity and function were assessed using measures of enzyme activity (Albrecht et al., 2020). Human PAECs were plated on glass coverslips and stained for all lysosomal measurements. For the LysoLive Assay (Marker Gene Technologies, Inc.; M27745), the β-glucosidase specific substrate GlucGreen was incubated at 5 µM in media for 30 minutes at 37ºC. Cells were washed three times with ice-cold PBS and subsequently fixed in 4% PFA for 15 minutes at room temperature. Slides were mounted with ProLong™ Gold Antifade Mountant with DAPI (ThermoFisher; P36935).

For the SiR-Lysosome Assay (Cytoskeleton, Inc.; CYSC012), a cell-permeable peptide conjugated to a silicon rhodamine (SiR) dye was incubated in human PAECs as a measure of active cathepsin D. SiR-Lysosome was incubated with cells at 1 µM and with the calcium channel blocker verapamil at 1 µM to improve signal intensity for 30 minutes at 37ºC. Cells were rinsed three times with ice-cold PBS, fixed in 4% PFA, and mounted as described above.

3.2.9 Assessment of Lysosomal Acidification

Lysosomal acidification was measured using the LysoSensor™ Yellow/Blue DND-160 (PDMPO) dye (ThermoFisher; L7545). The LysoSensor™ Yellow/Blue DND-160 (PDMPO) dye exhibits dual-excitation (*i.e.*, 329 and 384 nm) and dual-emission (*i.e.*, 440 and 540 nm) spectral peaks that are pH-dependent (pK_a 4.2). In acidic organelles, the dye has predominantly yellow fluorescence. In basic organelles, the dye has predominantly blue fluorescence. The unique spectral properties of this dye allow for ratiometric quantification.

Live human PAECs were incubated with 1 μM of dye in 0.1% FBS cell-specific media for 1 minute at 37°C. Cells were rinsed with PBS, trypsinized, pelleted in polystyrene tubes at 300 *g* for 5 minutes, and rinsed twice more with PBS. Cells were immediately analyzed on a BD LSRFortesssa™ Flow Cytometer (BD Biosciences) at the Unified Flow Core at the University of Pittsburgh. Median fluorescent intensity (MFI) ratio was calculated by using the yellow over the blue MFI fluorescent values.

3.2.10 Assessment of Lysosomal Lipid Content

Neutral lipids were stained with the fluorescent dye 4,4-difluoro-1,3,5,7,8-pentamethyl-4-bora-3a,4a-diaza-s-indacene (BODIPY®; ThermoFisher; D3922). Acidic organelles (*i.e.*, lysosomes) were stained with LysoTracker™ Red DND-99 (ThermoFisher; L7528). Live human PAECs were incubated in cell-type specific media containing 1 μM BODIPY® and 50 nM LysoTracker™ Red DND-99 for 30 minutes at 37°C. Cells were then washed with PBS three times before fixation with 4% PFA for 30 minutes at room temperature. Cells were rinsed with PBS three more times and then mounted with ProLong™ Gold Antifade Mountant with DAPI

(ThermoFisher; P36935). Images were acquired on a Nikon A1 Confocal Microscope at the Center for Biologic Imaging at the University of Pittsburgh.

Lysosomal lipid content was measured by the degree of colocalization between BODIPY® (*i.e.*, neutral lipids) and LysoTracker™ Red DND-99 (*i.e.*, acidic organelles). Colocalization was measured using EzColocalization in Fiji and quantified as Pearson's Correlation Coefficient (Stauffer et al., 2018).

3.3 Primary Data

3.3.1 The Creation of Molecular Tools to Study NCOA7

Data from the previous chapter support the notion that *NCOA7* is an immune-responsive element, most notably with the preferential upregulation of its short-length isoform. As these *in vitro* and *in vivo* models of PH indicated dynamic regulation of *NCOA7*, our next question was whether the manipulation of this molecule can alter the functional activity of endothelial cells to promote pulmonary vascular disease. To accomplish this, we confirmed that both *NCOA7* isoforms can be genetically manipulated through RNA interference or lentiviral delivery of expression vectors in human PAECs (Figure 12). The proceeding work will focus on the *in vitro* manipulation of NCOA7 and its effects on endothelial behavior using these tools.

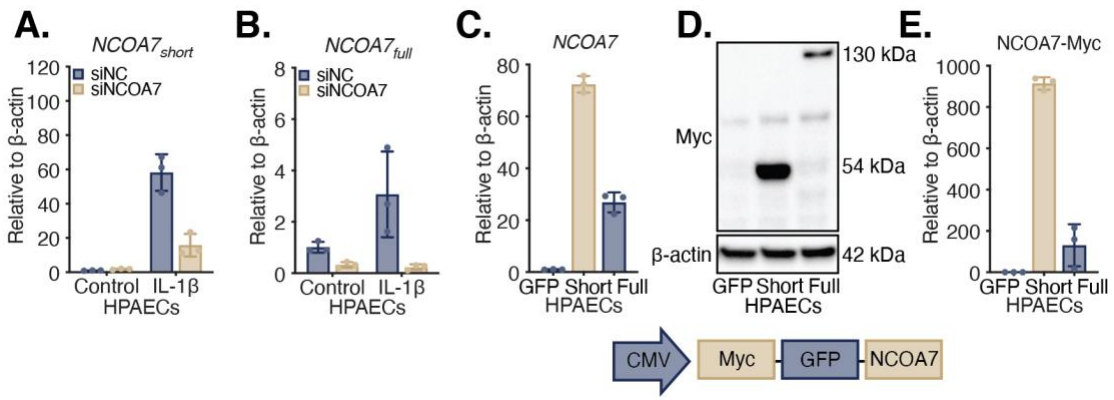

Figure 12. NCOA7 Manipulation *in vitro*

A & B. Expression of *NCOA7* isoforms via RT-qPCR in human PAECs subjected to RNAi against *NCOA7* under control or IL-1β conditions for 24 hours. **C.** Expression of *NCOA7* via RT-qPCR in human PAECs transduced with a lentivector containing the short- or full-length isoforms with GFP and Myc tags. **D.** Immunoblot against the Myc-tag of lentivector-generated NCOA7 in human PAECs with an internal control against β-actin. Short-length predicted molecular weight is 54 kDa and full-length predicted molecular weight is 130 kDa. **E.** Densitometry of human PAECs overexpressing NCOA7-Myc. N=3 per group. All data are presented as mean ± standard deviation.

3.3.2 NCOA7 Localizes at the Lysosome to Control Organelle Function

An unbiased, transcriptomic analysis of human PAECs deficient for NCOA7 revealed a global downregulation of genes related to lysosomal function. Notably, a number of these genes (*e.g.*, *ATP6V0A1*, *ATP6V1B2*, *ATP6V1C1*, *ATP6V1D*, *ATP6V1E1*, *ATP6V1G1*, and *ATP6V1H*) encode various subunits of V-ATPases—machinery necessary for lysosomal acidification and thus the function of pH-sensitive enzymes like cathepsins (Figure 13).

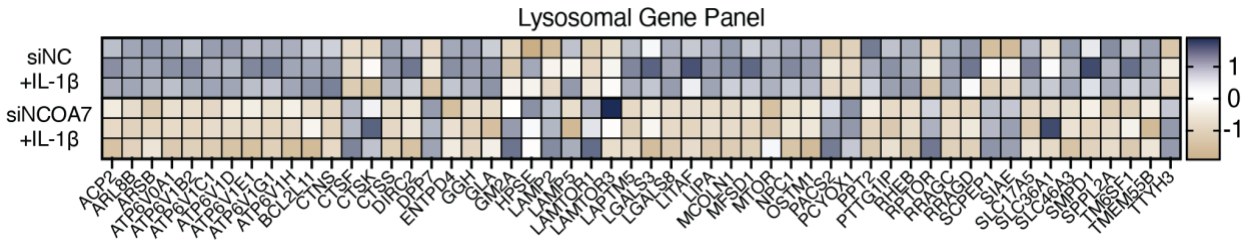

Figure 13. Loss of NCOA7 Downregulates Global Lysosomal Gene Expression

Unbiased, transcriptomic analysis of human PAECs deficient for NCOA7 reveal a global downregulation of genes related to lysosomal function. Genes presented have an FDR-corrected p-value less than 0.05.

Previous proteomics-based studies have mapped the V-ATPase interactome and they established that NCOA7 interacts with ATP6V1B1—a renal specific paralog of ATP6V1B2 (Huttlin et al., 2015; Merkulova et al., 2015). In human PAECs, the genetic knockdown of *NCOA7* abrogated the IL-1β-mediated upregulation of *ATP6V1B2*, and the forced overexpression of either the short- or full-length isoforms conversely upregulated *ATP6V1B2* (Figure 14). Taken together, these data suggest a functional, genetic regulatory element between *ATP6V1B2* and *NCOA7*.

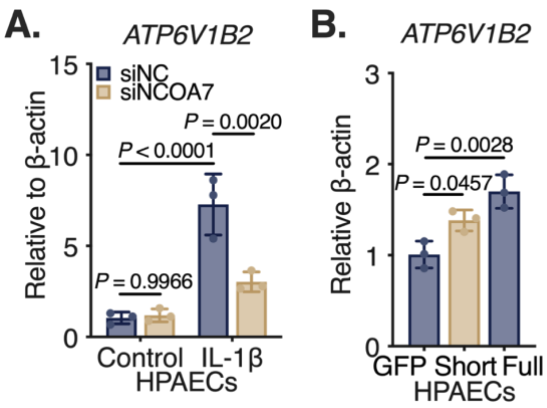

Figure 14. NCOA7 Modulates the Expression of ATP6V1B2

A. Expression of the V-ATPase subunit *ATP6V1B2* by RT-qPCR in human PAECs subjected to RNAi against *NCOA7* under control and IL-1β conditions for 24 hours. N=3; Two-way ANOVA. **B.** Expression of *ATP6V1B2* by RT-qPCR in human PAECs subjected to lentiviral delivery of $NCOA7_{short}$ (Short) or $NCOA7_{full}$ (Full) compared to control (GFP). N=3; One-way ANOVA. All data are presented as mean ± standard deviation.

Previously, homologs of NCOA7 identified in *Drosophila* were found to have protective effects in preventing bacterial pathogen entry via the endocytic pathway (Wang et al., 2012). And, most recently, NCOA7 was further confirmed to regulate endolysosomal physiology, as it relates to viral entry (Doyle et al., 2018). To confirm that NCOA7 operates at the lysosome in human PAECs, a proximity ligation assay was performed against ATP6V1B2 and NCOA7. In GFP-transduced human PAECs, there was a notable perinuclear staining of ATP6V1B2-NCOA7 interactions compared to the controls, which is consistent with a perinuclear distribution of lysosomes (Bright et al., 2016; Johnson et al., 2016). Moreover, the forced overexpression of $NCOA7_{short}$ or $NCOA7_{full}$ markedly upregulated the number of ATP6V1B2-NCOA7 interactions, demonstrating a natural localization of artificially expressed NCOA7 to the lysosome (Figure 15). These data confirmed a role for both short- and full-length NCOA7 as regulatory components of

the V-ATPase complex, potentially controlling acidification and downstream function of the lysosome.

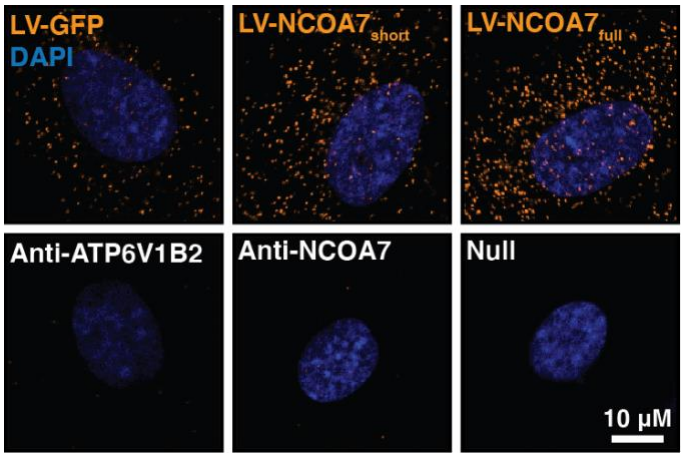

Figure 15. NCOA7 Physically Interacts with ATP6V1B2

Confocal images of a proximity ligation assay performed in human PAECs overexpessing NCOA7. Successful dimerization is indicated by orange signal and nuclei stain with DAPI in blue. In the top panels, antibodies were used against the V-ATPase subunit ATP6V1B2 and NCOA7. In the bottom panels, control images indicate sole or no antibody incubations, revealing amplification failure of the proximity ligation assay.

3.3.3 Loss of NCOA7 Results in Dysfunctional Lysosomes

To indirectly assess lysosomal acidification, two quantitative measures of lysosomal enzyme activity were utilized. First, the activity of β-glucosidase was assessed through the use of LysoLive—a specific substrate for β-glucosidase that becomes fluorescent upon cleavage (Harlan et al., 2016). With treatment of IL-1β, there was a significant increase of fluorescent signal, which was subsequently blocked with NCOA7 deficiency (Figure 16A & B). In addition, cathepsin D activity was assessed utilizing SiR-Lysosome—a cell-permeable peptide sequence of pepstatin A with a silicon rhodamine (SiR) dye that binds specifically to active cathepsin D (Lukinavičius et

al., 2016; Marciniszyn et al., 1976). In line with the IL-1β-mediated increase of *ATP6V1B2*, cathepsin D activity was significantly upregulated as noted by SiR-Lysosome fluorescence. With knockdown of NCOA7, the IL-1β-mediated increase in SiR-Lysosome fluorescence was abrogated, signifying a loss of cathepsin D activity (Figure 16C & D). In sum, the inhibition of lysosomal enzymatic activity with NCOA7 deficiency implies a failure of the V-ATPase complex to properly acidify the luminal space, which requires an acidic environment for the functioning of pH-sensitive enzymes.

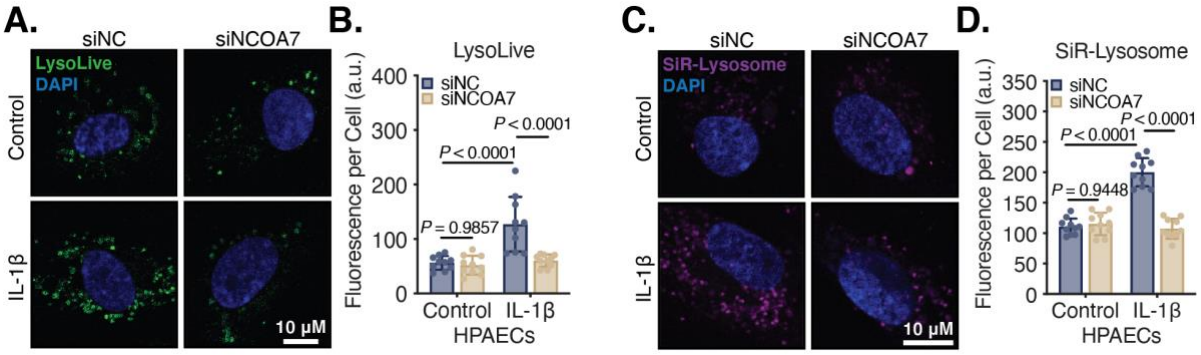

Figure 16. Loss of NCOA7 Inhibits Lysosomal Enzyme Activity

A. Confocal images of the LysoLive probe—a specific substrate for the lysosomal enzyme β-glucosidase that becomes fluorescent upon cleavage. The LysoLive probe was incubated in human PAECs deficient for NCOA7 under control and IL-1β conditions. Green signal indicates probe cleavage and blue signal indicates DAPI staining of nuclei. **B.** Fluorescence was quantified per cell using Fiji. N=10 cells per group were measured from N=3 images; Two-way ANOVA. **C.** Confocal images of a cell-permeable peptide of pepstatin A with silicone rhodamine (SiR) dye that binds to active cathepsin D. The SiR-Lysosome dye was incubated in human PAECs deficient for NCOA7 under control and IL-1β conditions. Purple signal indicates active cathepsin D and blue signal indicates DAPI staining of nuclei. **D.** Fluorescence was quantified per cell using Fiji. N=10 cells per group were measured from N=3 images; Two-way ANOVA. All data are presented as mean ± standard deviation.

To directly evaluate lysosomal acidification, a unique acidotropic probe with selective accumulation in acidic compartments (*i.e.*, lysosomes) was utilized. LysoSensor Yellow/Blue DND-160 specifically accumulates in lysosomes following its protonation. Moreover, this acidotropic probe serves as a ratiometric measure of lysosomal pH due to its conjugation to a compound with pH-dependent, dual-excitation and dual-emission spectral peaks (Albrecht et al., 2020; Diwu et al., 1999). Consistent with the IL-1β-mediated increase in lysosomal enzyme activity, there was a marked shift to yellow fluorescence in human PAECs, indicating enhanced acidification and decreased pH of the lysosomal compartment (Figure 17). Collectively, NCOA7 deficiency impaired lysosomal enzyme activity through attenuated luminal acidification. Such observations mimic the findings in lysosomal storage disorders, which characteristically are notable for the accumulation of undigested cellular components in the lysosomal compartment (Ballabio and Gieselmann, 2009; Platt et al., 2012).

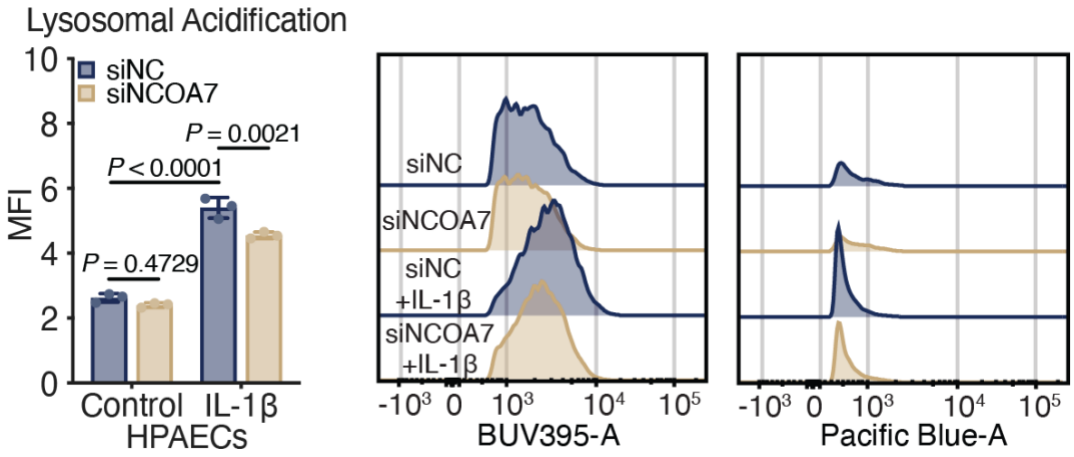

Figure 17. Loss of NCOA7 Inhibits Lysosomal Acidification

Median fluorescence intensity (MFI) ratio of LysoSensor™ Yellow/Blue DND-160 (PDMPO) dye via flow cytometry in human PAECs subjected to RNAi against *NCOA7* under control and IL-1β conditions. N=3; Two-way ANOVA. All data are presented as mean ± standard deviation.

Failure of V-ATPase complex formation or acidification is a well-accepted driver of lysosomal dysmorphology (Clague et al., 1994). Morphologic analysis of lysosomes using transmission electron microscopy of human PAECs deficient for NCOA7 revealed marked hypertrophy of lysosomes as quantified by lysosomal area (Figure 18), denoting an inability of the lysosomal compartment to breakdown and process cellular components. Moreover, the enlarged lysosomes in NCOA7-deficient cells carried lamellar-like inclusions (Figure 18; yellow arrows), suggestive of lipid buildup—again phenocopying many lysosomal storage disorders that present similarly with abnormal lysosomal lipid accumulation (de Araujo et al., 2020; Dierks et al., 2009; Leroy and Demars, 1967).

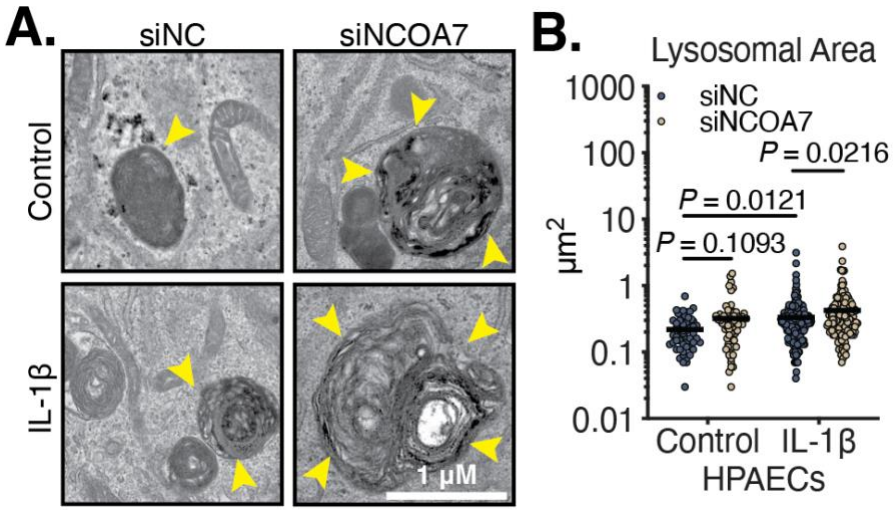

Figure 18. Loss of NCOA7 Results in Lysosomal Hypertrophy

A. Transmission electron micrographs of human PAECs deficient for NCOA7 under control and IL-1β conditions. Yellow arrows indicate lamellar-like inclusions within lysosomes, a morophology consistent with lipid accumulation. **B.** Lysosomal area was quantified using Fiji. N=20 images per group were quantified; Two-way ANOVA. All data are presented as mean ± standard deviation.

To address whether the lamellar-like structures observed in the electron micrographs were lipids, human PAECs were co-stained using a dye against neutral lipids (*i.e.*, BODIPY®) and a dye that specifically localizes to acidic compartments (*i.e.*, LysoTracker). With loss of NCOA7, there was an increase in lipid punctae throughout the cell, which specified vesicular accumulation. Correspondingly, the hyperintense lipid punctae were identified within acidic vesicles, supporting the idea that loss of NCOA7 caused in its lysosomal accumulation (Figure 19).

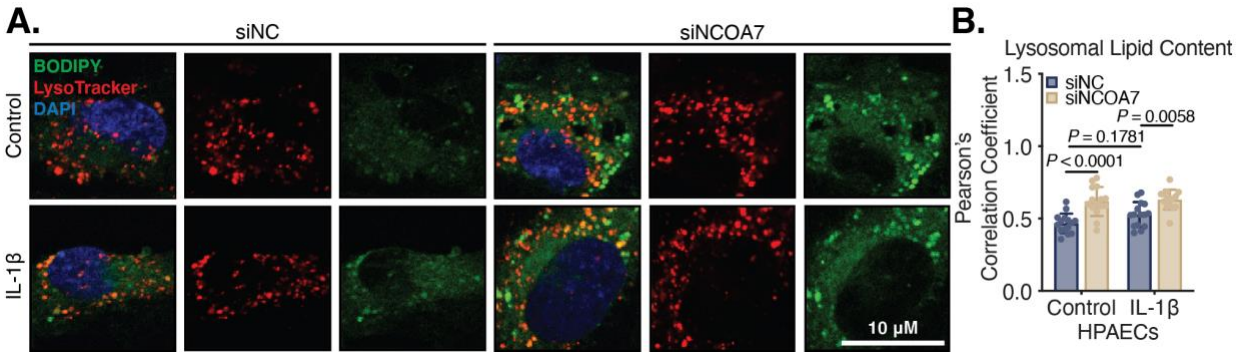

Figure 19. Loss of NCOA7 Results in Lysosomal Lipid Accumulation

A. Confocal images of human PAECs subjected to RNAi against NCOA7 under control or IL-1β conditions. Human PAECs were stained for neutral lipids with BODIPY® in green, acidic organelles with LysoTracker in red, and nuclei with DAPI in blue. **B.** Colocalization was measured using EzColocalization in Fiji and quantified as Pearson's Correlation Coefficient (Stauffer et al., 2018). N=15 cells per group were quantified from N=3 images; Two-way ANOVA. All data are presented as mean ± standard deviation.

3.4 Discussion

3.4.1 NCOA7 Regulates Lysosomal Behavior

A role for NCOA7 in endothelial biology has never been established. More specifically, we recognized that loss of NCOA7 resulted in a global shutdown of genes related to lysosomal function with a notable and prominent downregulation of various V-ATPase subunits, such as *ATP6V1B2*. Moreover, we confirmed that both NCOA7 isoforms act at the endolysosome through direct interaction with the V-ATPase subunit ATP6V1B2 via a proximity ligation assay. In addition, the perinuclear distribution of these punctae was consistent with reports of perinuclear lysosomes being highly acidic (*i.e.,* pH range of 4.5 to 5.5) and relatively immobile organelles (Bright et al., 2016; Johnson et al., 2016). The lack of ATP6V1B2-NCOA7 interactions in the surrounding area presents the question on when and how NCOA7 is recruited to an endosome destined for acidification. We confirmed that NCOA7 deficiency inhibited the activity of luminal hydrolases, presumably through elevated pH, via the immunofluorescent cleavage of enzyme-specific dyes for β-glucosidase and cathepsin D. Direct interrogation of vesicle acidification using a pH-sensitive dye confirmed the requirement of NCOA7 in lysosomal acidification—in line with previous published reports (Castroflorio et al., 2021; Doyle et al., 2018). In accordance with a failure of luminal acidification and thus hydrolase function, transmission electron micrographs confirmed lysosomal swelling with lamellar-like inclusions indicative of lipid content, which was subsequently confirmed with immunofluorescent staining noting lipid-like punctae colocalizing with acidic vesicles. The totality of these cell-based experiments are further strengthened by direct human evidence of lysosomal dysfunction in affected proband with loss-of-function variants in a homologue of *NCOA7* (Wang et al., 2019); despite this compelling evidence, no previous reports

have ever identified NCOA7 as a key regulatory molecule in the pathogenesis of pulmonary vascular disease.

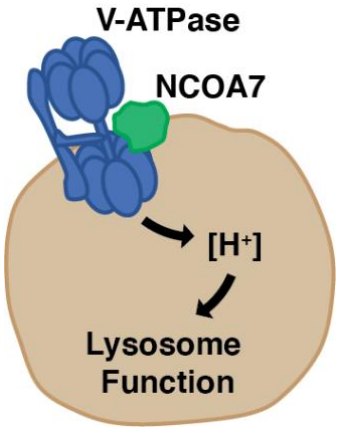

Figure 20. NCOA7 Interacts with V-ATPases to Acidify Lysosomes

Cartoon summary demonstrating that NCOA7 interacts with the ATP6V1B2 subunit of V-ATPases to modulate lysosomal acidification and thus its hydrolytic capacity to process cellular cargo.

3.4.2 Lysosomal Storage Disorders & Pulmonary Vascular Disease

First identified in the mid-20th century (De Duve and Wattiaux, 1966), lysosomes have attracted significant scientific interest for their capacity to regulate a multitude of diverse cellular functions (Luzio et al., 2007). Lysosomal degradative capacity is governed by the action of pH-dependent hydrolases within the vesicle lumen, which is maintained by V-ATPases that consume ATP to pump protons against a concentration gradient (Mindell, 2012). The failure of proper lysosomal acidification results in an elevated intraluminal pH, thereby inhibiting the activity of resident organelle hydrolases and consequently results in the accumulation of undigested cellular content. The inability of a lysosome to digest cellular content falls into a category of medical conditions known as lysosomal storage disorders, which often stem from inborn genetic errors

related to a single lysosomal hydrolase (Ballabio and Gieselmann, 2009; Platt et al., 2012). As such, a global shutdown of hydrolase activity within the lysosome secondary to a failure of the acidification complex would affect a multitude of hydrolases and fundamentally alter cellular behavior.

Although clinical observations and limited studies are suggestive of such, a definitive link between lysosomal dysfunction and PAH has never been firmly established. Previous reports reveal that rare mutations in various V-ATPase subunits cause manifestations of cardiopulmonary and vascular abnormalities with biallelic, loss-of-function variants. For instance, patients with a clinical diagnosis of cutis laxa—a connective tissue disorder—secondary to the mutations *ATP6V1A* or *ATP6V1E1* can present with arterial tortuosity, right ventricular hypertrophy in the absence of PH, and pulmonary arterial stenosis or hypoplasia (Van Damme et al., 2017). Moreover, other case reports have documented severe PAH in patients with mucolipidosis—a disease characterized by dysfunctional lysosomal enzyme processing and thus substrate accumulation (Alfadhel et al., 2013; Ishak et al., 2012; Recla et al., 2015). In a somewhat larger sampling, PH assessed by echocardiography was considerably high in a cohort of patients living with Gaucher's disease—a lysosomal enzyme defect in β-glucosidase (Figure 16A & B) that results in glucocerebroside accumulation (Elstein et al., 1998). This finding, in fact, has been recognized by the World Symposium on Pulmonary Hypertension and is reflected in the Group V classification of PH with unclear and/or multifactorial mechanisms (Simonneau et al., 2019). In addition, others lysosomal storage diseases, such as Niemann-Pick disease and Fabry disease, have severe pulmonary manifestations classified as interstitial lung disease (Borie et al., 2021), which often coexists with Group III PH (roughly 30 to 40%) due to lung diseases and/or hypoxia (Behr and Ryu, 2008). Although the aforementioned disease states are dependent upon the presence of rare,

homozygous alleles, they collectively display the importance of lysosomal function in the vasculature and the predisposition to pulmonary vascular disease. Notably, lysosomes have a principal role in modulating sterol metabolism as direct traffickers of cholesterol and sterols throughout the cell (Meng et al., 2020). For this reason, lysosomes have innate sterol sensing abilities that regulate cell growth regulatory pathways (Castellano et al., 2017).

Our future work hopes to examine the ability of common genetic variants (*i.e.*, the presence or absence of the G allele at SNP rs11154337 in iPSC-ECs) in altering lysosomal function, presumably through the modulation of NCOA7 expression. Thus, as an established regulatory factor of lysosomal function, NCOA7 may regulate cellular behavior through a reprogramming of cellular sterol homeostasis–a notion that we explore next.

4.0 Cholesterol Reprogramming in NCOA7 Deficiency

This work was adapted from a manuscript in submission:

Lloyd D. Harvey, Sanya Arshad, Mona Alotaibi, Anna Kirillova, Wei Sun, Neha Hafeez, Adam Handen, Yi-Yin Tai, Ying Tang, Chen-Shan C. Woodcock, Jingsi Zhao, Annie M. Watson, Yassmin Al Aaraj, Callen T. Wallace, Claudette M. St. Croix, Donna B. Stolz, Gang Li, Jeffrey McDonald, Haodi Wu, Thomas Bertero, Mohit Jain, and Stephen Y. Chan. NCOA7 Deficiency Coordinates Lysosomal Dysfunction and Sterol Metabolism to Promote Endothelial Dysfunction and Pulmonary Arterial Hypertension. *In submission*.

4.1 Introduction

The physiological importance of cholesterol in governing cellular behavior has been firmly established. Sterol metabolism is remarkably complex with its homeostasis coordinately regulated by an exquisite interplay of its uptake, *de novo* biosynthesis, storage, and export. Advancements over the last two decades have implicated lysosomes as the center of a regulatory network governing sterol homeostasis with many of these discoveries stemming from the observation and study of rare human disorders of lysosomal cholesterol handling (Meng et al., 2020). For example, lysosomes serve as critical organelles in the release of exogenous cholesterol from lipoprotein carriers (Heybrock et al., 2019; Winkler et al., 2019), cholesterol dispersal throughout the cell to organelles like the endoplasmic reticulum, the Golgi apparatus, mitochondria, and peroxisomes

(Chu et al., 2015; Hoglinger et al., 2019), and sterol sensing ability that governs the activity of expansive cellular signaling pathways like the mammalian target of rapamycin complex (mTORC) (Castellano et al., 2017; Thelen and Zoncu, 2017). When synthesizing this knowledge with our discovery that NCOA7 modulates lysosomal function, the question arises whether luminal hydrolase activity drives global reprogramming of sterol homeostasis within the cell.

Alterations of sterol metabolism in pulmonary vascular disease are poorly studied and remain largely undefined. Most work focusing on sterol metabolism in PAH has only just emerged in the last few years; however, these clinical observations focus exclusively on systemic markers of cholesterol metabolism, thereby failing to address the fundamental cellular dynamics of sterol handling in diseased tissue. Our understanding of systemic cholesterol metabolism markers is limited to a few generally reproducible observations. First, PAH patients demonstrate decreased low density lipoprotein-cholesterol (LDL-C) and total cholesterol levels in comparison to healthy controls and that disease severity and mortality associates with these parameters (Al-Naamani et al., 2016; Jonas et al., 2019; Kopec et al., 2017). Second, high density lipoprotein (HDL) is also decreased in PAH patients when compared to healthy controls and that it too associates with disease severity, clinical outcomes, and patient mortality (Harbaum et al., 2019; Heresi et al., 2010; Jonas et al., 2019; Larsen et al., 2016). Inhibition of *de novo* cholesterol synthesis through the administration of statins has demonstrated potential therapeutic benefit, noting its preservation of endothelial nitric oxide synthase activity in rats (Murata et al., 2005), reversal of proliferation and migratory capacity of smooth muscle cells derived from PAH patients (Ikeda et al., 2010), and the inhibition of fibroblast proliferation (Carlin et al., 2012; Zhu et al., 2018b). Attempts to translate these preclinical discoveries into patients suffering from PAH have yielded little clarity. For the most part, however, meta-analyses of clinical trials studying the efficacy of statins in PAH appear

to conclude that there is little benefit on clinical outcomes and disease progression (Wang et al., 2017).

Aberrant sterol metabolism within the endothelium has been directly linked to consequent cellular dysfunction (Goveia et al., 2014). For example, endothelial behaviors that can be contributory to pulmonary vascular disease like angiogenesis (Fang et al., 2013), immunoactivation (Whetzel et al., 2010), nitric oxide synthesis (Boger et al., 2000; Ivashchenko et al., 2010), and cell growth (Xu et al., 2010) have all been linked to dysregulation of cholesterol homeostasis, underlying the importance of sterol metabolism in regulating EC function. More recently and in the context of PAH, studies have shown that enhanced membrane fluidity (*i.e.*, decreased membrane cholesterol) modulates the vasodilatory effects of calcium-dependent, nitric oxide signaling in ECs (Zhang et al., 2017, 2018). Despite these advances in our understanding, a role for sterol metabolism and its subsequent dysregulation within the endothelium in pulmonary vascular disease remains undefined.

4.2 Materials & Methods

The following methods are in addition to those previously discussed in sections 2.2 and 3.2.

4.2.1 LC-MS for Cholesterol Intermediates and Oxysterols

Human PAECs were treated and collected for cholesterol intermediates and oxysterol analyses at 1 x 10^6 cells per glass 16 x 125 mm tube (Pyrex; 9826). Cells were subjected to a

liquid-liquid extraction of sterols using a modified form of the Bligh and Dyer method (Bligh and Dyer, 1959). Briefly, 1 mL of dichloromethane, methanol, and water were added to each sample. The sample was then vortexed and centrifuged to produce two liquid phases. The lower phase was carefully transferred to a new glass tube and dried under nitrogen. Samples were then resuspended in hexane and the resultant lipid species were analyzed by liquid chromatography-mass spectrometry (LC-MS) at the Center of Human Nutrition at the University of Texas Southwestern Medical Center by Jeffrey McDonald, Ph.D. (McDonald et al., 2012). Samples were run on the SCIEX QTRAP 6500+ equipped with a Shimadzu LC-30AD HPLC system and a 150 x 2.1-mm, 5 μm Supelco Ascentis silica column. The LC-MS data was analyzed using MultiQuant (SCIEX).

4.2.2 Staining for Neutral Lipids

Neutral lipids were stained in cells using the fluorescent dye 4,4-difluoro-1,3,5,7,8-pentamethyl-4-bora-3a,4a-diaza-s-indacene (BODIPY®) as previously described (Qiu and Simon, 2016). Live cells were grown on glass coverslips in plasticware. Cells were rinsed three times with PBS to remove residual media. A staining solution of 2 μM BODIPY® in PBS was applied to cells for 15 minutes at 37°C. Cells were rinsed three times with PBS before fixing with 4% paraformaldehyde for 15 minutes at room temperature. Coverslips were mounted with ProLong™ Gold Antifade Mountant with DAPI (ThermoFisher; P36935). Images were acquired on a Nikon A1 Confocal Microscope at the Center for Biologic Imaging at the University of Pittsburgh.

4.2.3 Measurement of Cholesterol Uptake

To assess cholesterol uptake, a Cholesterol Uptake Assay Kit was utilized per the manufacturer's specifications (abcam; ab236212). Briefly, treated human PAECs were incubated in 0.1% serum, cell-type specific media with supplemented fluorescent, NBD-cholesterol at 20 μg/mL for 24 hours. Cells were rinsed with PBS, trypsinized, pelleted in polystyrene tubes at 300 *g* for 5 minutes, and rinsed twice more with PBS. Cells were immediately analyzed on a BD LSRFortesssa™ Flow Cytometer (BD Biosciences) at the Unified Flow Core at the University of Pittsburgh. Flow cytometric analysis was chosen over confocal microscopy due to the high rate of photobleaching observed with NBD-cholesterol.

4.2.4 Assessment of Cholesterol Content

To assess cholesterol content, the Cholesterol/Cholesterol Ester-Glo™ Assay Kit was utilized (Promega; J3190). This assay measures cholesterol using a cholesterol dehydrogenase that links the presence of cholesterol to NADH production and thus proluciferin activation. Human PAECs were plated at a density of 20,000 cells per well in a 96-well plate in replicates of six. The assay was performed as the manufacturer specifies.

4.3 Primary Data

4.3.1 Loss of NCOA7 Reprograms Sterol Metabolism

The observation that NCOA7 deficiency results in lysosomal lipid accumulation suggests a dysregulation of sterol homeostasis within the cell, which is determined by a complex interplay of *de novo* biosynthesis, uptake, cellular localization, and export (Luo et al., 2020). In support of this, a transcriptomic analysis of human PAECs deficient for NCOA7 and subsequent gene-set enrichment analysis revealed a marked enrichment and downregulation of biosynthetic processes related to sterol metabolism (Figure 21A & B; red arrows).

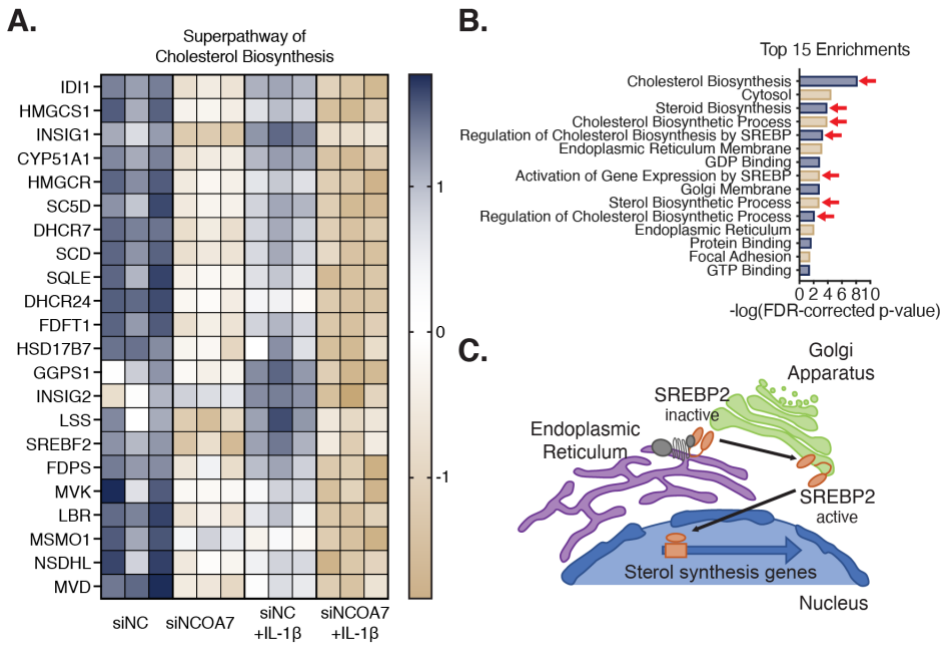

Figure 21. Loss of NCOA7 Reprograms Sterol Metabolism

A. Unbiased, transcriptomic analysis of human PAECs deficient for NCOA7 reveal a global downregulation of genes related to *de novo* cholesterol synthesis. Genes presented have an FDR-corrected p-value less than 0.05. **B.** Gene-set enrichment analysis revealed an enrichment for processes related to sterol metabolism (red arrows). **C.** Depiction of SREBP2 in its inactive form at the endoplasmic reticulum, where—in response to low sterol concentration—it is transported to the Golgi apparatus and subsequently cleaved into its active form. Active SREBP2 will translocate to the nucleus and bind to sterol responsive elements to upregulate genes related to cholesterol synthesis and homeostasis.

The observation that cholesterol synthesis is globally downregulated suggests that a master transcription factor governing sterol metabolism—such as the sterol regulatory element-binding protein 2 (SREBP2)—is either being inhibited through a failure of processing and translocation or through a negative feedback signal denoting a sterol satiated cellular state. Normally, SREBP2 remains in an inactive form within the endoplasmic reticulum, where it is finely attuned to sterol concentrations. If sterol levels reach a certain, activating threshold, SREBP2 is transported to the Golgi apparatus and subsequently cleaved into an active form capable of translocating to the

nucleus and binding to sterol responsive elements that govern *de novo* cholesterol synthesis (Figure 21C).

Moreover, we sought to exclude a defect in the *de novo* cholesterol synthetic pathway, as dysfunction can result in sterol intermediate accumulation and severe disease states (Porter and Herman, 2011). Case reports on rare, inborn errors of sterol metabolism have observed instances of pulmonary vascular disease. For example, individuals with defects in 7-dehydrocholesterol reductase (*DHCR7*)—the terminal reaction of *de novo* cholesterol synthesis—show instances of pulmonary vascular disease. Reports have noted persistent pulmonary hypertension of the newborn in the absence of any structural abnormalities (Katheria et al., 2010) and high rates of pulmonary vein stenosis in patients with a *DHCR7* mutation (Prosnitz et al., 2017)—both of which fall under the Group I PH classification. To address whether loss of NCOA7 may modulate the flux of sterol intermediates in the *de novo* synthesis of cholesterol, we performed LC-MS examining post-squalene intermediates in NCOA7-deficient human PAECs and found no appreciable differences in sterol intermediates (Figure 22). As such, the lack of any striking alteration in the biosynthetic pathway of cholesterol indicates that the observed downregulation of sterol metabolism is occurring secondary to an issue with cholesterol handling.

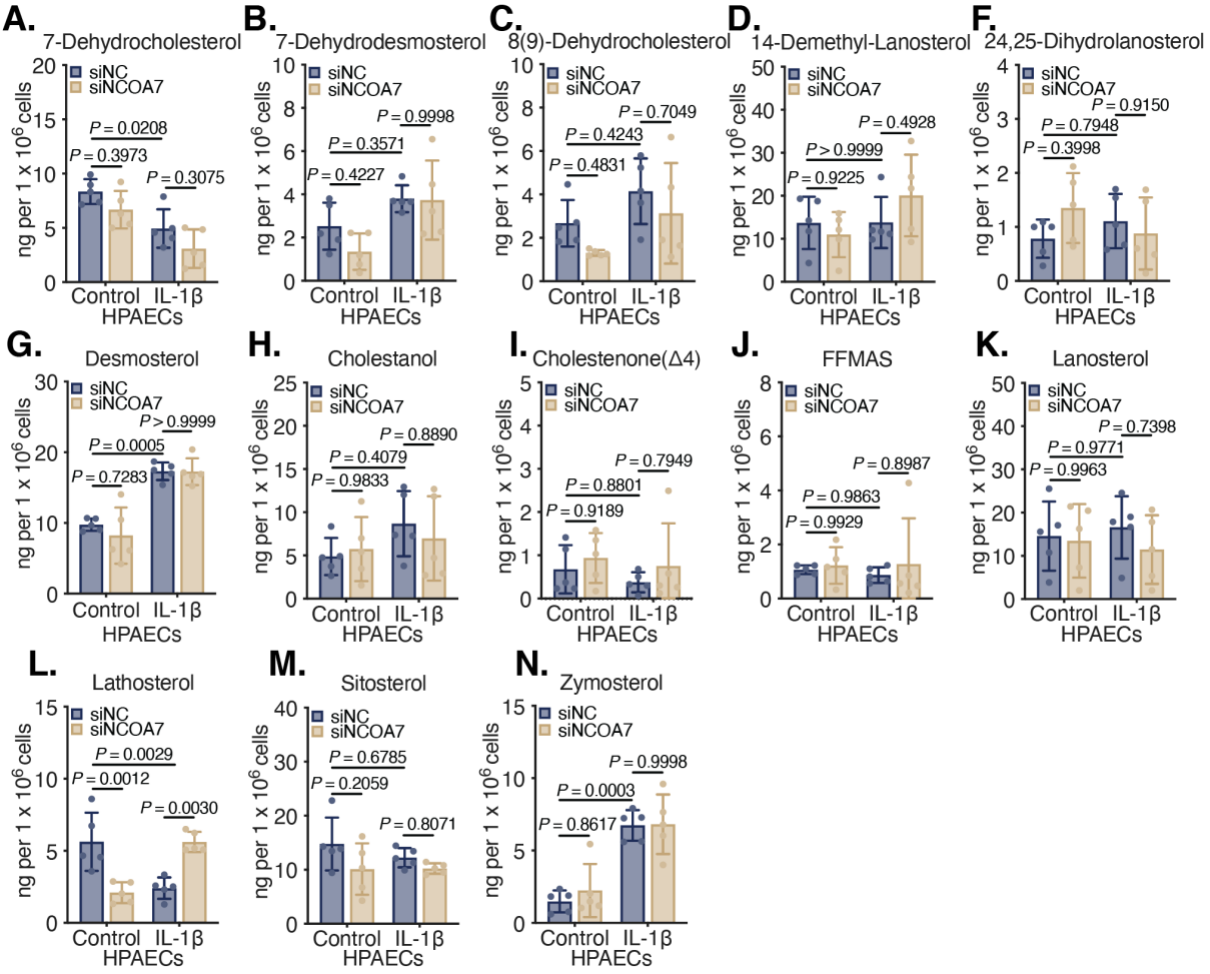

Figure 22. Loss of NCOA7 Does Not Alter Sterol Flux

A – N. The direct measurement of post-squalene intermediates by liquid chromatography-mass spectrometry in human PAECs subjected to RNAi against *NCOA7* under control and IL-1β conditions. N=5; Two-way ANOVA. All data are presented as mean ± standard deviation.

4.3.2 Loss of NCOA7 Results in Sterol Accumulation

As cholesterol homeostasis is dependent upon its uptake, *de novo* synthesis, storage, and export, our inability to identify any alterations in post-squalene intermediates to explain the transcriptomic findings implies that the loss of NCOA7 results in dysregulation of cholesterol handling throughout the cell. Accordingly, we set out to visualize cholesterol and its localization

within the cell using the BODIPY® stain against neutral lipids. We observed a marked upregulation of lipid content in NCOA7-deficient human PAECs with a punctated, perinuclear patterning—a finding that is consistent with mature (*i.e.*, acidic) lysosomes responsible for the breakdown of cellular content (Figure 23).

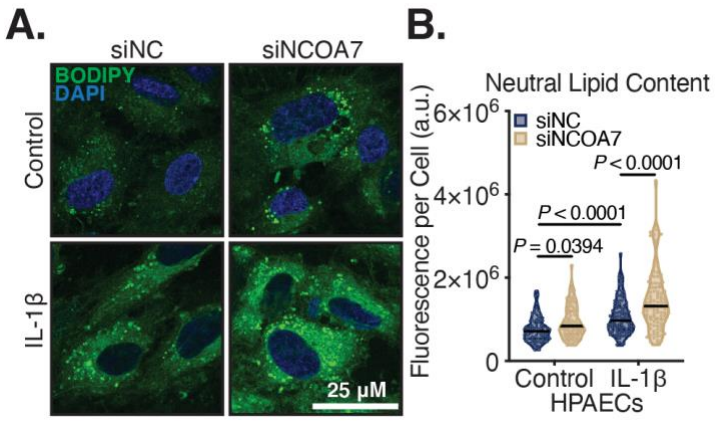

Figure 23. Loss of NCOA7 Results in Sterol Accumulation

A. Fluorescent staining against neutral lipids with BODIPY® in human PAECs subjected to RNAi against *NCOA7* under control and IL-1β conditions. Green signal indicates neutral lipid content. **B.** Quantification of total fluorescence per cell using Fiji. N=15-20 cells from N=5 images per condition; Two-way ANOVA. All data are presented as mean ± standard deviation.

In a sterol saturated cell, it is assumed that uptake pathways of extracellular cholesterol would be inhibited, namely through the actions of the low-density lipoprotein receptor (LDLR) (Figure 24A). Consistent with a sterol saturated state, expression of the *LDLR* was attenuated with loss of NCOA7, which similarly showed a reduction in the uptake of fluorescently labeled cholesterol in human PAECs (Figure 24B).

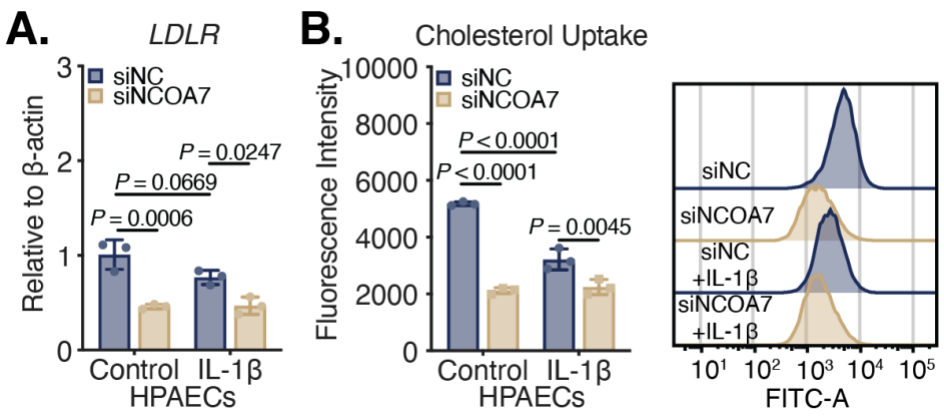

Figure 24. Loss of NCOA7 Inhibits Cholesterol Uptake

A. Expression of the lipid uptake receptor *LDLR* by RT-qPCR in human PAECs subjected to RNAi against *NCOA7* under control and IL-1β conditions. N=3; Two-way ANOVA. **B.** Uptake of fluorescently-tagged, NBD-cholesterol via flow cytometry in human PAECs subjected to RNAi against *NCOA7* under control and IL-1β conditions. N=3; Two-way ANOVA. All data are presented as mean ± standard deviation.

The direct interrogation of total cholesterol content in NCOA7-deficient human PAECs revealed substantial upregulation; conversely, forced overexpression of NCOA7 reduced total cholesterol content, which established the reciprocal nature of NCOA7 activity in regulating sterol homeostasis within the cell (Figure 25). These data indicate that the loss of NCOA7 resulted in a global reprogramming of sterol metabolism secondary to the aberrant accumulation of cholesterol.

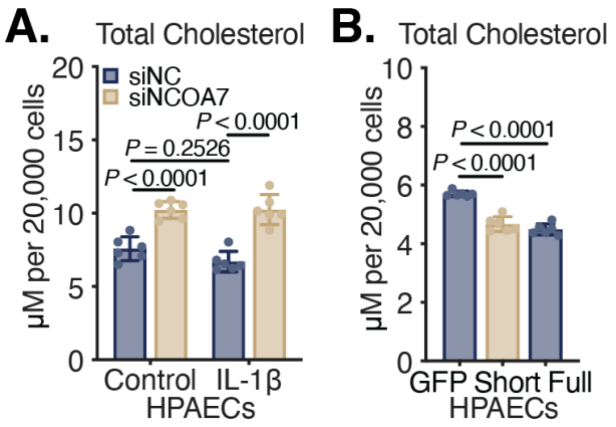

Figure 25. Loss of NCOA7 Results in Cholesterol Loading

A. Total cholesterol content via the production of NADH by cholesterol dehydrogenase and thus proluciferin activity in human PAECs subjected to RNAi against *NCOA7* under control and IL-1β conditions for 24 hours. 20,000 cells were plated per well. N=6; Two-way ANOVA. **B.** Total cholesterol content in human PAECs subjected to lentiviral delivery of $NCOA7_{short}$ (Short) or $NCOA7_{full}$ (Full) compared to control (GFP). N=6; One-way ANOVA. All data are presented as mean ± standard deviation.

4.3.3 Loss of NCOA7 Upregulates Oxysterol & Bile Acid Production

To combat cholesterol accumulation, the cell can engage in either its direct transport through transporters or by increasing its solubility through a series of oxidative steps. Appropriately, deficiency of NCOA7 was found to significantly upregulate both *CH25H* and *CYP27A1*—oxysterol generating enzymes that act on cholesterol to increase its solubility (Figure 26).

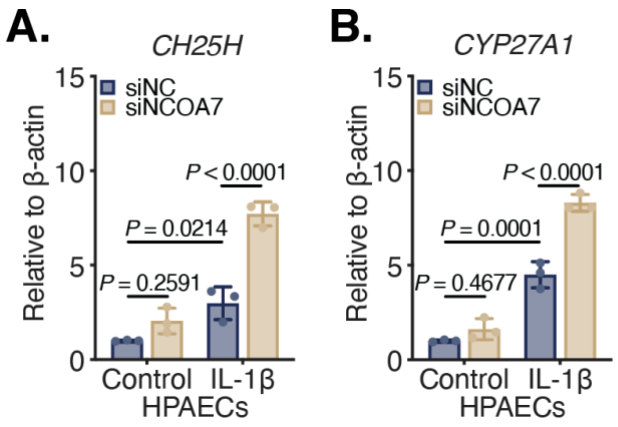

Figure 26. Loss of NCOA7 Upregulates Oxysterol Generating Enzymes

A & B. Expression of the oxysterol generating enzymes *CH25H* and *CYP27A1* by RT-qPCR in human PAECs subjected to RNAi against *NCOA7* under control and IL-1β conditions for 24 hours. N=3; Two-way ANOVA. All data are presented as mean ± standard deviation.

Looking at various proinflammatory rodent models of PH, we similarly found a marked upregulation of CH25H in pulmonary vessels (Figure 27). These data indicate a presumable augmented production of oxysterols and downstream bile acid derivatives.

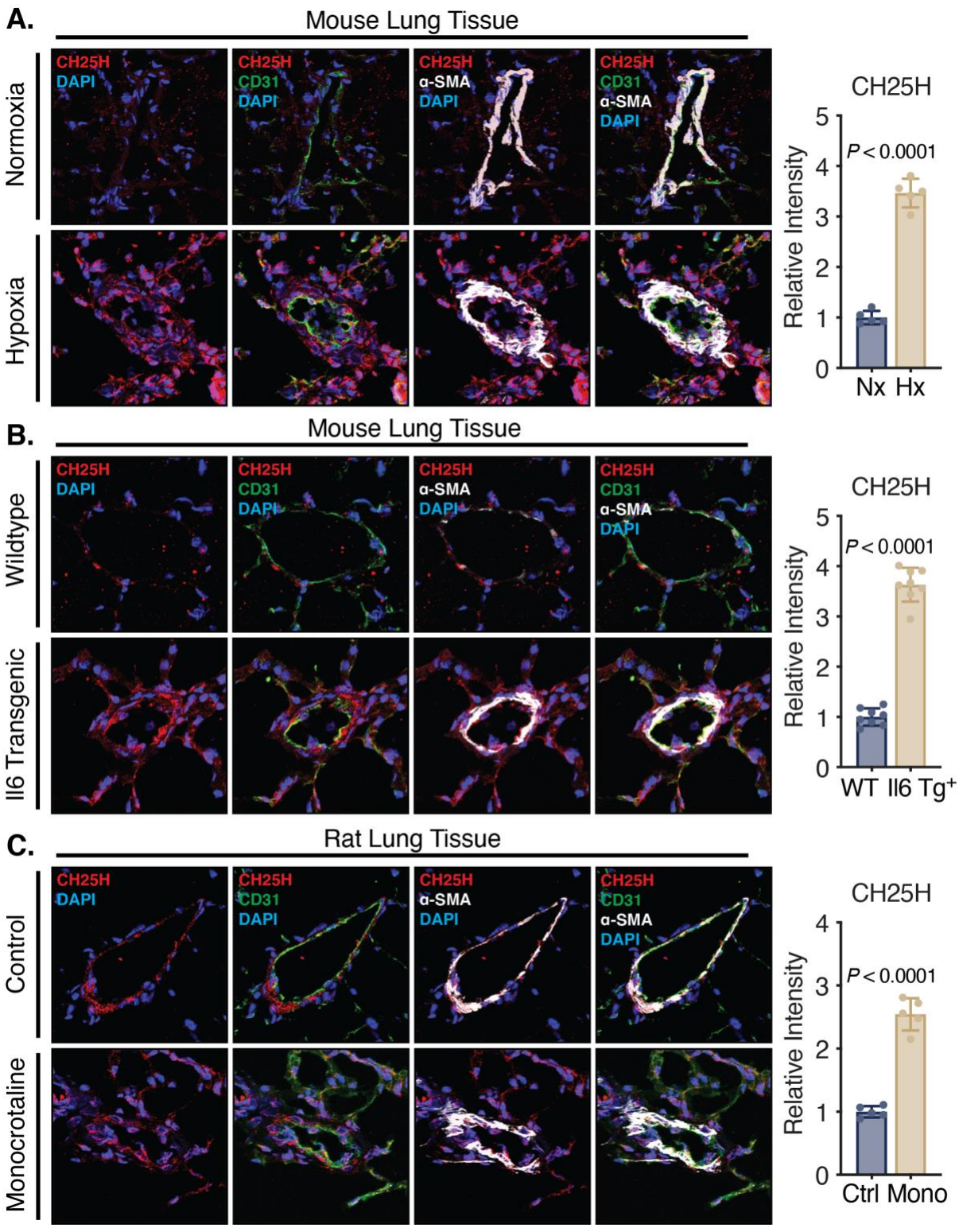

Figure 27. CH25H is Upregulated in Lungs of Rodent Models of PH

A. Pulmonary vessels from normoxic or hypoxia mice stained for CH25H (red), CD31 (endothelial cells; green), α-SMA (smooth muscle cells; white), and DAPI (blue). Quantification of relative intensity. N=5 per group; Student's *t*-

test. **B.** Pulmonary vessels from wildtype or *Il6* transgenic mice stained for CH25H (red), CD31 (green), α-SMA (white), and DAPI (blue). Quantification of relative intensity. N=8 per group; Student's *t*-test. **C.** Pulmonary vessels from control or monocrotaline-injected rats stained for CH25H (red), CD31 (green), α-SMA (white), and DAPI (blue). Quantification of relative intensity. N=5 per group; Student's *t*-test. All data are presented as mean ± standard deviation.

In addition, staining of pulmonary vessels in healthy control and patients with PAH confirmed the upregulation of CH25H in human tissue (Figure 28).

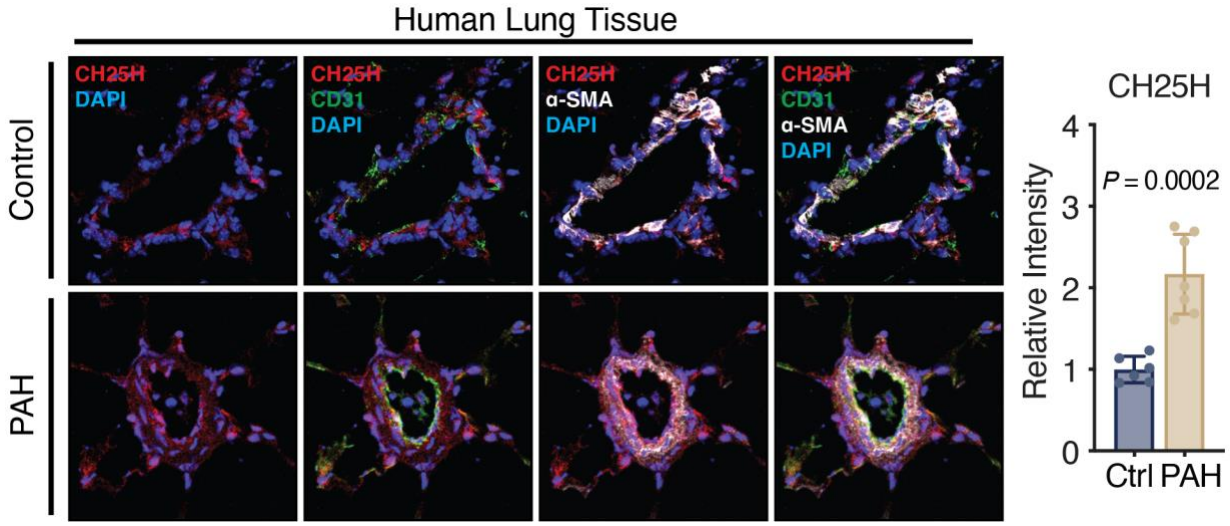

Figure 28. CH25H is Upregulated in Lungs of PAH Patients

Pulmonary vessels from healthy control or patients with PAH stained for CH25H (red), CD31 (endothelial cells; green), α-SMA (smooth muscle cells; white), and DAPI (blue). Quantification of relative intensity. N=6-7 patients per group with the average intensity of 4-7 vessels per patient plotted; Student's *t*-test. All data are presented as mean ± standard deviation.

To corroborate whether the observed upregulation of *CH25H* and *CYP27A1* enhanced oxysterol production, we performed targeted lipidomics using LC-MS by a different, independent laboratory (Figure 29A, E, & G). We found that the loss of NCOA7 in human PAECs under

conditions of IL-1β significantly upregulated the production of 25HC and 27HC, the two respective products of CH25H and CYP27A1. Interestingly, we also observed increased production of the autooxidation generated oxysterol 7α-hydroxycholesterol. The generation of such 7α-hydroxylated oxysterols can then be further metabolized into a variety of bile acid derivatives.

Using LC-MS in NCOA7-deficient human PAECs, we found that several downstream bile acid derivatives were upregulated in sequential pathways, such as 5-cholesten-3β-7α,25-triol, 5β-cholestane-3α,7α,12α-triol, and 5β-cholestane-3α,7α,12α,25,26-pentol (Figure 29B, C, & D). Similarly, another sequential pathway was identified: 3β,7α-dihydroxy-5-cholestenoate to 7α-hydroxy-3-oxo-4-cholestenoic acid (Figure 29H & I). Most importantly, we believe that the two metabolites identified by Alotaibi et al. correspond to 5β-cholestane-3α,7α,12α,25,26-pentol (665110; Figure 29D) and 7α-hydroxy-3-oxo-4-cholestenoic acid (667200; Figure 29I). Custom syntheses of these compounds are underway for direct validation.

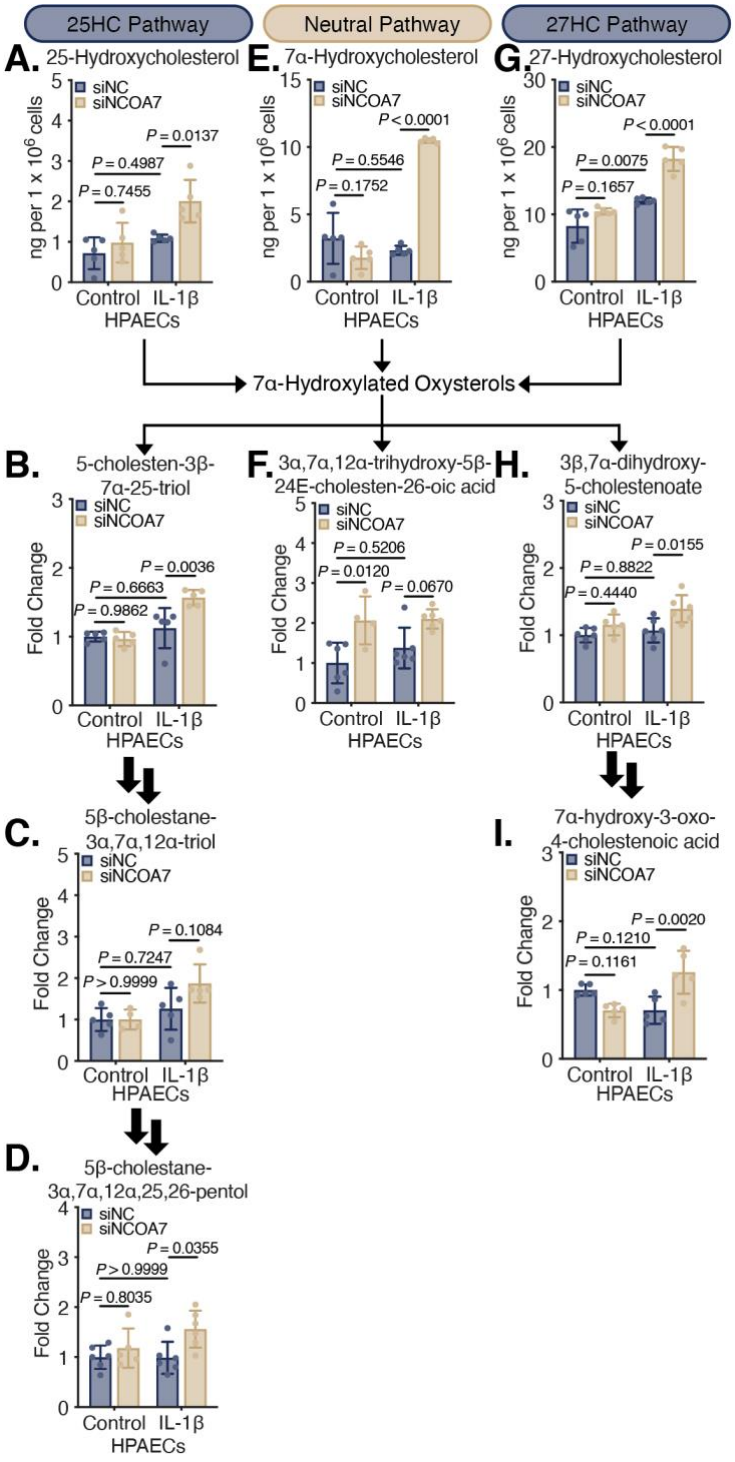

Figure 29. Loss of NCOA7 Upregulates Oxysterol & Bile Acid Synthesis

A, E, & G. Oxysterol content using LC-MS in human PAECs subjected to RNAi against *NCOA7* under control and IL-1β conditions for 24 hours. N=5; Two-way ANOVA. **B, C, D, F, H, I.** Bile acid relative fold change using LC-MS

in human PAECs subjected to RNAi against *NCOA7* under control and IL-1β conditions for 24 hours. N=4-6; Two-way ANOVA. All data are presented as mean ± standard deviation.

Ultimately, the upregulation of oxysterol generating enzymes suggests that there is increased production of oxidized cholesterol metabolites, which are well-documented as potent signaling and immunomodulatory molecules. As such, the production of oxysterols and downstream bile acid derivatives may therefore result in endothelial dysfunction and thus the pathogenesis of pulmonary vascular disease.

4.4 Discussion

4.4.1 NCOA7 as a Global Regulator of Sterol Metabolism

For the first time, a pivotal role has been established for NCOA7 deficiency as mediator of sterol reprogramming in the production bile acid synthesis. Our original observation stemmed from an unbiased, transcriptomic analysis on human PAECs deficient for NCOA7, where we observed a marked enrichment and downregulation of genes related to the biosynthetic enzymes of cholesterol. We had posited that the loss of NCOA7 caused such global inhibition either through a fundamental failure of SREBP2 processing and thus activation of *de novo* synthesis or through a failure in the handling of sterol species resulting in their accumulation and a consequent feedback onto inhibitory checkpoints. We found that loss of NCOA7 had no appreciable effect on post-squalene intermediates in the biosynthetic pathway of cholesterol, which, if they had accumulated, would have potentially explained a global inhibition of cholesterol synthesis.

Instead, we found that the loss of NCOA7 resulted in the marked accumulation of neutral lipid species, demonstrating a perinuclear and punctated patterning indicative of lysosomal accumulation. Further in line with this notion, we observed that NCOA7 deficiency downregulated the expression of *LDLR* and thus the physical uptake of fluorescently labeled cholesterol from the surrounding extracellular environment. These observations are interesting when coupled with the ability of NCOA7 to modulate V-ATPase activity and thus lysosomal acidification. The proper luminal acidification of endocytic vesicles is necessary for the release of internalized ligands from their receptors (Forgac, 2007), such as the release of a cholesterol carrying lipoprotein from LDLR. Normally, after the ligand is released within the intraluminal vesicle, the receptor can be recycled and returned to the plasma membrane. Failure of ligand-receptor separation and recycling would presumably result in lysosomal hypertrophy and the formation of lamellar-like inclusions, an observation we confirmed using transmission electron microscopy in NCOA7-deficient human PAECs.

In addition to the downregulation of biosynthetic enzymes and extracellular sterol uptake, we found via direct interrogation of cholesterol content in NCOA7-deficient human PAECs that there is a marked accumulation of cholesterol. Because of the observed accumulation of one of the most insoluble macromolecules in living systems, we posited that there would be a compensatory process to excrete excess cholesterol. As a cholesterol responsive enzymes, the high levels of *CH25H* and *CYP27A1* observed in the lung—namely ECs and macrophages—suggest a functional role in the maintenance of sterol homeostasis (Bjorkhem et al., 1994). In fact, the inhibition of CYP27A1 leads to cholesterol accumulation, which insinuates a critical task in cholesterol oxidation and excretion (Lund et al., 1996). The oxidation of cholesterol to produce 25HC and 27HC confers greater polarity and thus greater ease in crossing the plasma membrane, signifying

this pathway as an important mechanism of excess cholesterol removal from the cell (Lange et al., 1995; Meaney et al., 2002). Accordingly, the further oxidation of oxysterols into bile acids augments the excretory capacity of the cell. More specifically, we sought to determine if accumulated sterols were undergoing oxidation to increase solubility. Typically, the first oxidation step of cholesterol generates oxysterols, such as 25HC and 27HC. These molecules, however, can become further soluble through subsequent oxidative reactions, thereby becoming highly soluble bile acids.

In line with this theory, we found that NCOA7 deficiency significantly upregulated both *CH25H* and *CYP27A1* and their downstream oxysterol products 25HC and 27HC using targeted lipidomics. Both rodent models of PH and human PAH patients similarly had upregulated CH25H in pulmonary vessels—direct evidence of a key enzymatic step required for oxysterol and bile acid synthesis. Furthermore, we utilized an unbiased, metabolomics screen on human PAECs deficient for NCOA7 and found the upregulation of the downstream bile acid metabolites. Strikingly, we found that two of these downstream metabolites appear to match the chemical structures of the two identified metabolites by Alotaibi et al.: 5β-cholestane-3α,7α,12α,25,26-pentol (665110; Figure 29D) and 7α-hydroxy-3-oxo-4-cholestenoic acid (667200; Figure 29I). Moreover, and consistent with the associations, we found that loss of NCOA7 significantly upregulated both metabolites—in line with the notion that the presence of the G allele (*i.e.*, higher NCOA7 expression) negatively associated with these metabolites. Future work will determine if iPSC-ECs carrying the allelic variants will carry this observation of decreased bile acids with the presence of the G allele when compared to the homozygous C allele line.

The series of molecular aberrations that occur prior to the onset of endothelial dysfunction are diverse and remain poorly undefined. Over the last few years, however, a growing body of

evidence has grown suggesting a fundamental role for sterols, particularly oxidized sterols, in the pathogenesis of pulmonary vascular disease, noting their elevation in patient serum and lung tissue (Al-Husseini et al., 2015; Ross et al., 2015; Sharma et al., 2016). For example, an analysis on the methylation signatures of PAH patients revealed hypermethylation at the promoter site of ATP-binding cassette transporter A 1 (ABCA1)—a critically important transporter in the removal of lipids from the cell. Pulmonary arterial ECs isolated from these patients with idiopathic PAH demonstrated decreased mRNA and protein of ABCA1, supporting the finding of its promoter hypermethylation (Hautefort et al., 2017). Most recently, it was documented that patients with PH have increased oxidized LDL deposits in their lungs and pulmonary arteries, which correlated with decreased expression of LDLR in their lungs, as well. Moreover, they observed increased monocyte infiltration near lipid deposits, suggesting the proinflammatory nature of oxidized lipid species (Umar et al., 2020). Taken together, this observation suggests that a lipid-loading phenomenon within cells of the pulmonary vasculature may induce immune infiltration and thus disease.

Overall, these findings support a paucity of literature that previously demonstrated elevated bile acids in the serum and lungs of PAH patients (Zhao et al., 2014b) (Bujak et al., 2016). When coupled with our understanding of bile acids as having immunomodulatory actions, such as their ability to activate the endothelium via upregulation of cellular adhesion molecules for immune cell recruitment (Qin et al., 2006), there is considerable interest in how they may alter endothelial behavior.

4.4.2 Inborn Errors of Sterol Metabolism & Pulmonary Vascular Disease

Although our work excluded any effect of NCOA7 deficiency on direct sterol intermediate flux, there exists considerable medical literature documenting observations of inborn errors of sterol metabolism and pulmonary vascular disease. For example, patients with genetic defects in 7-dehydrocholesterol reductase (*DHCR7*; also known as Smith-Lemli-Opitz Syndrome [SLOS])—the terminal enzyme in the *de novo* synthesis of cholesterol—show instances of PAH. In a retrospective study of 170 patients with pulmonary veno-occlusive disease (PVOD)—a subtype of Group 1 PH—five patients were found to have pathogenic *DHCR7* mutations (Prosnitz et al., 2017). Similarly, persistent pulmonary hypertension of the newborn (also a subtype of Group I PH) has been documented in a patient with SLOS (Katheria et al., 2010). To further underscore a potential relevance for lysosomal function and defects in sterol metabolism in pulmonary vascular disease, a case report noted severe PAH in a young child with cholesteryl ester storage disease (CESD). Her disease was secondary to a mutation in the gene encoding lysosome acid lipase (*LIPA*)—a lysosomal enzyme responsible for the liberation of cholesteryl esters and triglycerides (Cagle et al., 1986). Despite the rarity of these disorders, the observations of pulmonary vascular disease with loss-of-function variants in sterol synthesis and handling suggests a fundamental role in vessel homeostasis and health.

The total failure of cholesterol synthesis can result in PAH, but what about individuals with monoallelic, so-called "recessive" mutations that hinder the efficiency of DHCR7? It is estimated that the most common pathogenic variant of *DHCR7* occurs at a rate of 1 in 100 for the Caucasian population in North America and is as high as 1 in 30 for Central European populations (Nowaczyk et al., 2006). Is the proverbial genetic gun now loaded and waiting for a second stimulus to pull the trigger of disease? Is that second, or even third, trigger the presence of other monoallelic

variants within the same molecular pathway? These questions give rise to an important scientific concept: complex genetic inheritance in the form of multiple, monoallelic mutations accumulating in several genes in a pathway that synergistically leads to a disruption of flux through a pathway, thereby mimicking a monogenic disorder caused by homozygous defects in a single gene in that same pathway—or more simply called synergistic heterozygosity (Vockley et al., 2000).

Beyond the scope of this body of work, we are currently in the process of studying *DHCR7* and its role in endothelial behaviors. We are utilizing powerful *in vitro* models, such as SLOS patient-derived iPSCs carrying pathogenic *DHCR7* with corresponding CRISPR-Cas9-corrected lines from the same patient. These iPSCs lines will be differentiated into iPSC-ECs for the modelling of disease in culture. We are also performing transcriptomic analysis on *DHCR7* deficient human PAECs to better understand the global reprogramming with loss of such a critical molecule. Lastly, we are nearing the completion of obtaining a unique mouse model. We are creating a *Dhcr7* floxed mouse with endothelial-specific knockout driven by *Cdh5*(PAC)-ERT2+-Cre on an *Il6* transgenic background (Payne et al., 2018). We hope that this work will establish the first mechanistic explanation to observations of PAH in patients suffering from SLOS.

5.0 NCOA7 Deficiency Promotes Pulmonary Arterial Hypertension

This work was adapted from a manuscript in submission:

Lloyd D. Harvey, Sanya Arshad, Mona Alotaibi, Anna Kirillova, Wei Sun, Neha Hafeez, Adam Handen, Yi-Yin Tai, Ying Tang, Chen-Shan C. Woodcock, Jingsi Zhao, Annie M. Watson, Yassmin Al Aaraj, Callen T. Wallace, Claudette M. St. Croix, Donna B. Stolz, Gang Li, Jeffrey McDonald, Haodi Wu, Thomas Bertero, Mohit Jain, and Stephen Y. Chan. NCOA7 Deficiency Coordinates Lysosomal Dysfunction and Sterol Metabolism to Promote Endothelial Dysfunction and Pulmonary Arterial Hypertension. *In submission*.

5.1 Introduction

There is a growing consensus within the field of pulmonary vascular disease that the incitement of endothelial dysfunction is central to a series of subsequent molecular events in the pathogenesis of PAH. Namely, this theory posits that the initial stimulus—whether it be acquired, environment, or genetic—results in an acute, molecular cascade triggering endothelial apoptosis and senescence that ultimately selects for an apoptosis-resistant, hyperproliferative, and immunoactivated clonal EC population (Culley et al., 2021; Lee et al., 1998; Masri et al., 2007). There have been very limited studies on the relationship between sterol metabolism and endothelial dysfunction in the context of pulmonary vascular disease; however, such work has shown that cholesterol content within the plasma membrane and thus membrane fluidity modulates the

production of the vasodilatory signaling molecule nitric oxide (Zhang et al., 2017, 2018). Beyond a pulmonary vascular perspective, sterol metabolism has been linked to canonical endothelial behaviors like angiogenesis (Fang et al., 2013), immunoactivation (Whetzel et al., 2010), nitric oxide synthesis (Boger et al., 2000; Ivashchenko et al., 2010), and cell growth regulatory pathways (Xu et al., 2010).

Although a series of clinical observations have reliably demonstrated the upregulation of bile acids in the lung and serum of PAH patients, there has been a paucity of work mechanistically defining how these molecules may alter cellular behavior to promote disease. Both oxysterols and bile acids have been documented to have immunomodulatory effects. For example, the application of bile acids activates the endothelium through the upregulation of cellular adhesion molecules, thereby allowing for immune cell attachment and recruitment into the vascular bed (Qin et al., 2006). In addition, oxysterols have shown to increase endothelial stiffness via atomic force microscopy (Shentu et al., 2012)—an important observation when considering vessel compliance and thus potential alterations in pulmonary pressures. Moreover, rich literature exists firmly establishing a role of oxysterols in the activation of immune cells and as chemoattractants (Choi and Finlay, 2020), which, in the context of pulmonary vascular disease, may explain both the systemic elevation of cytokines in serum and immune infiltration observed in the plexiform lesion of PAH patients.

Our previous work demonstrating that NCOA7 deficiency induces the upregulation of oxysterols and bile acids in human PAECs therefore indicates there is resultant endothelial dysfunction, such as immunoactivation. Accordingly, we aimed to assess whether the loss of NCOA7 could produce alterations in behavior of the endothelium.

5.2 Materials & Methods

The following methods are in addition to those previously discussed in sections 2.2, 3.2, and 4.2.

5.2.1 Apoptosis Measured via Caspase-3/7 Activity

Apoptosis was assessed using the Caspase -Glo® 3/7 Assay System (Promega; G8090). This assay functions by providing a luminogenic, caspase-3/7 substrate optimized for caspase activity. Cleavage of this substrate generates a luminescence-based signal through luciferase. Equal volumes of this substrate were added to wells containing human PAECs (5,000 per well) and left to incubate at room temperature for 30 minutes. Luminescence was measured via spectrophotometry. Luminescent signal was normalized to protein content per well, assessed using the Pierce™ BCA Protein Assay Kit (ThermoFisher; 23227).

5.2.2 Proliferation Measured via BrdU Incorporation

Proliferation was assessed using the BrdU Cell Proliferation Assay Kit (Cell Signaling Technology; 6813). This assay functions by measuring 5-bromo-2'-deoxyuridine (BrdU) into proliferating cells using an anti-BrdU antibody. BrdU was added to complete growth media containing 5% serum for two hours. Human PAECs (5,000 per well) were fixed and denatured before application of the mouse anti-BrdU antibody. Next, anti-mouse HRP-linked antibody was added. A development substrate was then added to detect with HRP-linked, antibody complexes to BrdU. Absorbance was measured at 450 nm using spectrophotometry.

5.2.3 Leukocyte and Monocyte Adhesion Assays

Immune activation of the endothelium was assessed by measuring the adhesion of immune cells to an endothelial monolayer. Human PAECs were cultured until a complete monolayer was formed. Immune cells were stained with either CellTrace™ Blue or CFSE (ThermoFisher; Blue, C34568; CFSE, C34554) per the manufacturer's protocol. Between 2.0 to 2.5 x 10^5 stained immune cells were added to each well of a six-well plate and allowed to incubate for 24 hours. Wells were then rinsed two times with PBS and subsequently fixed with 4% PFA for 15 minutes at room temperature. After fixation, the cells were rinsed once more with PBS. Fluorescent images were acquired at 4x magnification for each well. Immune cell number per image was quantified using Fiji. For the leukocyte adhesion assay, HuT 78 cutaneous T lymphocytes were used (ATCC). For the monocyte adhesion assay, THP-1 peripheral blood monocytes were used (ATCC).

5.2.4 Application of Oxysterols & Bile Acids

Oxysterols and bile acids were applied to human PAECs in 0.1% FBS, cell-specific media containing 1% (2-Hydroxypropyl)-β-cyclodextrin (Sigma-Aldrich; H5784). 25-hydroxycholesterol was dissolved in 100% ethanol (solubility 20 mg/mL) and applied to cells at a concentration of 25 μM for 24 hours (Millipore Sigma; H1015).

5.2.5 Animal Studies

All animal studies were approved by the Division of Laboratory Animal Resources at the University of Pittsburgh.

5.2.6 Genetic Models

The *Ncoa7* knockout mouse line (C57BL/6 Ncoa7tm1.1(KOMP)Vlcg) was obtained from the Knockout Mouse Project (KOMP; https://komp.org/) and generated using sperm for rederivation at the Genome Editing, Transgenic, & Virus Core at Magee Women's Research Institute. Obtained mice were bred in-house to generate homozygous, *Ncoa7* knockout mice. To elicit a model of pulmonary inflammation resulting in severe PH, *Ncoa7* knockout mice were crossbred with C56BL/6 Il6 transgenic (Tg^+) mice. The *Il6* Tg^+ mice contain a Clara cell 10-kD promoter (CC10) that drives constitutive expression of IL-6 within the lung (Steiner et al., 2009). Mice were taken to 15 weeks of age under normal oxygen tension before echocardiography, invasive hemodynamics measurement, and tissue harvesting.

5.2.7 Hemodynamic Measurements

Echocardiography was performed on 15-week-old mice using a 15- 45MHz transthoracic transducer and a VisualSonics Vevo770 system (Fujifilm). Anesthesia was administered with 2% isoflurane in 100% O_2 during animal positioning and hair removal, and subsequently decreased to 0.8% isoflurane during image acquisition. Data were analyzed in a blinded manner by a technician.

For right heart catheterization, mice were given ketamine/xylazine (9:1; Henry Schein) or subjected to isoflurane (Henry Schein). The isoflurane vaporizer was maintained at 1.5 to 2% with an oxygen gas flow rate of 1 L/min. Right ventricular systolic pressure was measured with Millar catheters (SPR-513 and SPR-671). Catheters were inserted into the jugular vein and then guided through the right atrium and into the right ventricle. Steady right ventricular systolic pressure

waveforms were measured for two minutes. Analysis of waveforms were performed in a blinded manner.

5.2.8 Bile Acid Analysis of Plasma

Plasma samples were thawed at 4C overnight; 20 µL of plasma was transferred into a 96-well extraction plate. Proteins were precipitated with the addition of 80 µL of ice-cold extraction solvent (consisting of ethanol for reversed phase method), as described (Kantz et al., 2019; Lagerborg et al., 2019; Watrous et al., 2019). Plates were sealed, vortexed and centrifuged to precipitate proteins with the supernatant containing extract metabolites pipetted into a clean microtiter plate for LC-MS analysis. For the reversed phase methods, samples were passed across a reverse phase SPE column (Phenomenex 8B-S199-UB), and lipid species eluted using 1ml methanol, as described (Kantz et al., 2019; Watrous et al., 2019), before being transferred into a clean microtiter plate for LC-MS analysis.

Bioactive metabolites analysis was performed on plasma samples using state of the art LC-MS, using a Vanquish UPLC coupled to high resolution, QExactive orbitrap mass spectrometer (Thermo) using a Phenomenex Kinetex C18 column. All generated spectral data underwent daily Qc/Qa analysis, as described in the section below. Data was extracted using image processing and machine learning based spectral optimization. Each sample MS data file was initially represented as an image using mass to charge and retention time coordinates. A watershed algorithm was applied to image files using peak apex density as a guide to define regions containing putative spectral peaks. An optimized neural network was subsequently applied to all putative spectra peaks to isolate true spectral peaks from ‘false’ background signals. Following data extraction, spectral peaks were cross aligned among datasets using landmark-based algorithms to allow for

comparison of signals among cohorts. Data was subsequently normalized to account for plate-to-plate variation using a simple batch median normalization metric with correction for median absolute deviation. Following normalization, metabolite peaks were further compressed for multiple adducts and in source fragments. Normalized, aligned, filtered datasets were subsequently used for statistical analyses, as described below. Metabolites were annotated by using an in-house library of commercially available standards or MS/MS fragmentation patterns.

Qc/Qa of data has been standardized using a panel of deuterated internal standards as well as interval pooled plasma samples to monitor fluctuations in extraction efficiency, instrument sensitivity, matrix artifact and mass accuracy. Any samples not meeting Qc/Qa thresholds underwent reinjection. The assay was highly reproducible over several days and independent measures with median coefficient of variance (CV) across analytes at low standard amount of 0.15 ng.

5.3 Primary Data

5.3.1 NCOA7 Deficiency Promotes Endothelial Dysfunction

In line with the theory of an apoptosis-resistant and hyperproliferative endothelium in pulmonary vascular disease, we observed that NCOA7 deficiency in human PAECs abrogated IL-1β-mediated apoptosis while simultaneously enhancing proliferative capacity (Figure 30A & C). In addition, there was a striking upregulation of the vascular cellular adhesion molecule 1 (*VCAM1*) with NCOA7 deficiency—a critical molecule in the transmigration of immune cells out of circulation and into the vascular bed (Figure 30E). The marked upregulation of *VCAM1*—a

surrogate of endothelium immunoactivation—further corresponded to the significant attachment of both leukocytes and monocytes to an endothelial monolayer deficient for NCOA7 (Figure 30G & I). Taken together, these data demonstrate that loss of NCOA7 in human PAECs resulted in the creation of an apoptosis-resistant, hyperproliferative, and immunoactivated endothelium—consistent with the prevailing theory of EC dysfunction in PAH (Figure 30K).

Reciprocally, we observed that the forced overexpression of NCOA7 reversed these phenotypes. Apoptosis was worsened with the overexpression of NCOA7 with the induction more noticeable under proinflammatory conditions (Figure 30B). Similarly, proliferation was attenuated with the inhibition more pronounced with IL-1β (Figure 30D). Lastly, the induction of VCAM1 with IL-1β was reversed with NCOA7 overexpression that corresponded to a decreased ability of both leukocytes and monocytes to adhere to the endothelium (Figure 30F, H, & J). The total summation of these findings demonstrates that the overexpression of NCOA7 in human PAECs induced apoptosis, inhibited proliferation, and prevented endothelium immunoactivation.

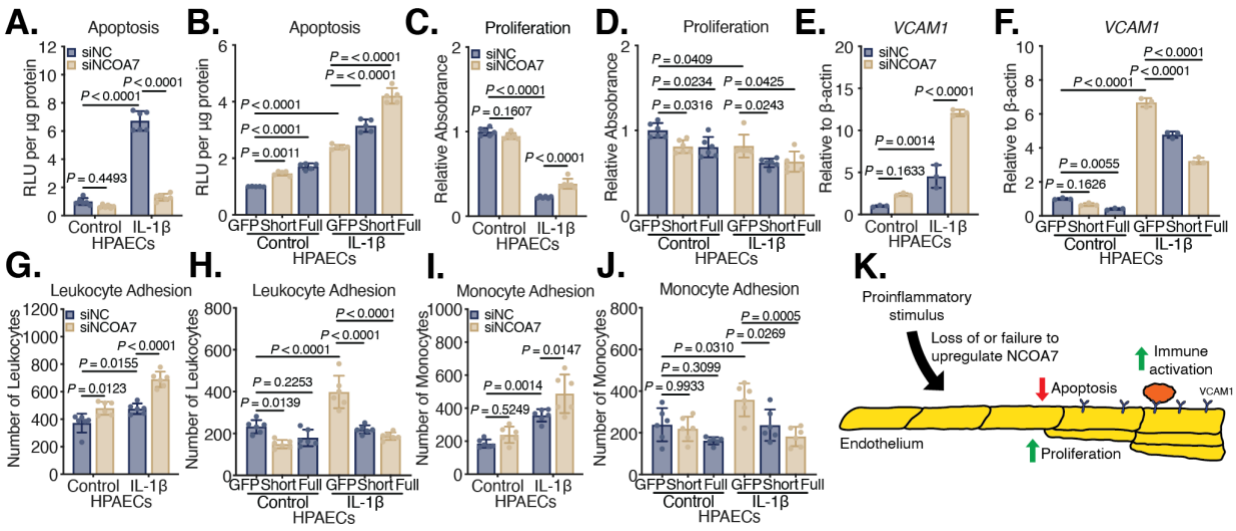

Figure 30. Loss of NCOA7 Promotes Endothelial Dysfunction

A & B. Apoptosis assessed via caspase-3/7 activity in human PAECs subjected to RNAi against *NCOA7* or lentiviral delivery of $NCOA7_{short}$ (Short) or $NCOA7_{full}$ (Full) under control and IL-1β conditions. N=6; Two-way ANOVA. **C & D.** Proliferation asssessed via BrdU incorporation in human PAECs subjected to RNAi against *NCOA7* or lentiviral delivery of $NCOA7_{short}$ or $NCOA7_{full}$ under control and IL-1β conditions. N=6; Two-way ANOVA. **E & F.** Expression of *VCAM1* by RT-qPCR in human PAECs subjected to RNAi against *NCOA7* or lentiviral delivery of $NCOA7_{short}$ or $NCOA7_{full}$ under control and IL-1β conditions. N=3; Two-way ANOVA. **G & H.** Leukocyte adhesion measured through direct binding to a human PAEC monolayer subjected to RNAi against *NCOA7* or lentiviral delivery of $NCOA7_{short}$ (Short) or $NCOA7_{full}$ (Full) under control and IL-1β conditions. N=6; Two-way ANOVA. **I & J.** Monocyte adhesion measured through direct binding to a human PAEC monolayer subjected to RNAi against *NCOA7* or lentiviral delivery of $NCOA7_{short}$ (Short) or $NCOA7_{full}$ (Full) under control and IL-1β conditions. N=6; Two-way ANOVA. **K.** Cartoon summary demonstrating how a loss of or failure to upregulate NCOA7 results in an apoptosis-resistant, hyperproliferative, and immunoactivated endothelium. All data are presented as mean ± standard deviation.

To determine if observed phenotypes in human PAECs were dependent upon the generation of downstream, oxidized forms of cholesterol, concomitant knockdown experiments against the oxysterol generating enzyme *CH25H*, which is upregulated with NCOA7 deficiency, were performed. Notably, inhibition of CH25H upregulation reversed the attenuation of apoptosis,

while enhancing the proliferative capacity of the cells (Figure 31A &B). The loss of CH25H prevented the upregulation of *VCAM1*, thereby reversing the immune cell adhesion of both leukocytes and monocytes observed in NCOA7-deficient human PAECs (Figure 31C – E). In sum, these data reveal the necessity of the oxysterol and thus bile acid generating enzymes in mediating observed EC dysfunction with NCOA7 deficiency.

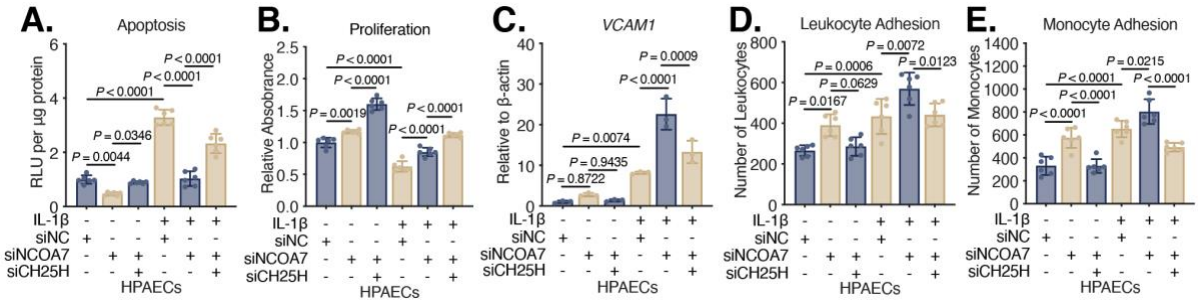

Figure 31. Inhibition of CH25H Reverses Endothelial Immune Activation

A. Apoptosis assessed via caspase-3/7 activity in human PAECs subjected to RNAi against *NCOA7* and *CH25H* under control and IL-1β conditions. N=6; Two-way ANOVA. **B.** Proliferation asssessed via BrdU incorporation in human PAECs subjected to RNAi against *NCOA7* and *CH25H* under control and IL-1β conditions. N=6; Two-way ANOVA. **C.** Expression of *VCAM1* by RT-qPCR in human PAECs subjected to RNAi against *NCOA7* and *CH25H* under control and IL-1β conditions. N=3; Two-way ANOVA. **D.** Leukocyte adhesion measured through direct binding to a human PAEC monolayer subjected to RNAi against *NCOA7* and *CH25H* under control and IL-1β conditions. N=6; Two-way ANOVA. **E.** Monocyte adhesion measured through direct binding to a human PAEC monolayer subjected to RNAi against *NCOA7* and *CH25H* under control and IL-1β conditions. N=6; Two-way ANOVA. All data are presented as mean ± standard deviation.

To determine if 25HC, as an upstream derivative of bile acids and the product of CH25H, directly activates the endothelium, this oxysterol was directly applied to human PAECs in culture. In support of their proinflammatory nature, we observed that 25HC significantly upregulated *VCAM1* (Figure 32A). The upregulation of this inflammatory cellular adhesion molecule was

further corroborated by a marked and striking increase of both leukocytes and monocytes to a monolayer of human PAECs (Figure 32B & C).

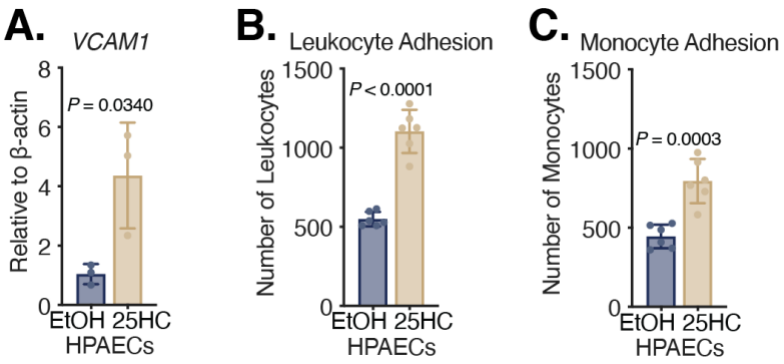

Figure 32. Application of 25-Hydroxycholesterol Immunoactivates The Endothelium

A. Expression of *VCAM1* by RT-qPCR in human PAECs subjected to ethanol or 25HC (25 μM) for 24 hours.N=3; Student's *t*-test. **B.** Leukocyte adhesion measured through direct binding to a human PAEC monolayer subjected to ethanol or 25HC (25 μM) for 24 hours. N=6; Student's *t*-test. **E.** Monocyte adhesion measured through direct binding to a human PAEC monolayer subjected to ethanol or 25HC (25 μM) for 24 hours. N=6; Student's *t*-test. All data are presented as mean ± standard deviation.

To determine if the differential, SNP-dependent expression of *NCOA7* in isogenic iPSC-ECs carried over to immunoactivation parameters, we sought to examine *VCAM1* expression and immune cell adhesion to an endothelial monolayer. To reiterate, we found that the presence of the G allele at SNP rs11154337 allowed for higher *NCOA7* expression when compared to the isogenic, homozygous C/C parent line. Moreover, we found that the loss of NCOA7 significantly enhanced *VCAM1* expression and, conversely, NCOA7 overexpression attenuated *VCAM1* expression—an index of immunoactivation that carried over to direct immune cell adhesion. In accordance with our previous observations, we discovered decreased *VCAM1* expression and immune cell adhesion in iPSC-ECs with the G allele when compared to the isogenic homozygous C/C line (Figure 33).

Strangely, the baseline adhesion of immune cells to the iPSC-EC lines under control conditions was quite high in comparison to human PAECs. For this reason, the application of IL-1β did not induce as robust of an increase in immune cell adhesion to previous observations in human PAECs. We believe this heightened state may be in part a function of the iPSC model and the stressful conditions required to induce endothelial differentiation.

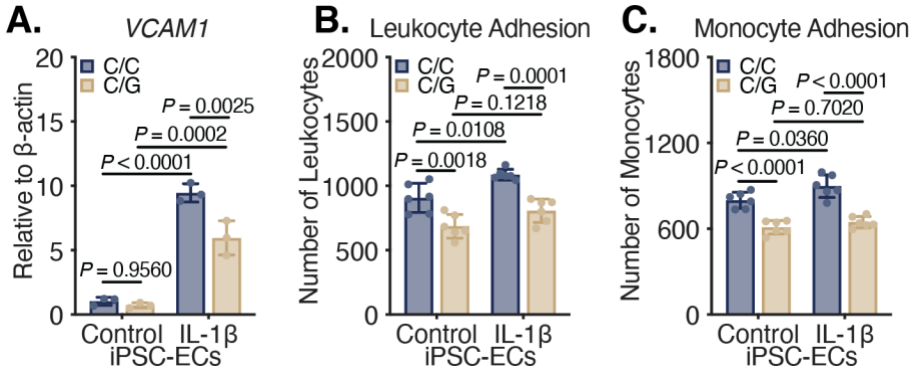

Figure 33. SNP Rs11154337 Modulates Immunoactivation of The Endothelium

A. Expression of *VCAM1* by RT-qPCR in isogenic, SNP-edited, iPSC-ECs subjected to control or IL-1β for 24 hours. N=3; Student's *t*-test. **B.** Leukocyte adhesion measured through direct binding to an isogenic, SNP-edited, iPSC-EC monolayer subjected to control or IL-1β for 24 hours. N=6; Student's *t*-test. **C.** Monocyte adhesion measured through direct binding to an isogenic, SNP-edited, iPSC-EC monolayer subjected to control or IL-1β for 24 hours. N=6; Student's *t*-test. All data are presented as mean ± standard deviation.

Our previous work has solidified a role for NCOA7 in the modulation of lysosomal behavior and thus sterol homeostasis within the endothelium in a way that governs its immunoactivation. To corroborate these finding *in vivo*, we utilized an *Il6* transgenic (Tg^+) mouse to elicit severe pulmonary inflammation as a model of angioproliferative PAH (Steiner et al., 2009). A whole-body knockout mouse for *Ncoa7* was crossed onto *Il6* Tg^+ mice to determine if loss of NCOA7 would worsen indices of PH *in vivo*. Assessment of Fulton's Index—a

measurement of right ventricular hypertrophy that indirectly reflects increased pulmonary vascular resistance—revealed a significant enlargement in *Ncoa7* knockout mice (0.3485 ± 0.02837) compared to controls (0.3028 ± 0.03670) (Figure 34A). Direct hemodynamic interrogation via right heart catheterization determined a baseline right ventricular systolic pressure (RVSP)—a surrogate for the clinical measurement of mean pulmonary arterial pressure—in *Il6* Tg^{+} control mice of 27.99 ± 2.913 mmHg. With the global loss *Ncoa7*, the RVSP was significantly worsened to a value of 34.19 ± 6.247 mmHg (Figure 34B). To ensure that these hemodynamic alterations were not secondary to potential off-target effects of a global knockout (*i.e.*, left ventricular hypertrophy), echocardiographic imaging was performed prior to invasive right heart catheterization. Echocardiographic assessment revealed no gross alterations in left ventricular function, as noted by left ventricular fractional shortening (LVFS), left ventricular ejection fraction (LVEF), and left ventricular posterior wall distance during diastole (LVPW;d) (Figure 34C – F).

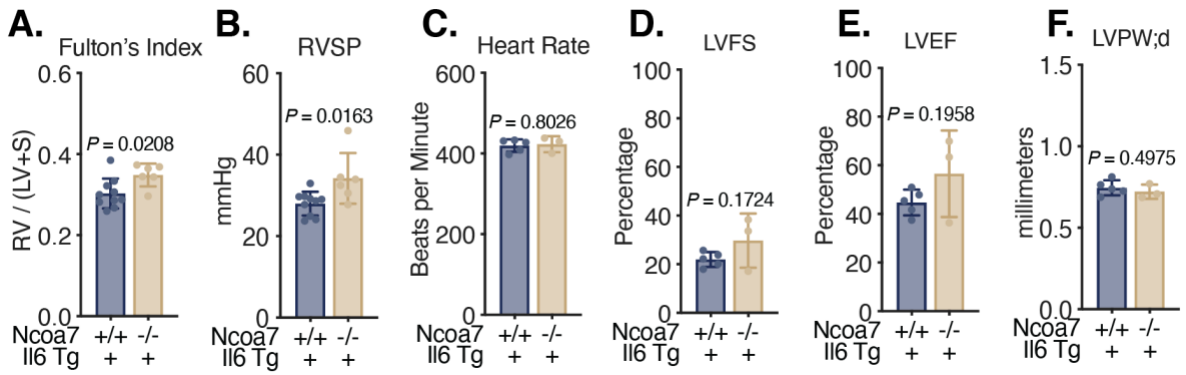

Figure 34. Loss of Ncoa7 Worsens Pulmonary Hypertension in Il6 Transgenic Mice

A. The mass of the right ventricle divided by the mass of the left ventricle and septum ($\frac{RV}{LV+S}$) was calculated to produce Fulton's Index—a measure of right ventricular hypertrophy. **B.** Right ventricular systolic pressure measured through right heart catheterization. **C**. Heart rate measured through echocardiography. **D.** Left ventricular fraction shortening (LVFS). **E.** Left venitricular ejection fraction **F.** Left ventricular posterior wall thickness during diastole (LVPW;d). N=3-10; Student's *t*-test. All data are presented as mean ± standard deviation.

In confirmation of our *in vitro* mechanism, we found that mice deficient for *Ncoa7* had elevated CH25H expression in pulmonary arterioles with subsequently elevated VCAM1 expression and CD11b^{+} monocyte infiltration (Figure 35). Moreover, quantification of the relative degree of arteriole muscularization, as noted by the thickness of the α-SMA^{+} layer, revealed worsening with loss of *Ncoa7* (Figure 35).

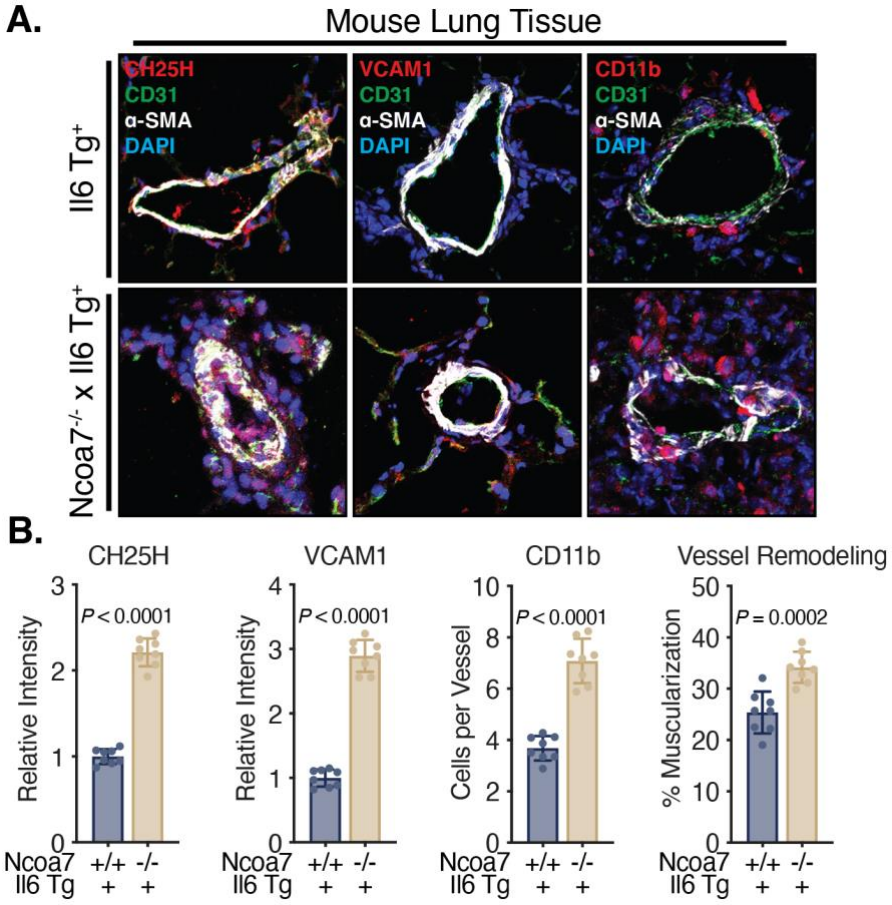

Figure 35. Loss of Ncoa7 Immunoactivates the Endothelium in Il6 Transgenic Mice

A. Pulmonary vessels from *Il6* Tg^{+} versus *Ncoa7*$^{-/-}$ x *Il6* Tg^{+} mice stained for a target protein (*i.e.*, CH25H, VCAM1, or CD11b; red), the endothelial layer (CD31; green), the smooth muscle layer (α-SMA; white), and nuclear counterstain (DAPI; blue). **B.** Quantification of the relative intensity of CH25H or VCAM1, the number of CD11b^{+} cells per vessel, or the degree of vessel muscularization defined by α-SMA layer thickness to total vessel diameter. Student's *t*-test. All data are presented as mean ± standard deviation.

We also sought to confirm if the loss of *Ncoa7* in mice would produce similar serum elevations of downstream bile acids that were identified by Alotaibi et al. in a cohort of PAH patients and that were confirmed to be upregulated in human PAECs with genetic loss of NCOA7. Importantly, we observed a significant upregulation of the downstream bile acid 5β-cholestane-3α,7 α,12α,26-tetrol in the serum of *Ncoa7* knockout mice (Figure 36)—the metabolite immediately prior to a single oxidative step away from 5β-cholestane-3α,7α,12α,25,26-pentol (665110; Figure 29D).

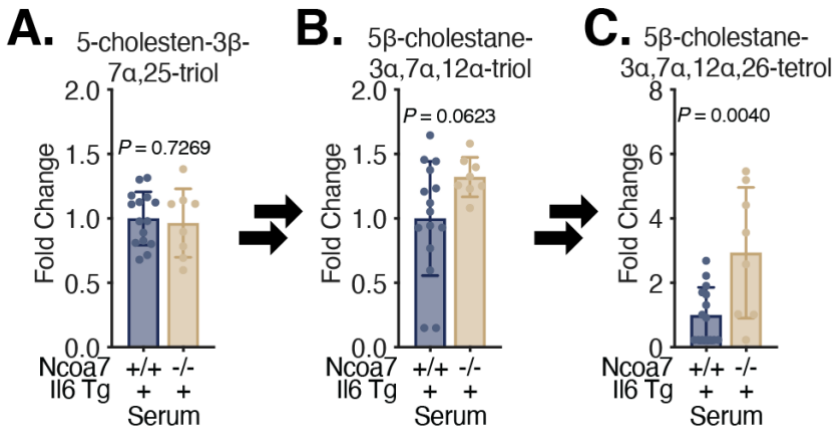

Figure 36. Loss of Ncoa7 Upregulates Bile Acids in Il6 Transgenic Mice

A – C. Measurement of bile acids using LC-MS in the serum of IL-6 transgenic mice with and without *Ncoa7* knockout. N=8-15; Student's *t*-test. All data are presented as mean ± standard deviation.

5.4 Discussion

5.4.1 NCOA7 Deficiency & Endothelial Dysfunction

The molecular origins of pulmonary vascular disease are founded on the notion of an inciting, pathologic stimulus that induces endothelial dysfunction. Our work is the first to demonstrate a functional role of NCOA7 in altering fundamental cellular behaviors. In the context of endothelial dysfunction, we show that the loss of NCOA7 completely abrogates proinflammatory cytokine-mediated apoptosis—in line with the apoptosis-resistant observation seen in ECs isolated from PAH patients (Lee et al., 1998; Masri et al., 2007; Sakao et al., 2005). Moreover, we show that under proinflammatory conditions, NCOA7 deficiency results in enhanced proliferative capacity human PAECs. Again, this observation is consistent with decades of work documenting the hyperproliferative nature of ECs in pulmonary vascular disease (Lee et al., 1998; Masri et al., 2007; Sakao et al., 2005). In addition, and most interestingly, we demonstrate a profound immunoactivation of the endothelium, as noted by significant upregulation of *VCAM1* and immune cell adhesion, with loss of NCOA7. This finding, when interpreted in the context of observed immune activation of the endothelium in PAH (Rabinovitch et al., 2014), further implicates the loss of NCOA7 as consequential in the pathogenesis of this disease.

5.4.2 NCOA7 Deficiency Generates Oxysterols to Induce Pulmonary Arterial Hypertension

To determine if these endothelial aberrations were secondary to the NCOA7 deficiency-mediated upregulation of the oxysterol generating enzyme CH25H, we performed concomitant knockdown experiments of both *NCOA7* and *CH25H*. Interestingly, we found that this double

knockdown partially reversed IL-1β-mediated apoptosis, suggesting that 25HC and/or its downstream metabolites exert anti-apoptotic effects. This finding is in contrast to literature indicating that 25HC induces apoptosis in a variety of cell types (Choi et al., 2008; Le Goff et al., 2006); however, recent work suggests that the actions of 25HC are context-specific, with reported ability to resolve lung inflammation (Madenspacher et al., 2020) and suppress IL-1β signaling pathways (Reboldi et al., 2014). Other studies in support of this show that 25HC derivatives (*i.e.*, bile acids) do in fact have anti-apoptotic properties (Ren and Ning, 2014; Zhang et al., 2012). Moreover, previous studies showcasing the apoptosis-inducing effect of 25HC have a noticeable limitation in that the direct application of supra-physiologic concentrations of this oxysterol are perhaps misrepresentative of the true biology, for they fail to properly replicate the spatiotemporal dynamic of oxysterol generation and localization within the cell. To address this, future work should optimize a more suitable delivery of 25HC, such as through the lentivector delivery of CH25H under a moderately expressing promoter. We also note that the additional knockdown of CH25H in NCOA7-deficient cells further enhanced proliferation—an interesting finding that indicates these molecules may act as an inhibitory break on proliferative capacity. In B cells, the presence of 25HC was found to inhibit proliferative capacity (Bauman et al., 2009), yet, in hepatocytes and macrophages, 25HC promotes their proliferative potential (Ren and Ning, 2014). These conflicting data further support the idea that 25HC function is not easily discrete, depending highly on its microenvironment, cellular localization, and source tissue.

Examining the role in immune activation of the endothelium, we observed that the loss of CH25H reversed the IL-1β-mediated upregulation of *VCAM1*, which further prevented the adhesion of both leukocytes and monocytes to an endothelial monolayer. These data suggest that inhibition of 25HC production served as a protective mechanism of resultant immune

dysregulation. We also show that the direct application of 25HC into the media of human PAECs upregulated *VCAM1* with the expected attachment of leukocytes and monocytes to the endothelium. In addition, we confirmed that iPSC-ECs containing the allelic variants of SNP rs11154337 have differential VCAM1 expression and immune activation—noting that the presence of the G allele (*i.e.*, more *NCOA7* expression) had lower immunoactivation. Taken together, these data support limited literature demonstrating the role of downstream oxysterol derivatives in immunoactivation of the endothelium (Qin et al., 2006). Future work will establish whether these observations can be explained by differential oxysterol and bile acid production in iPSC-ECs containing the allelic variants of SNP rs11154337.

Beyond direct relevance to pulmonary vascular disease, there is growing evidence to support a role for abnormal bile acid elevation in other disorders of the lung. For instance, the aspiration of bile acids into the lungs of patients with respiratory diseases (*i.e.*, cystic fibrosis) has been recognized as a major comorbidity (Navarro et al., 2001) and driver of inflammation (Aseeri et al., 2012; Pauwels et al., 2012). Moreover, recent molecular work has demonstrated a role for bile acids in the induction of epithelial cell apoptosis and increased proinflammatory cytokine secretion (Aldhahrani et al., 2017).

To translate our findings *in vivo*, we utilized a severe proinflammatory model of PH—the *Il6* transgenic mouse (Steiner et al., 2009). We found that the total body knockout of *Ncoa7* in *Il6* transgene-positive mice worsened PH as noted by increased right ventricular hypertrophy and worsened RVSP. Moreover, we confirmed that the loss of *Ncoa7* upregulates CH25H in the pulmonary vessels, which resulted in enhanced VCAM1 expression and monocyte infiltration into the vessel as defined by CD11b positivity. The enhanced immunoactivation of the pulmonary vessel was further confirmed by worsened arteriole muscularization. Consistent with the work of

Alotaibi et al. and increased CH25H in knockout mice, we found significant elevation of the bile acid metabolite immediately upstream of and one oxidative step away from 5β-cholestane-3α,7α,12α,25,26-pentol (665110; Figure 29D). As such, the knockout of *Ncoa7* in a rodent model similarly upregulated bile acids to promote progression of PH. Future work will further characterize the degree of vessel remodeling in these mice, as noted by the degree of arteriole muscularization and the degree of immune cell infiltration into the vascular bed.

One major limitation of our *in vivo* work is the global loss of *Ncoa7*. Although we have ruled out via echocardiography left ventricular disease, not every variable in a global knockout model can be addressed. To correct this, future studies are planned to utilize the 7C1 nanoparticle delivery of silencing RNA against *Ncoa7* in mice that specifically localizes to the endothelium. With our prior experience utilizing the 7C1 nanoparticle delivery model, we hope to establish the necessity of *Ncoa7* in the proper functioning of the endothelium (Culley et al., 2021; Yu et al., 2019). Specifically, we hypothesize that RNA silencing of *Ncoa7* within the endothelium of *Il6* Tg^+ mice will similarly worsen PH as did our total body knockout model. In addition, we are currently delivering 25HC to mice via both intraperitoneal and tail vein injections to understand if the direct application of such molecules can induce PH in mice. We are also planning to do this experiment with the metabolites identified by Alotaibi et al., as we have commissioned custom chemical syntheses of these compounds. Lastly, as we believe NCOA7 upregulation is beneficial in response to proinflammatory conditions (*i.e.*, its reversal of endothelial immune activation), we are developing adeno-associated virus vectors containing both isoforms of NCOA7 for overexpression in rodent models of PH with the goal of preventing or reversing disease.

In sum, these data demonstrate that loss of NCOA7 causes abnormal sterol accumulation and thus secondary mechanisms to excrete excess content in the form of soluble oxysterols and

bile acids. These oxidized sterols have important functions in immune activation of the endothelium, suggesting that their upregulation in response to a loss of or failure to upregulate NCOA7 promotes pulmonary vascular disease.

5.4.3 NCOA7 Homologues & Pulmonary Vascular Disease

Beyond our work establishing NCOA7 as a key modulator of pulmonary vascular disease, there exists a variety of other, relatively unstudied proteins within its family. The unifying feature among NCOA7 and these proteins is the presence of the Tre2/Bub2/Cdc16 (TBC), lysin motif (LysM), domain catalytic (TLDc) domain. This family of proteins (*i.e.*, NCOA7, oxidation resistance protein 1 [OXR1], TBC1 domain family member 24 [TBC1D24], TBC/LysM-associated domain containing 1 [KIAA1609], and TBC/LysM-associated domain containing 2 [C20ORF118]) has poorly defined features (Finelli and Oliver, 2017; Finelli et al., 2016); however, previous work has established an apparent function for OXR1 and TBC1D24 in oxidation resistance within the central nervous system.

In addition to its oxidative scavenging potential, OXR1 is similarly implicated in the immune response, where its overexpression in *Drosophila* increased tolerance to oral *Vibrio cholerae* infection. Moreover, truncated overexpression of the TLDc domain recapitulated full OXR1 overexpression, suggesting that the domain alone could exert functional modulation of an immune response (Wang et al., 2012). Interestingly, this highly truncated TLDc domain is what $NCOA7_{short}$ represents. In support of a role for OXR1 in the immune system, mouse strains with inflammation-resistant kidneys had significantly higher levels of *Oxr1* than sensitive strains (Li et al., 2014)—a finding which indicates that *more* OXR1 is anti-inflammatory and beneficial. In addition, this study implanted mesenchymal stem cells expressing OXR1 into an autoimmune

mouse model of systemic lupus erythematosus and found that implanted mice had reduced cytokine and interleukin levels in the serum and decreased T cell and macrophage infiltration into the kidney (Li et al., 2014)—similar to our data demonstrating that overexpression of NCOA7 reversed immune activation of the endothelium as measured by decreased leukocyte and monocyte adhesion. Moreover, direct confirmation of OXR1 relevance in human disease was recently validated in consanguineous families that have bi-allelic, loss-of-function variants, where affected proband demonstrate dysfunctional lysosomes by electron microscopy in comparison to unaffected kin (Wang et al., 2019). The combination of these data suggests that both OXR1 and NCOA7 appear to have endolysosomal and immunomodulatory functions. As such, the question is raised on whether a compensatory mechanism exists when one TLDc protein is disrupted (*i.e.*, a deficiency of NCOA7 inducing a compensatory increase of OXR1). Moreover, both NCOA7 and OXR1 possess similar isoforms (*i.e.*, full-and short-length) but the extent of their exact cellular localization and responsiveness to stimuli has not been well characterized. The importance in delineating such nuance could potentially have implications for therapeutic intervention. For instance, could a deficiency of one TLDc protein be supplemented with the delivery (*i.e.*, "rescued") of a different TLDc protein? Overall, our work on establishing a mechanism for the function of NCOA7 in modulating lysosomal behavior and thus sterol metabolism prompt numerous questions on potential supporting roles of other TLDc family members.

5.4.4 Sex Differences, Sterol Metabolism, & Pulmonary Vascular Disease

Since the early observations of the gender paradox in PAH, studies have attempted to understand the way in which sex hormones (*i.e.*, estrogen) may be contributory. In the context of previous literature on NCOA7, the high female predominance of PAH (*i.e.*, 4.8 to 1) might be

explained by its control of sterol metabolism, especially since the discovery of NCOA7 was based upon the full-length isoform directly binding to the estrogen receptor α (Shao et al., 2002). In addition, a series of *–omics*-based studies have identified NCOA7 in female specific cancers. Although somewhat contradictory, there are a series of reports that have linked NCOA7 involvement in breast cancer (Gao et al., 2019; Higginbotham et al., 2011; Sullner et al., 2012). A meta-analysis on three genome-wide association studies for endometrial cancer identified a risk locus near the *NCOA7* (Cheng et al., 2016). In line with these observations, molecular analysis found that $NCOA7_{short}$ is highly-enriched in ovarian and uterine tissues and that its induction is responsive to gonadotropins (Shkolnik et al., 2008). Potential explanations of this sex paradox, perhaps superficially, have focused on estrogen metabolism and signaling. For instance, one theory put forward suggests a dose-dependence of estrogen and its metabolites (Foderaro and Ventetuolo, 2016), noting that at low doses estrogen acts as a pro-oxidant and at high doses has anti-oxidant properties. In addition, estrogen metabolites show contradictory effects on vascular cells with studies demonstrating pro-apoptotic and anti-proliferative effects while others show the opposite (Docherty et al., 2018). The basis of these studies believe that it is a fundamental imbalance of estrogen and its metabolites that may explain the increased incidence of PAH in females (Paulin and Michelakis, 2012). Interestingly, female sex, despite conferring increased risk of PAH, also confers increased survivability. As we show a protective role for NCOA7 in endothelial function and others have shown its gonadotropin induction, perhaps there is a role for NCOA7 in the conference of disease protection in females versus males. Ultimately, the work on teasing apart the sex-specific molecular events underlying pulmonary vascular disease remain vastly understudied. Future work must ensure equitable representation and study of the female sex, especially within the context of *in vivo* rodent models.

5.4.5 NCOA7 Deficiency & Atherosclerosis

Our work defining a fundamental role for NCOA7 in the modulation of sterol metabolism and how its deficiency causes the production of proinflammatory oxysterols and bile acids suggests potential relevance in the pathogenesis of atherosclerosis. Atherosclerosis is a systemic disease state characterized by the formation of lipid deposits, or plaques, within the vessel lumen. Although typically thought of as a disease of aging, evidence suggests that the deposition of lipid plaques within the vessel lumen is also a direct function of systemic inflammation and immunoactivation of the endothelium. For example, shear stress on the endothelium (*i.e.*, as a model of vulnerable regions in an arterial tree and thus impaired laminar flow) is known to activate the proinflammatory NF-κB pathway, which subsequently upregulates a multitude of cellular adhesion molecules like *VCAM1* and the expression of various proinflammatory cytokines (Tzima et al., 2005; Zaragoza et al., 2012). Moreover, one study demonstrated in an atherosclerosis mouse model that the inhibition of NF-κB within the endothelium significantly decreased the lesion area and the recruitment of macrophages to the vessel lesion (Gareus et al., 2008).

We have demonstrated that the lack of NCOA7 within the endothelium significantly upregulated the expression of *VCAM1* and this corresponded to increased attachment of monocytes to an endothelial monolayer. Conversely, we show that the forced overexpression of NCOA7 prevents the IL-1β-mediated upregulation of *VCAM1* and attachment of monocytes to the endothelium. Coupling this knowledge, a rational thread appears to suggest that loss of NCOA7 may also contribute to systemic vascular disease and thus predispose or worsen the progression of atherosclerotic lesion development. In addition, and beyond the scope of this body of work, we have performed preliminary experiments in mice subjected to a high-fat Western diet (42% kCal from fat) for three months with the concomitant delivery of an adeno-associated vector (AAV)

containing a hyperactive, mutant version of proprotein convertase subtilisin/kexin type 9 serine protease (*PCSK9*; D33Y mutation) in wildtype or *Ncoa7* knockout mice. Our initial and limited physical observations noted a striking splenic mass increase in *Ncoa7*-/- mice (174 ± 26.20 mg) compared to wildtype mice (109 ± 10.17 mg; $P = 0.0006$; Student's *t*-test; N=5-6 per group)—a fascinating observation given the emerging literature of a splenic-monocytic-atherosclerosis axis (Potteaux et al., 2015). However, more concrete work must be completed, such as morphometric and histological analyses, to determine a more definitive role for NCOA7 and the development of atherosclerosis.

6.0 Concluding Remarks

6.1 Functional Multi-Omics: NCOA7 & Pulmonary Arterial Hypertension

A role for bile acids in the development of PAH has been alluded to through small (*i.e.*, less than 20 PAH patients for a given cohort), metabolomics-based studies over the years, which demonstrate the elevation of bile acids in both the lungs and serum of patients (Bujak et al., 2016; Chouvarine et al., 2020; Zhao et al., 2014b). Our colleagues Alotaibi et al. have lent credence to the concept of bile acids as mediators of disease by assembling the largest cohort of over 2,000 PAH patients to date for unbiased, metabolomics screening. Their landmark study found a significant upregulation of bile acids in the serum of PAH patients that correlate with clinical parameters of disease, such as hemodynamics, six-minute walk distance, and mortality. Utilizing parallel metabolomics and orthogonal genomics data from The FINRISK Study of nearly 8,000 people, we and Alotaibi et al. determined that two of these bile acids were negatively associated with the presence of G allele at SNP rs11154337 in an intronic region of *NCOA7*, indicating that an absence of the G allele allows for higher levels of these oxidized lipid species (Chapter 1). Our work, in complement, has sought to map the mechanistic underpinnings of this observation as the first report to ever integrate large, multi-omics datasets in the discovery of a functional genomic variant with direct biological activity in the production of a pathologic, metabolomic signature with direct clinical utility in the progression and management of human disease.

In Chapter 2, we demonstrated using a variety of modalities, such as through cytokine application to human PAECs, in inflammatory rodent models of PH, and in single-endothelial cell transcriptomic analysis of PAH patients that proinflammatory stimuli integrate and converge upon

p65/RelA of NF-κB to upregulate *NCOA7*. In addition, using SNP-edited, isogenic, iPSC-ECs, we have demonstrated a biological function for the SNP rs11154337 regulatory region where p65/RelA bind to perhaps form a transcription factor complex that alters consequent *NCOA7* expression. Although not directly located in the canonical or non-canonical promoter, this genetic variant appears to modulate the enhancer activity of this region to ultimately affect the expression of both isoforms.

In Chapters 3 and 4, we directly implicated NCOA7 as a critical regulatory factor of lysosomal function and thus sterol metabolism. Unbiased, transcriptomic analysis of human PAECs deficient for NCOA7 revealed a global downregulation of genes related to lysosomal biology and *de novo* cholesterol synthesis. Furthermore, we revealed a direct function of NCOA7 at the V-ATPase complex, through the subunit ATP6V1B2, in the control of lysosomal acidification and subsequent hydrolase activity. The inhibition of luminal acidification—through loss of NCOA7—resulted in the accumulation of lipid species within lysosomes. Because of abnormal sterol processing and accumulation, we observed an upregulation of oxysterol generating enzymes as a mechanism to excrete and offload accumulating sterol species. We confirmed this offloading mechanism using targeted lipidomics and unbiased metabolomics to reveal the upregulation of upstream oxysterols and downstream bile acid derivatives, respectively. Strikingly, we found that two of these downstream metabolites appear to match the chemical structures of the two identified metabolites by Alotaibi et al.: 5β-cholestane-3α,7α,12α,25,26-pentol (665110; Figure 29D) and 7α-hydroxy-3-oxo-4-cholestenoic acid (667200; Figure 29I). Most importantly, and consistent with the associations, we found that loss of NCOA7 significantly upregulated both metabolites—in line with the notion that the presence of the G allele (*i.e.*, higher NCOA7 expression) negatively associates with the metabolites.

In Chapter 5, we demonstrated that either a complete genetic loss or a failure to induce robust expression of *NCOA7* resulted in aberrant bile acid synthesis and subsequent endothelial dysfunction. Specifically, the loss of NCOA7 produced an apoptosis-resistant, hyperproliferative, and immunoactivated endothelium—a finding consistent with decades of research (Lee et al., 1998; Masri et al., 2007; Sakao et al., 2005). Through inhibition of the upstream oxysterol generating enzyme CH25H, we reversed immune activation of the endothelium, thereby implicating oxysterol and bile acid production as key to this phenotypic aberration. We further confirmed that the direct application of 25HC mimicked the loss of NCOA7 in human PAECs, and, using iPSC-ECs, that the degree of immune activation was SNP-dependent. Moving to *in vivo* models, we found that the genetic loss of *Ncoa7* in an angioproliferative rodent model exacerbated disease progression as noted by worsened right ventricular hypertrophy, elevated right ventricular systolic pressure, and vessel muscularization. We further confirmed that loss of *Ncoa7* similarly upregulated CH25H *in vivo*. In accordance with our mechanism, the upregulation of CH25H in the pulmonary vessel produced upregulation of VCAM1 and immune infiltration into the pulmonary vessel. Lastly, we found the upregulation of the bile acid 5β-cholestane-3α,7 α,12α,26-tetrol in the serum of these mice)—the metabolite immediately prior to a single oxidative step away from 5β-cholestane-3α,7α,12α,25,26-pentol (metabolite 665110).

In summary, this work—in conjunction with Alotaibi et al.— demonstrates the successful integration of both genomics and metabolomics datasets in the identification of a functional nucleotide variant with direct, mechanistic underpinnings in the synthesis of oxysterol and bile acid species with demonstrable, disease-inciting activity and clinical utility in the progression and management of pulmonary vascular disease. As such, this work not only unleashes a fundamentally new mechanism underlying PAH through NCOA7 deficiency-mediated aberrations

in lysosomal behavior and sterol metabolism but also implicates NCOA7—and by proxy SNP rs11154337—as potential diagnostic and therapeutic targets.

6.2 Sterol Metabolism & Pulmonary Vascular Disease: A New Mechanism

For the first time, we have demonstrated a mechanistic link between sterol metabolism aberrations and pulmonary vascular disease. Moreover, our report is the first to identify a fundamental regulatory role for NCOA7 in sterol homeostasis and oxysterol generation, as discussed in previous chapters. We hope that the culmination of this work lays the foundational substrate from which future studies can investigate observations of pulmonary vascular disease in a myriad of disorders related to sterol metabolism—whether through direct inborn errors of biosynthetic enzymes (*i.e.*, Smith-Lemli Opitz Syndrome [*DHCR7*] and Cholesteryl Ester Storage Disease [*LIPA*]) or through indirect handling of sterols through mutations in lysosomal hydrolases (*i.e.*, Fabry Disease [*GLA*], Gaucher Disease [*GBA*], and Niemann-Pick Disease [*NPC1* and *NPC2*]) or V-ATPase subunits (*i.e.*, Cutis Laxa [*ATP6V1A* or *ATP6V1E1*]). Although these disease states are due to the presence of rare, biallelic, loss-of-function variants, the manifestation of pulmonary vascular disease in these patients lends insight into complex genetic inheritance. For example, does the possession of a loss-of-function variant for a specific enzyme predispose the patient to PAH overtime? Could other variants involved in lysosomal behavior and sterol homeostasis act in synergy to cause disease? Examples of such synergistic heterozygosity were first documented in disorders of mitochondrial metabolism (Vockley et al., 2019; Vockley et al., 2000). Ironically, one of the next early reports of this genetic phenomenon was the demonstration

of nucleotide variants in transforming growth factor-β signaling pathways that affected the penetration of *BMPR2* mutations in familial PAH (Phillips et al., 2008).

6.3 The Challenge of Biomarker Discovery in Pulmonary Arterial Hypertension

Inherent to the management of rare disease is difficulty in its diagnosis and subsequent therapeutic intervention. One of the most obvious barriers in the current diagnostic algorithm is the deference to a center of care with clinical expertise in pulmonary vascular disease, as the gold standard requires invasive right heart catheterization and/or a vasodilator challenge study. For this reason, clinicians have toiled to find diagnostic biomarkers. Although numerous potential biomarkers have been identified to various metrics of disease (*i.e.*, clinical parameters, inflammation, and endothelial cell dysfunction) (McMahon and Bryan, 2017), they have failed to demonstrate sensitivity and specificity for diagnosis, risk assessment, and management of pulmonary vascular disease (Frost et al., 2019). Moreover, clinicians have invested much effort in the stratification of patients (*i.e.*, low-, intermediate-, or high-risk status) to better initiate a tailored treatment regimen (*i.e.*, monotherapy versus combination therapies).

In attempting to address these challenges, we and Alotaibi et al. have demonstrated that serum bile acids identified in PAH patients associated clinical parameters of disease (*i.e.*, six-minute walk distance, mRAP, and mortality), stratified patients into risk status, and, most importantly, were inversely associated with the G allele of SNP rs11154337. Accordingly, the combined efforts of our work suggest that either targeted serum metabolite analysis or SNP genotyping of rs11154337 may have direct clinical utility in the management of patients suffering from this devastating disorder. In addition, the ability to risk stratify patients based on serum bile

acids indicates an underlying disease process that may not be specific to all Group I PH patients, meaning that subclassification may define as-of-yet discovered therapies for specific patients. Overall, much future work must be completed to translate these discoveries into clinical application in the betterment of individuals suffering from pulmonary vascular disease.

6.4 The Challenge of Therapeutic Development in Pulmonary Arterial Hypertension

Our discovery of a fundamentally new mechanism underlying the pathogenesis of pulmonary vascular disease reveals a new set of molecular factors for therapeutic intervention. The generation of oxysterols and downstream bile acid derivatives implicate the generating enzymes, such as CH25H, as potential therapeutic targets. Metabolism, however, is an exquisitely complex series of molecular events. For this reason, the therapeutic targeting of metabolism in PH confers both advantages and disadvantages. Metabolism is tightly coordinated in time and space, meaning that therapeutic intervention of metabolic pathways can be difficult and result in unintended side-effects. For example, our work indicates that the generation of oxidized sterol species is a direct, homeostatic response to sterol accumulation. As such, it is reasonable to posit that inhibition of excretory mechanisms (*i.e.*, CH25H) may cause even more immediate damage to the cell than allowing for the generation and excretion of proinflammatory bile acids. Our *in vitro* work, however, demonstrated that concomitant loss of *NCOA7* and *CH25H* prevented the acute immunoactivation of the endothelium. To truly implicate CH25H as a viable therapeutic target, future work must recapitulate this finding in the complexity of an *in vivo* system.

Beyond oxysterol generating enzymes, our work also implicates NCOA7 as a potential therapeutic target. We demonstrated that the forced overexpression of NCOA7 reverses the IL-1β-

mediated immunoactivation of the endothelium. To confirm this finding *in vivo*, we are preparing experiments for the adeno-associated virus delivery of NCOA7 to the pulmonary system of PH rodent models. If corroborated, our work will solidify that either small molecule activators of NCOA7 (or even V-ATPase subunits) or gene delivery vectors may serve as promising treatment options in the prevention or reversal of pulmonary vascular disease. In addition, future work in therapeutic discovery must consider systemic versus local administration of an intervention. To address this, work must focus on the nanoscale delivery of treatments to the *lung* endothelium, whether it may be through recombinant proteins or encapsulated pharmacological agents. One immediate challenge in the study of new therapies is that such new agents must be tested in patients with the current standard of care (*i.e.*, combination therapy), meaning that clinical trials and attempts to discern efficacy can be complicated. Ultimately, future work must commit to finding new therapies, as our current clinical arsenal of interventions provides only symptomatic relief with no effect on disease progression or cure.

Appendix A Primers & Oligonucleotides

Table 3. Custom Primers for Gene Expression

Gene Target	Species	Primer Sequences 5' to 3'
ACTB	Human	Forward: CATGTACGTTGCTATCCAGGC Reverse: CTCCTTAATGTCACGCACGAT
NCOA7$_{short}$	Human	Forward GCCACACTTCTCACTGCTCA Reverse TAGGACAGGCAGCACCTCTT
NCOA7$_{full}$	Human	Forward CTCCGCTGCAAGATGGAAGG Reverse CGAGTAGCCATCCTGCAACT
Actb	Mouse	Forward: ACCTTCTACAATGAGCTGCG Reverse: CTGGATGGCTACGTACATGG
Ncoa7$_{short}$	Mouse	Forward GCAGGCAACCAGAGAAAGAC Reverse CGTTTTGCCTCCTCAACTGT
Ncoa7$_{full}$	Mouse	Forward ATGGAAAGGGTGTGGTTGGG Reverse CTCCAGGCCTGTACAGAGGA

Table 4. Custom Primers for ChIP qPCR

DNA Target	Species	Primer Sequences 5' to 3'
Non-canonical Promoter (*i.e.*, *NCOA7$_{short}$*)	Human	Forward AAAGCTAGGTTCACTGGAGGG Reverse GGCATCGCTGTGAGACTGTAA
Canonical Promoter (*i.e.*, *NCOA7$_{full}$*)	Human	Forward TGGGTGGTATGCCTAGTGAA Reverse TTAAGGCTGGGCTGTAAGGT
SNP rs11154337 Region	Human	Forward ACCTCCTGGCCAGTATCCTT Reverse ACTCACATAGTGCCCCTCCT

Table 5. Oligonucleotides for Genome Editing

Oligonucleotides	Species	Sequence 5' to 3'
NCOA7 gRNAs	Human	Forward: CACCGTTCAAATATATAGCAGGATA Reverse: AAACTATCCTGCTATATATTTGAAC
NCOA7 ssODN	Human	CTAAACCAAGAAAATGATCATTTGA CAGTGTTTACCTTGGCAAGGATACT GGCCAGGAGGTGTCTTCCCATTAGG GACATGACTATGGACTCACTATCCT GCTATATATTTGAAGACACAGATCAA
NCOA7 Sequencing Primer Set #1	Human	Forward: CTTCATGGCCTCCTTTGGTA Reverse: AAGGATACTGGCCAGGAGGT
NCOA7 Sequencing Primer Set #2	Human	Forward: CCAGGTTGAAGTGGAAAGGA Reverse: GGACAGGCCTCACCTGATTA

Table 6. TaqMan Primers

Gene Target	Species	TaqMan Assay ID
ACTB	Human	Hs99999903_m1
ATP6V1B2	Human	Hs00156037_m1
CH25H	Human	Hs02379634_s1
CYP27A1	Human	Hs01017992_g1
LDLR	Human	Hs01092524_m1
NCOA7	Human	Hs00906291_m1
VCAM1	Human	Hs01003372_m1

Table 7. Silencing RNA Species

siRNA Gene Target	Species	*Silencer*™ Assay ID
CH25H	Human	289454
CYP27A1	Human	106239
NCOA7	Human	242114
Negative Control No. 1	Human	AM4611

Appendix B Antibodies

Table 8. Antibodies for Protein Detection

Target	Species	Concentration	Vendor
Flow Cytometry			
CD34-FITC	Mouse	1:200	BD Biosciences; 555821
CD144-APC	Mouse	1:200	BioLegend; 348508
CD309-PE	Mouse	1:200	BD Biosciences; 560872
Immunoblot			
Myc	Rabbit	1:1000	Cell Signaling Technologies; 2278S
Immunofluorescence			
αSMA	Goat	1:100	Sigma-Aldrich; A5228
CD31/PECAM-1	Goat	1:100	R&D Systems; AF3628
CH25H	Rabbit	1:100	abcam; ab214295
NCOA7	Rabbit	1:100	abcam; ab224481
Proximity Ligation Assay			
ATP6V1B2	Rabbit	1:50	abcam; ab73404
NCOA7	Mouse	1:50	Santa Cruz Biotechnology; sc-393427

Appendix C Software

Table 9. Software for Data Analyses

Software	Access Link
EndNote X9.3.3	https://endnote.com
Fiji 2.1.0/1.53c	https://imagej.net
FlowJo 10.7.1	https://flowjo.com
LabChart v8.1.14	https://adinstruments.com
Prism 9.1.0	https://graphpad.com

Appendix D Publications

Appendix D.1 Graduate Training (2017 – current)

Acharya AP, Tang Y, Bertero T, Tai YY, Harvey LD, Woodcock CC, Sun W, Pineda R, Mitash N, Königshoff M, Little SR, Chan SY. Simultaneous Pharmacologic Inhibition of Yes-Associated Protein 1 and Glutaminase 1 via Inhaled Poly(Lactic-co-Glycolic) Acid-Encapsulated Microparticles Improves Pulmonary Hypertension. J Am Heart Assoc. 2021 Jun 15;10(12):e019091. doi: 10.1161/JAHA.120.019091. Epub 2021 May 29. PubMed PMID: 34056915.

Woodcock CC, Hafeez N, Handen A, Tang Y, Harvey LD, Estephan LE, Speyer G, Kim S, Bertero T, Chan SY. Matrix stiffening induces a pathogenic QKI-miR-7-SRSF1 signaling axis in pulmonary arterial endothelial cells. Am J Physiol Lung Cell Mol Physiol. 2021 May 1;320(5):L726-L738. doi: 10.1152/ajplung.00407.2020. Epub 2021 Feb 10. PubMed PMID: 33565360; PubMed Central PMCID: PMC8174827.

Harvey LD, Chan SY. Evolving systems biology approaches to understanding non-coding RNAs in pulmonary hypertension. J Physiol. 2019 Feb;597(4):1199-1208. doi: 10.1113/JP275855. Epub 2018 Sep 2. Review. PubMed PMID: 30113078; PubMed Central PMCID: PMC6375871.

Harvey LD, Chan SY. YAPping About Glutaminolysis in Hepatic Fibrosis. Gastroenterology. 2018 Apr;154(5):1231-1233. doi: 10.1053/j.gastro.2018.03.007. Epub 2018 Mar 3. PubMed PMID: 29510133; PubMed Central PMCID: PMC6456336.

Ranchoux B, Harvey LD, Ayon RJ, Babicheva A, Bonnet S, Chan SY, Yuan JX, Perez VJ. Endothelial dysfunction in pulmonary arterial hypertension: an evolving landscape (2017 Grover Conference Series). Pulm Circ. 2018 Jan-Mar;8(1):2045893217752912. doi: 10.1177/2045893217752912. Epub 2017 Dec 28. PubMed PMID: 29283043; PubMed Central PMCID: PMC5798691.

Harvey LD, Chan SY. Emerging Metabolic Therapies in Pulmonary Arterial Hypertension. J Clin Med. 2017 Apr 4;6(4). doi: 10.3390/jcm6040043. Review. PubMed PMID: 28375184; PubMed Central PMCID: PMC5406775.

Appendix D.2 Undergraduate Training (2011 – 2015)

Harvey LD, Yin Y, Attarwala IY, Begum G, Deng J, Yan HQ, Dixon CE, Sun D. Administration of DHA Reduces Endoplasmic Reticulum Stress-Associated Inflammation and Alters Microglial or Macrophage Activation in Traumatic Brain Injury. ASN Neuro. 2015 Nov-Dec;7(6). doi: 10.1177/1759091415618969. Print 2015 Nov-Dec. PubMed PMID: 26685193; PubMed Central PMCID: PMC4710127.

Zonouzi M, Scafidi J, Li P, McEllin B, Edwards J, Dupree JL, Harvey L, Sun D, Hübner CA, Cull-Candy SG, Farrant M, Gallo V. GABAergic regulation of cerebellar NG2 cell development is altered in perinatal white matter injury. Nat Neurosci. 2015 May;18(5):674-82. doi: 10.1038/nn.3990. Epub 2015 Mar 30. PubMed PMID: 25821912; PubMed Central PMCID: PMC4459267.

Begum G*, Harvey L*, Dixon CE, Sun D. ER stress and effects of DHA as an ER stress inhibitor. Transl Stroke Res. 2013 Dec;4(6):635-42. doi: 10.1007/s12975-013-0282-1. Epub 2013 Aug 20. Review. PubMed PMID: 24323417; PubMed Central PMCID: PMC3864671. *Denotes co-first authorship.

Appendix D.3 Access & Citation Metrics

List of Publications on PubMed

Citation Metrics on Google Scholar

Bibliography

Al-Husseini, A., Wijesinghe, D.S., Farkas, L., Kraskauskas, D., Drake, J.I., Van Tassel, B., Abbate, A., Chalfant, C.E., and Voelkel, N.F. (2015). Increased eicosanoid levels in the Sugen/chronic hypoxia model of severe pulmonary hypertension. PLoS One *10*, e0120157.

Al-Naamani, N., Palevsky, H.I., Lederer, D.J., Horn, E.M., Mathai, S.C., Roberts, K.E., Tracy, R.P., Hassoun, P.M., Girgis, R.E., Shimbo, D., *et al.* (2016). Prognostic Significance of Biomarkers in Pulmonary Arterial Hypertension. Ann Am Thorac Soc *13*, 25-30.

Albrecht, L.V., Tejeda-Munoz, N., and De Robertis, E.M. (2020). Protocol for Probing Regulated Lysosomal Activity and Function in Living Cells. STAR Protoc *1*, 100132.

Aldhahrani, A., Verdon, B., Ward, C., and Pearson, J. (2017). Effects of bile acids on human airway epithelial cells: implications for aerodigestive diseases. ERJ Open Res *3*.

Alfadhel, M., AlShehhi, W., Alshaalan, H., Al Balwi, M., and Eyaid, W. (2013). Mucolipidosis II: first report from Saudi Arabia. Ann Saudi Med *33*, 382-386.

Aran, D., Looney, A.P., Liu, L., Wu, E., Fong, V., Hsu, A., Chak, S., Naikawadi, R.P., Wolters, P.J., Abate, A.R., *et al.* (2019). Reference-based analysis of lung single-cell sequencing reveals a transitional profibrotic macrophage. Nat Immunol *20*, 163-172.

Archer, S.L., Weir, E.K., and Wilkins, M.R. (2010). Basic science of pulmonary arterial hypertension for clinicians: new concepts and experimental therapies. Circulation *121*, 2045-2066.

Aseeri, A., Brodlie, M., Lordan, J., Corris, P., Pearson, J., Ward, C., and Manning, N. (2012). Bile acids are present in the lower airways of people with cystic fibrosis. Am J Respir Crit Care Med *185*, 463.

Ashburner, M., Ball, C.A., Blake, J.A., Botstein, D., Butler, H., Cherry, J.M., Davis, A.P., Dolinski, K., Dwight, S.S., Eppig, J.T., *et al.* (2000). Gene ontology: tool for the unification of biology. The Gene Ontology Consortium. Nat Genet *25*, 25-29.

Austin, E.D., Ma, L., LeDuc, C., Berman Rosenzweig, E., Borczuk, A., Phillips, J.A., 3rd, Palomero, T., Sumazin, P., Kim, H.R., Talati, M.H., *et al.* (2012). Whole exome sequencing to identify a novel gene (caveolin-1) associated with human pulmonary arterial hypertension. Circ Cardiovasc Genet *5*, 336-343.

Babiker, A., Andersson, O., Lindblom, D., van der Linden, J., Wiklund, B., Lütjohann, D., Diczfalusy, U., and Björkhem, I. (1999). Elimination of cholesterol as cholestenoic acid in human lung by sterol 27-hydroxylase: evidence that most of this steroid in the circulation is of pulmonary origin. J Lipid Res *40*, 1417-1425.

Babiker, A., Andersson, O., Lund, E., Xiu, R.J., Deeb, S., Reshef, A., Leitersdorf, E., Diczfalusy, U., and Björkhem, I. (1997). Elimination of cholesterol in macrophages and endothelial cells by the sterol 27-hydroxylase mechanism. Comparison with high density lipoprotein-mediated reverse cholesterol transport. J Biol Chem *272*, 26253-26261.

Babiker, A., Dzeletovic, S., Wiklund, B., Pettersson, N., Salonen, J., Nyyssonen, K., Eriksson, M., Diczfalusy, U., and Bjorkhem, I. (2005). Patients with atherosclerosis may have increased circulating levels of 27-hydroxycholesterol and cholestenoic acid. Scand J Clin Lab Invest *65*, 365-375.

Badesch, D.B., Champion, H.C., Gomez Sanchez, M.A., Hoeper, M.M., Loyd, J.E., Manes, A., McGoon, M., Naeije, R., Olschewski, H., Oudiz, R.J., *et al.* (2009). Diagnosis and assessment of pulmonary arterial hypertension. J Am Coll Cardiol *54*, S55-S66.

Ballabio, A., and Gieselmann, V. (2009). Lysosomal disorders: from storage to cellular damage. Biochim Biophys Acta *1793*, 684-696.

Barnes, H., Brown, Z., Burns, A., and Williams, T. (2019). Phosphodiesterase 5 inhibitors for pulmonary hypertension. Cochrane Database Syst Rev *1*, CD012621.

Barst, R.J., McGoon, M., Torbicki, A., Sitbon, O., Krowka, M.J., Olschewski, H., and Gaine, S. (2004). Diagnosis and differential assessment of pulmonary arterial hypertension. J Am Coll Cardiol *43*, 40S-47S.

Bauman, D.R., Bitmansour, A.D., McDonald, J.G., Thompson, B.M., Liang, G., and Russell, D.W. (2009). 25-Hydroxycholesterol secreted by macrophages in response to Toll-like receptor activation suppresses immunoglobulin A production. Proc Natl Acad Sci U S A *106*, 16764-16769.

Behr, J., and Ryu, J.H. (2008). Pulmonary hypertension in interstitial lung disease. Eur Respir J *31*, 1357-1367.

Benza, R.L., Gomberg-Maitland, M., Demarco, T., Frost, A.E., Torbicki, A., Langleben, D., Pulido, T., Correa-Jaque, P., Passineau, M.J., Wiener, H.W., *et al.* (2015). Endothelin-1 Pathway Polymorphisms and Outcomes in Pulmonary Arterial Hypertension. Am J Respir Crit Care Med *192*, 1345-1354.

Benza, R.L., Gomberg-Maitland, M., Miller, D.P., Frost, A., Frantz, R.P., Foreman, A.J., Badesch, D.B., and McGoon, M.D. (2012a). The REVEAL Registry risk score calculator in patients newly diagnosed with pulmonary arterial hypertension. Chest *141*, 354-362.

Benza, R.L., Miller, D.P., Barst, R.J., Badesch, D.B., Frost, A.E., and McGoon, M.D. (2012b). An evaluation of long-term survival from time of diagnosis in pulmonary arterial hypertension from the REVEAL Registry. Chest *142*, 448-456.

Beshay, S., Sahay, S., and Humbert, M. (2020). Evaluation and management of pulmonary arterial hypertension. Respir Med *171*, 106099.

Best, D.H., Sumner, K.L., Austin, E.D., Chung, W.K., Brown, L.M., Borczuk, A.C., Rosenzweig, E.B., Bayrak-Toydemir, P., Mao, R., Cahill, B.C., *et al.* (2014). EIF2AK4 mutations in pulmonary capillary hemangiomatosis. Chest *145*, 231-236.

Bjorkhem, I., Andersson, O., Diczfalusy, U., Sevastik, B., Xiu, R.J., Duan, C., and Lund, E. (1994). Atherosclerosis and sterol 27-hydroxylase: evidence for a role of this enzyme in elimination of cholesterol from human macrophages. Proc Natl Acad Sci U S A *91*, 8592-8596.

Bligh, E.G., and Dyer, W.J. (1959). A rapid method of total lipid extraction and purification. Can J Biochem Physiol *37*, 911-917.

Boger, R.H., Sydow, K., Borlak, J., Thum, T., Lenzen, H., Schubert, B., Tsikas, D., and Bode-Boger, S.M. (2000). LDL cholesterol upregulates synthesis of asymmetrical dimethylarginine in human endothelial cells: involvement of S-adenosylmethionine-dependent methyltransferases. Circ Res *87*, 99-105.

Borie, R., Crestani, B., Guyard, A., and Lidove, O. (2021). Interstitial lung disease in lysosomal storage disorders. Eur Respir Rev *30*.

Borodulin, K., Tolonen, H., Jousilahti, P., Jula, A., Juolevi, A., Koskinen, S., Kuulasmaa, K., Laatikainen, T., Mannisto, S., Peltonen, M., *et al.* (2018). Cohort Profile: The National FINRISK Study. Int J Epidemiol *47*, 696-696i.

Braganza, M., Shaw, J., Solverson, K., Vis, D., Janovcik, J., Varughese, R.A., Thakrar, M.V., Hirani, N., Helmersen, D., and Weatherald, J. (2019). A Prospective Evaluation of the Diagnostic Accuracy of the Physical Examination for Pulmonary Hypertension. Chest *155*, 982-990.

Bright, N.A., Davis, L.J., and Luzio, J.P. (2016). Endolysosomes Are the Principal Intracellular Sites of Acid Hydrolase Activity. Curr Biol *26*, 2233-2245.

Brown, L.M., Chen, H., Halpern, S., Taichman, D., McGoon, M.D., Farber, H.W., Frost, A.E., Liou, T.G., Turner, M., Feldkircher, K., *et al.* (2011). Delay in recognition of pulmonary arterial hypertension: factors identified from the REVEAL Registry. Chest *140*, 19-26.

Budhiraja, R., Tuder, R.M., and Hassoun, P.M. (2004). Endothelial dysfunction in pulmonary hypertension. Circulation *109*, 159-165.

Bujak, R., Mateo, J., Blanco, I., Izquierdo-Garcia, J.L., Dudzik, D., Markuszewski, M.J., Peinado, V.I., Laclaustra, M., Barbera, J.A., Barbas, C., *et al.* (2016). New Biochemical Insights into the Mechanisms of Pulmonary Arterial Hypertension in Humans. PLoS One *11*, e0160505.

Butler, A., Hoffman, P., Smibert, P., Papalexi, E., and Satija, R. (2018). Integrating single-cell transcriptomic data across different conditions, technologies, and species. Nat Biotechnol *36*, 411-420.

Cagle, P.T., Ferry, G.D., Beaudet, A.L., and Hawkins, E.P. (1986). Pulmonary hypertension in an 18-year-old girl with cholesteryl ester storage disease (CESD). Am J Med Genet *24*, 711-722.

Carlin, C.M., Celnik, D.F., Pak, O., Wadsworth, R., Peacock, A.J., and Welsh, D.J. (2012). Low-dose fluvastatin reverses the hypoxic pulmonary adventitial fibroblast phenotype in experimental pulmonary hypertension. Am J Respir Cell Mol Biol *47*, 140-148.

Caslin, A.W., Heath, D., Madden, B., Yacoub, M., Gosney, J.R., and Smith, P. (1990). The histopathology of 36 cases of plexogenic pulmonary arteriopathy. Histopathology *16*, 9-19.

Castellano, B.M., Thelen, A.M., Moldavski, O., Feltes, M., van der Welle, R.E., Mydock-McGrane, L., Jiang, X., van Eijkeren, R.J., Davis, O.B., Louie, S.M., *et al.* (2017). Lysosomal cholesterol activates mTORC1 via an SLC38A9-Niemann-Pick C1 signaling complex. Science *355*, 1306-1311.

Castroflorio, E., den Hoed, J., Svistunova, D., Finelli, M.J., Cebrian-Serrano, A., Corrochano, S., Bassett, A.R., Davies, B., and Oliver, P.L. (2021). The Ncoa7 locus regulates V-ATPase formation and function, neurodevelopment and behaviour. Cell Mol Life Sci *78*, 3503-3524.

Chan, S.Y., and Loscalzo, J. (2008). Pathogenic mechanisms of pulmonary arterial hypertension. J Mol Cell Cardiol *44*, 14-30.

Chaouat, A., Coulet, F., Favre, C., Simonneau, G., Weitzenblum, E., Soubrier, F., and Humbert, M. (2004). Endoglin germline mutation in a patient with hereditary haemorrhagic telangiectasia and dexfenfluramine associated pulmonary arterial hypertension. Thorax *59*, 446-448.

Chen, R., Jiang, M., Li, B., Zhong, W., Wang, Z., Yuan, W., and Yan, J. (2018). The role of autophagy in pulmonary hypertension: a double-edge sword. Apoptosis *23*, 459-469.

Cheng, C.C., Chang, S.J., Chueh, Y.N., Huang, T.S., Huang, P.H., Cheng, S.M., Tsai, T.N., Chen, J.W., and Wang, H.W. (2013). Distinct angiogenesis roles and surface markers of early and late endothelial progenitor cells revealed by functional group analyses. BMC Genomics *14*, 182.

Cheng, T.H., Thompson, D.J., O'Mara, T.A., Painter, J.N., Glubb, D.M., Flach, S., Lewis, A., French, J.D., Freeman-Mills, L., Church, D., *et al.* (2016). Five endometrial cancer risk loci identified through genome-wide association analysis. Nat Genet *48*, 667-674.

Chichger, H., Rounds, S., and Harrington, E.O. (2019). Endosomes and Autophagy: Regulators of Pulmonary Endothelial Cell Homeostasis in Health and Disease. Antioxid Redox Signal *31*, 994-1008.

Choi, C., and Finlay, D.K. (2020). Diverse Immunoregulatory Roles of Oxysterols-The Oxidized Cholesterol Metabolites. Metabolites *10*.

Choi, Y.K., Kim, Y.S., Choi, I.Y., Kim, S.W., and Kim, W.K. (2008). 25-hydroxycholesterol induces mitochondria-dependent apoptosis via activation of glycogen synthase kinase-3beta in PC12 cells. Free Radic Res *42*, 544-553.

Chouvarine, P., Giera, M., Kastenmüller, G., Artati, A., Adamski, J., Bertram, H., and Hansmann, G. (2020). Trans-right ventricle and transpulmonary metabolite gradients in human pulmonary arterial hypertension. Heart *106*, 1332-1341.

Chu, B.B., Liao, Y.C., Qi, W., Xie, C., Du, X., Wang, J., Yang, H., Miao, H.H., Li, B.L., and Song, B.L. (2015). Cholesterol transport through lysosome-peroxisome membrane contacts. Cell *161*, 291-306.

Clague, M.J., Urbe, S., Aniento, F., and Gruenberg, J. (1994). Vacuolar ATPase activity is required for endosomal carrier vesicle formation. J Biol Chem *269*, 21-24.

Consortium, E.P. (2012). An integrated encyclopedia of DNA elements in the human genome. Nature *489*, 57-74.

Croft, D., Mundo, A.F., Haw, R., Milacic, M., Weiser, J., Wu, G., Caudy, M., Garapati, P., Gillespie, M., Kamdar, M.R., *et al.* (2014). The Reactome pathway knowledgebase. Nucleic Acids Res *42*, D472-477.

Culley, M.K., Zhao, J., Tai, Y.Y., Tang, Y., Perk, D., Negi, V., Yu, Q., Woodcock, C.C., Handen, A., Speyer, G., *et al.* (2021). Frataxin deficiency promotes endothelial senescence in pulmonary hypertension. J Clin Invest *131*.

D'Alonzo, G.E., Barst, R.J., Ayres, S.M., Bergofsky, E.H., Brundage, B.H., Detre, K.M., Fishman, A.P., Goldring, R.M., Groves, B.M., Kernis, J.T., *et al.* (1991). Survival in patients with primary pulmonary hypertension. Results from a national prospective registry. Ann Intern Med *115*, 343-349.

Davie, N., Haleen, S.J., Upton, P.D., Polak, J.M., Yacoub, M.H., Morrell, N.W., and Wharton, J. (2002). ET(A) and ET(B) receptors modulate the proliferation of human pulmonary artery smooth muscle cells. Am J Respir Crit Care Med *165*, 398-405.

de Araujo, M.E.G., Liebscher, G., Hess, M.W., and Huber, L.A. (2020). Lysosomal size matters. Traffic *21*, 60-75.

De Duve, C., and Wattiaux, R. (1966). Functions of lysosomes. Annu Rev Physiol *28*, 435-492.

DeCicco-Skinner, K.L., Henry, G.H., Cataisson, C., Tabib, T., Gwilliam, J.C., Watson, N.J., Bullwinkle, E.M., Falkenburg, L., O'Neill, R.C., Morin, A., *et al.* (2014). Endothelial cell tube formation assay for the in vitro study of angiogenesis. J Vis Exp, e51312.

Deng, Z., Morse, J.H., Slager, S.L., Cuervo, N., Moore, K.J., Venetos, G., Kalachikov, S., Cayanis, E., Fischer, S.G., Barst, R.J., *et al.* (2000). Familial primary pulmonary hypertension (gene PPH1) is caused by mutations in the bone morphogenetic protein receptor-II gene. Am J Hum Genet *67*, 737-744.

Dierks, T., Schlotawa, L., Frese, M.A., Radhakrishnan, K., von Figura, K., and Schmidt, B. (2009). Molecular basis of multiple sulfatase deficiency, mucolipidosis II/III and Niemann-Pick C1 disease - Lysosomal storage disorders caused by defects of non-lysosomal proteins. Biochim Biophys Acta *1793*, 710-725.

Diwu, Z., Chen, C.S., Zhang, C., Klaubert, D.H., and Haugland, R.P. (1999). A novel acidotropic pH indicator and its potential application in labeling acidic organelles of live cells. Chem Biol *6*, 411-418.

Docherty, C.K., Harvey, K.Y., Mair, K.M., Griffin, S., Denver, N., and MacLean, M.R. (2018). The Role of Sex in the Pathophysiology of Pulmonary Hypertension. Adv Exp Med Biol *1065*, 511-528.

Doyle, T., Moncorge, O., Bonaventure, B., Pollpeter, D., Lussignol, M., Tauziet, M., Apolonia, L., Catanese, M.T., Goujon, C., and Malim, M.H. (2018). The interferon-inducible isoform of NCOA7 inhibits endosome-mediated viral entry. Nat Microbiol *3*, 1369-1376.

Dresdale, D.T., Schultz, M., and Michtom, R.J. (1951). Primary pulmonary hypertension. I. Clinical and hemodynamic study. Am J Med *11*, 686-705.

Elstein, D., Klutstein, M.W., Lahad, A., Abrahamov, A., Hadas-Halpern, I., and Zimran, A. (1998). Echocardiographic assessment of pulmonary hypertension in Gaucher's disease. Lancet *351*, 1544-1546.

Evans, C.E., Cober, N.D., Dai, Z., Stewart, D.J., and Zhao, Y.Y. (2021). Endothelial Cells in the Pathogenesis of Pulmonary Arterial Hypertension. Eur Respir J.

Eyries, M., Montani, D., Girerd, B., Perret, C., Leroy, A., Lonjou, C., Chelghoum, N., Coulet, F., Bonnet, D., Dorfmuller, P., *et al.* (2014). EIF2AK4 mutations cause pulmonary veno-occlusive disease, a recessive form of pulmonary hypertension. Nat Genet *46*, 65-69.

Fabregat, A., Jupe, S., Matthews, L., Sidiropoulos, K., Gillespie, M., Garapati, P., Haw, R., Jassal, B., Korninger, F., May, B., *et al.* (2017). The Reactome Pathway Knowledgebase. Nucleic Acids Res.

Fang, L., Choi, S.H., Baek, J.S., Liu, C., Almazan, F., Ulrich, F., Wiesner, P., Taleb, A., Deer, E., Pattison, J., *et al.* (2013). Control of angiogenesis by AIBP-mediated cholesterol efflux. Nature *498*, 118-122.

Fessel, J.P., Hamid, R., Wittmann, B.M., Robinson, L.J., Blackwell, T., Tada, Y., Tanabe, N., Tatsumi, K., Hemnes, A.R., and West, J.D. (2012). Metabolomic analysis of bone morphogenetic protein receptor type 2 mutations in human pulmonary endothelium reveals widespread metabolic reprogramming. Pulm Circ *2*, 201-213.

Finelli, M.J., and Oliver, P.L. (2017). TLDc proteins: new players in the oxidative stress response and neurological disease. Mamm Genome *28*, 395-406.

Finelli, M.J., Sanchez-Pulido, L., Liu, K.X., Davies, K.E., and Oliver, P.L. (2016). The Evolutionarily Conserved Tre2/Bub2/Cdc16 (TBC), Lysin Motif (LysM), Domain Catalytic (TLDc) Domain Is Neuroprotective against Oxidative Stress. J Biol Chem *291*, 2751-2763.

Foderaro, A., and Ventetuolo, C.E. (2016). Pulmonary Arterial Hypertension and the Sex Hormone Paradox. Curr Hypertens Rep *18*, 84.

Forgac, M. (2007). Vacuolar ATPases: rotary proton pumps in physiology and pathophysiology. Nat Rev Mol Cell Biol *8*, 917-929.

Frost, A., Badesch, D., Gibbs, J.S.R., Gopalan, D., Khanna, D., Manes, A., Oudiz, R., Satoh, T., Torres, F., and Torbicki, A. (2019). Diagnosis of pulmonary hypertension. Eur Respir J *53*.

Frost, A.E., Badesch, D.B., Barst, R.J., Benza, R.L., Elliott, C.G., Farber, H.W., Krichman, A., Liou, T.G., Raskob, G.E., Wason, P., *et al.* (2011). The changing picture of patients with pulmonary arterial hypertension in the United States: how REVEAL differs from historic and non-US Contemporary Registries. Chest *139*, 128-137.

Gao, Q., Lopez-Knowles, E., Cheang, M.C.U., Morden, J., Ribas, R., Sidhu, K., Evans, D., Martins, V., Dodson, A., Skene, A., *et al.* (2019). Impact of aromatase inhibitor treatment on global gene expression and its association with antiproliferative response in ER+ breast cancer in postmenopausal patients. Breast Cancer Res *22*, 2.

Gareus, R., Kotsaki, E., Xanthoulea, S., van der Made, I., Gijbels, M.J., Kardakaris, R., Polykratis, A., Kollias, G., de Winther, M.P., and Pasparakis, M. (2008). Endothelial cell-specific NF-kappaB inhibition protects mice from atherosclerosis. Cell Metab *8*, 372-383.

Giannotta, M., Trani, M., and Dejana, E. (2013). VE-cadherin and endothelial adherens junctions: active guardians of vascular integrity. Dev Cell *26*, 441-454.

Goldthorpe, H., Jiang, J.Y., Taha, M., Deng, Y., Sinclair, T., Ge, C.X., Jurasz, P., Turksen, K., Mei, S.H., and Stewart, D.J. (2015). Occlusive lung arterial lesions in endothelial-targeted, fas-induced apoptosis transgenic mice. Am J Respir Cell Mol Biol *53*, 712-718.

Gomberg-Maitland, M., and Olschewski, H. (2008). Prostacyclin therapies for the treatment of pulmonary arterial hypertension. Eur Respir J *31*, 891-901.

Goveia, J., Stapor, P., and Carmeliet, P. (2014). Principles of targeting endothelial cell metabolism to treat angiogenesis and endothelial cell dysfunction in disease. EMBO Mol Med *6*, 1105-1120.

Gu, M. (2018). Efficient Differentiation of Human Pluripotent Stem Cells to Endothelial Cells. Curr Protoc Hum Genet, e64.

Gurtner, H.P. (1972). [Pulmonary hypertension following appetite depressants]. Med Welt *23*, 1036-1041.

Hafemeister, C., and Satija, R. (2019). Normalization and variance stabilization of single-cell RNA-seq data using regularized negative binomial regression. Genome Biol *20*, 296.

Harbaum, L., Ghataorhe, P., Wharton, J., Jimenez, B., Howard, L.S.G., Gibbs, J.S.R., Nicholson, J.K., Rhodes, C.J., and Wilkins, M.R. (2019). Reduced plasma levels of small HDL particles transporting fibrinolytic proteins in pulmonary arterial hypertension. Thorax *74*, 380-389.

Harlan, F.K., Lusk, J.S., Mohr, B.M., Guzikowski, A.P., Batchelor, R.H., Jiang, Y., and Naleway, J.J. (2016). Fluorogenic Substrates for Visualizing Acidic Organelle Enzyme Activities. PLoS One *11*, e0156312.

Harrison, R.E., Berger, R., Haworth, S.G., Tulloh, R., Mache, C.J., Morrell, N.W., Aldred, M.A., and Trembath, R.C. (2005). Transforming growth factor-beta receptor mutations and pulmonary arterial hypertension in childhood. Circulation *111*, 435-441.

Harvey, L.D., and Chan, S.Y. (2019). Evolving systems biology approaches to understanding non-coding RNAs in pulmonary hypertension. J Physiol *597*, 1199-1208.

Hatano, S., and Strasser, T. (1975). Primary pulmonary hypertension : report on a WHO meeting, Geneva, 15-17 October 1973 (Geneva
Albany, N.Y.: World Health Organization ;
distributed by Q Corporation).

Hautefort, A., Chesne, J., Preussner, J., Pullamsetti, S.S., Tost, J., Looso, M., Antigny, F., Girerd, B., Riou, M., Eddahibi, S., *et al.* (2017). Pulmonary endothelial cell DNA methylation signature in pulmonary arterial hypertension. Oncotarget *8*, 52995-53016.

Heresi, G.A., Aytekin, M., Newman, J., DiDonato, J., and Dweik, R.A. (2010). Plasma levels of high-density lipoprotein cholesterol and outcomes in pulmonary arterial hypertension. Am J Respir Crit Care Med *182*, 661-668.

Heybrock, S., Kanerva, K., Meng, Y., Ing, C., Liang, A., Xiong, Z.J., Weng, X., Ah Kim, Y., Collins, R., Trimble, W., *et al.* (2019). Lysosomal integral membrane protein-2 (LIMP-2/SCARB2) is involved in lysosomal cholesterol export. Nat Commun *10*, 3521.

Higginbotham, K.S., Breyer, J.P., Bradley, K.M., Schuyler, P.A., Plummer, W.D., Jr., Freudenthal, M.E., Trentham-Dietz, A., Newcomb, P.A., Sanders, M.E., Page, D.L., *et al.* (2011). A multistage association study identifies a breast cancer genetic locus at NCOA7. Cancer Res *71*, 3881-3888.

Hoeper, M.M., Bogaard, H.J., Condliffe, R., Frantz, R., Khanna, D., Kurzyna, M., Langleben, D., Manes, A., Satoh, T., Torres, F., *et al.* (2013). Definitions and diagnosis of pulmonary hypertension. J Am Coll Cardiol *62*, D42-50.

Hoglinger, D., Burgoyne, T., Sanchez-Heras, E., Hartwig, P., Colaco, A., Newton, J., Futter, C.E., Spiegel, S., Platt, F.M., and Eden, E.R. (2019). NPC1 regulates ER contacts with endocytic organelles to mediate cholesterol egress. Nat Commun *10*, 4276.

Hu, Y., Chi, L., Kuebler, W.M., and Goldenberg, N.M. (2020). Perivascular Inflammation in Pulmonary Arterial Hypertension. Cells *9*.

Humbert, M., Guignabert, C., Bonnet, S., Dorfmuller, P., Klinger, J.R., Nicolls, M.R., Olschewski, A.J., Pullamsetti, S.S., Schermuly, R.T., Stenmark, K.R., *et al.* (2019). Pathology and pathobiology of pulmonary hypertension: state of the art and research perspectives. Eur Respir J *53*.

Humbert, M., Sitbon, O., and Simonneau, G. (2004). Treatment of pulmonary arterial hypertension. N Engl J Med *351*, 1425-1436.

Huttlin, E.L., Ting, L., Bruckner, R.J., Gebreab, F., Gygi, M.P., Szpyt, J., Tam, S., Zarraga, G., Colby, G., Baltier, K., *et al.* (2015). The BioPlex Network: A Systematic Exploration of the Human Interactome. Cell *162*, 425-440.

Ikeda, T., Nakamura, K., Akagi, S., Kusano, K.F., Matsubara, H., Fujio, H., Ogawa, A., Miura, A., Miura, D., Oto, T., *et al.* (2010). Inhibitory effects of simvastatin on platelet-derived growth factor signaling in pulmonary artery smooth muscle cells from patients with idiopathic pulmonary arterial hypertension. J Cardiovasc Pharmacol *55*, 39-48.

International, P.P.H.C., Lane, K.B., Machado, R.D., Pauciulo, M.W., Thomson, J.R., Phillips, J.A., 3rd, Loyd, J.E., Nichols, W.C., and Trembath, R.C. (2000). Heterozygous germline mutations in BMPR2, encoding a TGF-beta receptor, cause familial primary pulmonary hypertension. Nat Genet *26*, 81-84.

Ishak, M., Zambrano, E.V., Bazzy-Asaad, A., and Esquibies, A.E. (2012). Unusual pulmonary findings in mucolipidosis II. Pediatr Pulmonol *47*, 719-721.

Ivashchenko, C.Y., Bradley, B.T., Ao, Z., Leiper, J., Vallance, P., and Johns, D.G. (2010). Regulation of the ADMA-DDAH system in endothelial cells: a novel mechanism for the sterol response element binding proteins, SREBP1c and -2. Am J Physiol Heart Circ Physiol *298*, H251-258.

James, D., Nam, H.S., Seandel, M., Nolan, D., Janovitz, T., Tomishima, M., Studer, L., Lee, G., Lyden, D., Benezra, R., *et al.* (2010). Expansion and maintenance of human embryonic stem cell-derived endothelial cells by TGFbeta inhibition is Id1 dependent. Nat Biotechnol *28*, 161-166.

Javitt, N.B. (1994). Bile acid synthesis from cholesterol: regulatory and auxiliary pathways. FASEB J *8*, 1308-1311.

Johnson, D.E., Ostrowski, P., Jaumouille, V., and Grinstein, S. (2016). The position of lysosomes within the cell determines their luminal pH. J Cell Biol *212*, 677-692.

Jonas, K., Magon, W., Waligora, M., Seweryn, M., Podolec, P., and Kopec, G. (2018). Highdensity lipoprotein cholesterol levels and pulmonary artery vasoreactivity in patients with idiopathic pulmonary arterial hypertension. Pol Arch Intern Med *128*, 440-446.

Jonas, K., Waligora, M., Magon, W., Zdrojewski, T., Stokwiszewski, J., Plazak, W., Podolec, P., and Kopec, G. (2019). Prognostic role of traditional cardiovascular risk factors in patients with idiopathic pulmonary arterial hypertension. Arch Med Sci *15*, 1397-1406.

Kanehisa, M., Furumichi, M., Tanabe, M., Sato, Y., and Morishima, K. (2017). KEGG: new perspectives on genomes, pathways, diseases and drugs. Nucleic Acids Res *45*, D353-D361.

Kantz, E.D., Tiwari, S., Watrous, J.D., Cheng, S., and Jain, M. (2019). Deep Neural Networks for Classification of LC-MS Spectral Peaks. Anal Chem *91*, 12407-12413.

Katheria, A.C., Masliah, E., Benirschke, K., Jones, K.L., and Kim, J.H. (2010). Idiopathic persistent pulmonary hypertension in an infant with Smith-Lemli-Opitz syndrome. Fetal Pediatr Pathol *29*, 373-379.

Kent, W.J., Sugnet, C.W., Furey, T.S., Roskin, K.M., Pringle, T.H., Zahler, A.M., and Haussler, D. (2002). The human genome browser at UCSC. Genome Res *12*, 996-1006.

Kerstjens-Frederikse, W.S., Bongers, E.M., Roofthooft, M.T., Leter, E.M., Douwes, J.M., Van Dijk, A., Vonk-Noordegraaf, A., Dijk-Bos, K.K., Hoefsloot, L.H., Hoendermis, E.S., *et al.* (2013). TBX4 mutations (small patella syndrome) are associated with childhood-onset pulmonary arterial hypertension. J Med Genet *50*, 500-506.

Kopec, G., Waligora, M., Tyrka, A., Jonas, K., Pencina, M.J., Zdrojewski, T., Moertl, D., Stokwiszewski, J., Zagozdzon, P., and Podolec, P. (2017). Low-density lipoprotein cholesterol and survival in pulmonary arterial hypertension. Sci Rep *7*, 41650.

Kovacs, G., Berghold, A., Scheidl, S., and Olschewski, H. (2009). Pulmonary arterial pressure during rest and exercise in healthy subjects: a systematic review. Eur Respir J *34*, 888-894.

Krietenstein, N., Abraham, S., Venev, S.V., Abdennur, N., Gibcus, J., Hsieh, T.S., Parsi, K.M., Yang, L., Maehr, R., Mirny, L.A., *et al.* (2020). Ultrastructural Details of Mammalian Chromosome Architecture. Mol Cell *78*, 554-565.e557.

Lagerborg, K.A., Watrous, J.D., Cheng, S., and Jain, M. (2019). High-Throughput Measure of Bioactive Lipids Using Non-targeted Mass Spectrometry. Methods Mol Biol *1862*, 17-35.

Lange, Y., Ye, J., and Strebel, F. (1995). Movement of 25-hydroxycholesterol from the plasma membrane to the rough endoplasmic reticulum in cultured hepatoma cells. J Lipid Res *36*, 1092-1097.

Larsen, C.M., McCully, R.B., Murphy, J.G., Kushwaha, S.S., Frantz, R.P., and Kane, G.C. (2016). Usefulness of High-Density Lipoprotein Cholesterol to Predict Survival in Pulmonary Arterial Hypertension. Am J Cardiol *118*, 292-297.

Lau, E.M.T., Giannoulatou, E., Celermajer, D.S., and Humbert, M. (2017). Epidemiology and treatment of pulmonary arterial hypertension. Nat Rev Cardiol *14*, 603-614.

Le Goff, D., Viville, C., and Carreau, S. (2006). Apoptotic effects of 25-hydroxycholesterol in immature rat Sertoli cells: prevention by 17beta-estradiol. Reprod Toxicol *21*, 329-334.

Lee, S.D., Shroyer, K.R., Markham, N.E., Cool, C.D., Voelkel, N.F., and Tuder, R.M. (1998). Monoclonal endothelial cell proliferation is present in primary but not secondary pulmonary hypertension. J Clin Invest *101*, 927-934.

Leroy, J.G., and Demars, R.I. (1967). Mutant enzymatic and cytological phenotypes in cultured human fibroblasts. Science *157*, 804-806.

Levine, D.J. (2021). Pulmonary arterial hypertension: updates in epidemiology and evaluation of patients. Am J Manag Care *27*, S35-S41.

Levy, M., Eyries, M., Szezepanski, I., Ladouceur, M., Nadaud, S., Bonnet, D., and Soubrier, F. (2016). Genetic analyses in a cohort of children with pulmonary hypertension. Eur Respir J *48*, 1118-1126.

Lewis, G.D. (2014). The emerging role of metabolomics in the development of biomarkers for pulmonary hypertension and other cardiovascular diseases (2013 Grover Conference series). Pulm Circ *4*, 417-423.

Li, Y., Li, W., Liu, C., Yan, M., Raman, I., Du, Y., Fang, X., Zhou, X.J., Mohan, C., and Li, Q.Z. (2014). Delivering Oxidation Resistance-1 (OXR1) to Mouse Kidney by Genetic Modified Mesenchymal Stem Cells Exhibited Enhanced Protection against Nephrotoxic Serum Induced Renal Injury and Lupus Nephritis. J Stem Cell Res Ther *4*.

Lian, X., Zhang, J., Zhu, K., Kamp, T.J., and Palecek, S.P. (2013). Insulin inhibits cardiac mesoderm, not mesendoderm, formation during cardiac differentiation of human pluripotent stem cells and modulation of canonical Wnt signaling can rescue this inhibition. Stem Cells *31*, 447-457.

Liu, C., Chen, J., Gao, Y., Deng, B., and Liu, K. (2021). Endothelin receptor antagonists for pulmonary arterial hypertension. Cochrane Database Syst Rev *3*, CD004434.

Long, L., Yang, X., Southwood, M., Lu, J., Marciniak, S.J., Dunmore, B.J., and Morrell, N.W. (2013). Chloroquine prevents progression of experimental pulmonary hypertension via inhibition of autophagy and lysosomal bone morphogenetic protein type II receptor degradation. Circ Res *112*, 1159-1170.

Lukinavičius, G., Reymond, L., Umezawa, K., Sallin, O., D'Este, E., Göttfert, F., Ta, H., Hell, S.W., Urano, Y., and Johnsson, K. (2016). Fluorogenic Probes for Multicolor Imaging in Living Cells. J Am Chem Soc *138*, 9365-9368.

Lund, E., Andersson, O., Zhang, J., Babiker, A., Ahlborg, G., Diczfalusy, U., Einarsson, K., Sjovall, J., and Bjorkhem, I. (1996). Importance of a novel oxidative mechanism for elimination of intracellular cholesterol in humans. Arterioscler Thromb Vasc Biol *16*, 208-212.

Luo, J., Yang, H., and Song, B.L. (2020). Mechanisms and regulation of cholesterol homeostasis. Nat Rev Mol Cell Biol *21*, 225-245.

Luthy, E. (1975). Proceedings: The epidemic of primary pulmonary hypertension in Europe. Pathol Microbiol (Basel) *43*, 246-247.

Luzio, J.P., Pryor, P.R., and Bright, N.A. (2007). Lysosomes: fusion and function. Nat Rev Mol Cell Biol *8*, 622-632.

Ma, L., Roman-Campos, D., Austin, E.D., Eyries, M., Sampson, K.S., Soubrier, F., Germain, M., Tregouet, D.A., Borczuk, A., Rosenzweig, E.B., *et al.* (2013). A novel channelopathy in pulmonary arterial hypertension. N Engl J Med *369*, 351-361.

Madenspacher, J.H., Morrell, E.D., Gowdy, K.M., McDonald, J.G., Thompson, B.M., Muse, G., Martinez, J., Thomas, S., Mikacenic, C., Nick, J.A., *et al.* (2020). Cholesterol 25-hydroxylase promotes efferocytosis and resolution of lung inflammation. JCI Insight *5*.

Mai, J., Virtue, A., Shen, J., Wang, H., and Yang, X.F. (2013). An evolving new paradigm: endothelial cells--conditional innate immune cells. J Hematol Oncol *6*, 61.

Marciniszyn, J., Hartsuck, J.A., and Tang, J. (1976). Mode of inhibition of acid proteases by pepstatin. J Biol Chem *251*, 7088-7094.

Masri, F.A., Xu, W., Comhair, S.A., Asosingh, K., Koo, M., Vasanji, A., Drazba, J., Anand-Apte, B., and Erzurum, S.C. (2007). Hyperproliferative apoptosis-resistant endothelial cells in idiopathic pulmonary arterial hypertension. Am J Physiol Lung Cell Mol Physiol *293*, L548-554.

McDonald, J.G., Smith, D.D., Stiles, A.R., and Russell, D.W. (2012). A comprehensive method for extraction and quantitative analysis of sterols and secosteroids from human plasma. J Lipid Res *53*, 1399-1409.

McGoon, M.D., Krichman, A., Farber, H.W., Barst, R.J., Raskob, G.E., Liou, T.G., Miller, D.P., Feldkircher, K., and Giles, S. (2008). Design of the REVEAL registry for US patients with pulmonary arterial hypertension. Mayo Clin Proc *83*, 923-931.

McGoon, M.D., and Miller, D.P. (2012). REVEAL: a contemporary US pulmonary arterial hypertension registry. Eur Respir Rev *21*, 8-18.

McMahon, T.J., and Bryan, N.S. (2017). Biomarkers in Pulmonary Vascular Disease: Gauging Response to Therapy. Am J Cardiol *120*, S89-S95.

Meaney, S., Bodin, K., Diczfalusy, U., and Bjorkhem, I. (2002). On the rate of translocation in vitro and kinetics in vivo of the major oxysterols in human circulation: critical importance of the position of the oxygen function. J Lipid Res *43*, 2130-2135.

Meng, Y., Heybrock, S., Neculai, D., and Saftig, P. (2020). Cholesterol Handling in Lysosomes and Beyond. Trends Cell Biol *30*, 452-466.

Merkulova, M., Paunescu, T.G., Azroyan, A., Marshansky, V., Breton, S., and Brown, D. (2015). Mapping the H(+) (V)-ATPase interactome: identification of proteins involved in trafficking, folding, assembly and phosphorylation. Sci Rep *5*, 14827.

Mindell, J.A. (2012). Lysosomal acidification mechanisms. Annu Rev Physiol *74*, 69-86.

Murata, T., Kinoshita, K., Hori, M., Kuwahara, M., Tsubone, H., Karaki, H., and Ozaki, H. (2005). Statin protects endothelial nitric oxide synthase activity in hypoxia-induced pulmonary hypertension. Arterioscler Thromb Vasc Biol *25*, 2335-2342.

Nasim, M.T., Ogo, T., Ahmed, M., Randall, R., Chowdhury, H.M., Snape, K.M., Bradshaw, T.Y., Southgate, L., Lee, G.J., Jackson, I., *et al.* (2011). Molecular genetic characterization of SMAD signaling molecules in pulmonary arterial hypertension. Hum Mutat *32*, 1385-1389.

Navarro, J., Rainisio, M., Harms, H.K., Hodson, M.E., Koch, C., Mastella, G., Strandvik, B., and McKenzie, S.G. (2001). Factors associated with poor pulmonary function: cross-sectional analysis of data from the ERCF. European Epidemiologic Registry of Cystic Fibrosis. Eur Respir J *18*, 298-305.

Nishimura, D. (2001). BioCarta. Biotechnology Software & Internet Journal *2*, 117-120.

Nowaczyk, M.J., Waye, J.S., and Douketis, J.D. (2006). DHCR7 mutation carrier rates and prevalence of the RSH/Smith-Lemli-Opitz syndrome: where are the patients? Am J Med Genet A *140*, 2057-2062.

Paulin, R., and Michelakis, E.D. (2012). The estrogen puzzle in pulmonary arterial hypertension. Circulation *126*, 1016-1019.

Paulin, R., and Michelakis, E.D. (2014). The metabolic theory of pulmonary arterial hypertension. Circ Res *115*, 148-164.

Pauwels, A., Decraene, A., Blondeau, K., Mertens, V., Farre, R., Proesmans, M., Van Bleyenbergh, P., Sifrim, D., and Dupont, L.J. (2012). Bile acids in sputum and increased airway inflammation in patients with cystic fibrosis. Chest *141*, 1568-1574.

Payne, S., De Val, S., and Neal, A. (2018). Endothelial-Specific Cre Mouse Models. Arterioscler Thromb Vasc Biol *38*, 2550-2561.

Peacock, A.J. (1999). Primary pulmonary hypertension. Thorax *54*, 1107-1118.

Phillips, J.A., 3rd, Poling, J.S., Phillips, C.A., Stanton, K.C., Austin, E.D., Cogan, J.D., Wheeler, L., Yu, C., Newman, J.H., Dietz, H.C., *et al.* (2008). Synergistic heterozygosity for TGFbeta1 SNPs and BMPR2 mutations modulates the age at diagnosis and penetrance of familial pulmonary arterial hypertension. Genet Med *10*, 359-365.

Platt, F.M., Boland, B., and van der Spoel, A.C. (2012). The cell biology of disease: lysosomal storage disorders: the cellular impact of lysosomal dysfunction. J Cell Biol *199*, 723-734.

Porter, F.D., and Herman, G.E. (2011). Malformation syndromes caused by disorders of cholesterol synthesis. J Lipid Res *52*, 6-34.

Potteaux, S., Ait-Oufella, H., and Mallat, Z. (2015). Role of splenic monocytes in atherosclerosis. Curr Opin Lipidol *26*, 457-463.

Price, L.C., Caramori, G., Perros, F., Meng, C., Gambaryan, N., Dorfmuller, P., Montani, D., Casolari, P., Zhu, J., Dimopoulos, K., *et al.* (2013). Nuclear factor κ-B is activated in the pulmonary vessels of patients with end-stage idiopathic pulmonary arterial hypertension. PLoS One *8*, e75415.

Prosnitz, A.R., Leopold, J., Irons, M., Jenkins, K., and Roberts, A.E. (2017). Pulmonary vein stenosis in patients with Smith-Lemli-Opitz syndrome. Congenit Heart Dis *12*, 475-483.

Qin, P., Tang, X., Elloso, M.M., and Harnish, D.C. (2006). Bile acids induce adhesion molecule expression in endothelial cells through activation of reactive oxygen species, NF-kappaB, and p38. Am J Physiol Heart Circ Physiol *291*, H741-747.

Qiu, B., and Simon, M.C. (2016). BODIPY 493/503 Staining of Neutral Lipid Droplets for Microscopy and Quantification by Flow Cytometry. Bio Protoc *6*.

Rabinovitch, M., Guignabert, C., Humbert, M., and Nicolls, M.R. (2014). Inflammation and immunity in the pathogenesis of pulmonary arterial hypertension. Circ Res *115*, 165-175.

Ran, F.A., Hsu, P.D., Wright, J., Agarwala, V., Scott, D.A., and Zhang, F. (2013). Genome engineering using the CRISPR-Cas9 system. Nat Protoc *8*, 2281-2308.

Reboldi, A., Dang, E.V., McDonald, J.G., Liang, G., Russell, D.W., and Cyster, J.G. (2014). Inflammation. 25-Hydroxycholesterol suppresses interleukin-1-driven inflammation downstream of type I interferon. Science *345*, 679-684.

Recla, S., Hahn, A., and Apitz, C. (2015). Pulmonary arterial hypertension associated with impaired lysosomal endothelin-1 degradation. Cardiol Young *25*, 773-776.

Reiss, A.B., Martin, K.O., Javitt, N.B., Martin, D.W., Grossi, E.A., and Galloway, A.C. (1994). Sterol 27-hydroxylase: high levels of activity in vascular endothelium. J Lipid Res *35*, 1026-1030.

Ren, S., and Ning, Y. (2014). Sulfation of 25-hydroxycholesterol regulates lipid metabolism, inflammatory responses, and cell proliferation. Am J Physiol Endocrinol Metab *306*, E123-130.

Rhodes, C.J., Batai, K., Bleda, M., Haimel, M., Southgate, L., Germain, M., Pauciulo, M.W., Hadinnapola, C., Aman, J., Girerd, B., *et al.* (2019). Genetic determinants of risk in pulmonary arterial hypertension: international genome-wide association studies and meta-analysis. Lancet Respir Med *7*, 227-238.

Rhodes, C.J., Ghataorhe, P., Wharton, J., Rue-Albrecht, K.C., Hadinnapola, C., Watson, G., Bleda, M., Haimel, M., Coghlan, G., Corris, P.A., *et al.* (2017). Plasma Metabolomics Implicates Modified Transfer RNAs and Altered Bioenergetics in the Outcomes of Pulmonary Arterial Hypertension. Circulation *135*, 460-475.

Rich, S., Dantzker, D.R., Ayres, S.M., Bergofsky, E.H., Brundage, B.H., Detre, K.M., Fishman, A.P., Goldring, R.M., Groves, B.M., Koerner, S.K., *et al.* (1987). Primary pulmonary hypertension. A national prospective study. Ann Intern Med *107*, 216-223.

Ross, D.J., Hough, G., Hama, S., Aboulhosn, J., Belperio, J.A., Saggar, R., Van Lenten, B.J., Ardehali, A., Eghbali, M., Reddy, S., *et al.* (2015). Proinflammatory high-density lipoprotein results from oxidized lipid mediators in the pathogenesis of both idiopathic and associated types of pulmonary arterial hypertension. Pulm Circ *5*, 640-648.

Runo, J.R., and Loyd, J.E. (2003). Primary pulmonary hypertension. Lancet *361*, 1533-1544.

Sakao, S., Taraseviciene-Stewart, L., Lee, J.D., Wood, K., Cool, C.D., and Voelkel, N.F. (2005). Initial apoptosis is followed by increased proliferation of apoptosis-resistant endothelial cells. FASEB J *19*, 1178-1180.

Schermuly, R.T., Stasch, J.P., Pullamsetti, S.S., Middendorff, R., Muller, D., Schluter, K.D., Dingendorf, A., Hackemack, S., Kolosionek, E., Kaulen, C., *et al.* (2008). Expression and function of soluble guanylate cyclase in pulmonary arterial hypertension. Eur Respir J *32*, 881-891.

Sehgal, P.B., and Lee, J.E. (2011). Protein trafficking dysfunctions: Role in the pathogenesis of pulmonary arterial hypertension. Pulm Circ *1*, 17-32.

Shao, W., Halachmi, S., and Brown, M. (2002). ERAP140, a conserved tissue-specific nuclear receptor coactivator. Mol Cell Biol *22*, 3358-3372.

Shapiro, S., Traiger, G.L., Turner, M., McGoon, M.D., Wason, P., and Barst, R.J. (2012). Sex differences in the diagnosis, treatment, and outcome of patients with pulmonary arterial hypertension enrolled in the registry to evaluate early and long-term pulmonary arterial hypertension disease management. Chest *141*, 363-373.

Sharma, S., Ruffenach, G., Umar, S., Motayagheni, N., Reddy, S.T., and Eghbali, M. (2016). Role of oxidized lipids in pulmonary arterial hypertension. Pulm Circ *6*, 261-273.

Shatat, M.A., Tian, H., Zhang, R., Tandon, G., Hale, A., Fritz, J.S., Zhou, G., Martinez-Gonzalez, J., Rodriguez, C., Champion, H.C., *et al.* (2014). Endothelial Kruppel-like factor 4 modulates pulmonary arterial hypertension. Am J Respir Cell Mol Biol *50*, 647-653.

Shentu, T.P., Singh, D.K., Oh, M.J., Sun, S., Sadaat, L., Makino, A., Mazzone, T., Subbaiah, P.V., Cho, M., and Levitan, I. (2012). The role of oxysterols in control of endothelial stiffness. J Lipid Res *53*, 1348-1358.

Shi, Y., Inoue, H., Wu, J.C., and Yamanaka, S. (2017). Induced pluripotent stem cell technology: a decade of progress. Nat Rev Drug Discov *16*, 115-130.

Shintani, M., Yagi, H., Nakayama, T., Saji, T., and Matsuoka, R. (2009). A new nonsense mutation of SMAD8 associated with pulmonary arterial hypertension. J Med Genet *46*, 331-337.

Shkolnik, K., Ben-Dor, S., Galiani, D., Hourvitz, A., and Dekel, N. (2008). Molecular characterization and bioinformatics analysis of Ncoa7B, a novel ovulation-associated and reproduction system-specific Ncoa7 isoform. Reproduction *135*, 321-333.

Simonneau, G., Montani, D., Celermajer, D.S., Denton, C.P., Gatzoulis, M.A., Krowka, M., Williams, P.G., and Souza, R. (2019). Haemodynamic definitions and updated clinical classification of pulmonary hypertension. Eur Respir J *53*.

Sitbon, O., Channick, R., Chin, K.M., Frey, A., Gaine, S., Galie, N., Ghofrani, H.A., Hoeper, M.M., Lang, I.M., Preiss, R., *et al.* (2015). Selexipag for the Treatment of Pulmonary Arterial Hypertension. N Engl J Med *373*, 2522-2533.

Soon, E., Holmes, A.M., Treacy, C.M., Doughty, N.J., Southgate, L., Machado, R.D., Trembath, R.C., Jennings, S., Barker, L., Nicklin, P., *et al.* (2010). Elevated levels of inflammatory cytokines predict survival in idiopathic and familial pulmonary arterial hypertension. Circulation *122*, 920-927.

Stauffer, W., Sheng, H., and Lim, H.N. (2018). EzColocalization: An ImageJ plugin for visualizing and measuring colocalization in cells and organisms. Sci Rep *8*, 15764.

Steiner, M.K., Syrkina, O.L., Kolliputi, N., Mark, E.J., Hales, C.A., and Waxman, A.B. (2009). Interleukin-6 overexpression induces pulmonary hypertension. Circ Res *104*, 236-244, 228p following 244.

Stenmark, K.R., Fagan, K.A., and Frid, M.G. (2006). Hypoxia-induced pulmonary vascular remodeling: cellular and molecular mechanisms. Circ Res *99*, 675-691.

Stuart, T., Butler, A., Hoffman, P., Hafemeister, C., Papalexi, E., Mauck, W.M., 3rd, Hao, Y., Stoeckius, M., Smibert, P., and Satija, R. (2019). Comprehensive Integration of Single-Cell Data. Cell *177*, 1888-1902 e1821.

Sullner, J., Lattrich, C., Haring, J., Gorse, R., Ortmann, O., and Treeck, O. (2012). A polymorphism in the nuclear receptor coactivator 7 gene and breast cancer susceptibility. Oncol Lett *3*, 131-134.

Taraseviciene-Stewart, L., Scerbavicius, R., Choe, K.H., Cool, C., Wood, K., Tuder, R.M., Burns, N., Kasper, M., and Voelkel, N.F. (2006). Simvastatin causes endothelial cell apoptosis and attenuates severe pulmonary hypertension. Am J Physiol Lung Cell Mol Physiol *291*, L668-676.

The Gene Ontology, C. (2017). Expansion of the Gene Ontology knowledgebase and resources. Nucleic Acids Res *45*, D331-D338.

Thelen, A.M., and Zoncu, R. (2017). Emerging Roles for the Lysosome in Lipid Metabolism. Trends Cell Biol *27*, 833-850.

Thomson, J.R., Machado, R.D., Pauciulo, M.W., Morgan, N.V., Humbert, M., Elliott, G.C., Ward, K., Yacoub, M., Mikhail, G., Rogers, P., *et al.* (2000). Sporadic primary pulmonary hypertension is associated with germline mutations of the gene encoding BMPR-II, a receptor member of the TGF-beta family. J Med Genet *37*, 741-745.

Trembath, R.C., Thomson, J.R., Machado, R.D., Morgan, N.V., Atkinson, C., Winship, I., Simonneau, G., Galie, N., Loyd, J.E., Humbert, M., *et al.* (2001). Clinical and molecular genetic features of pulmonary hypertension in patients with hereditary hemorrhagic telangiectasia. N Engl J Med *345*, 325-334.

Tu, L., Dewachter, L., Gore, B., Fadel, E., Dartevelle, P., Simonneau, G., Humbert, M., Eddahibi, S., and Guignabert, C. (2011). Autocrine fibroblast growth factor-2 signaling contributes to altered endothelial phenotype in pulmonary hypertension. Am J Respir Cell Mol Biol *45*, 311-322.

Tuder, R.M., Davis, L.A., and Graham, B.B. (2012). Targeting energetic metabolism: a new frontier in the pathogenesis and treatment of pulmonary hypertension. Am J Respir Crit Care Med *185*, 260-266.

Tuder, R.M., Groves, B., Badesch, D.B., and Voelkel, N.F. (1994). Exuberant endothelial cell growth and elements of inflammation are present in plexiform lesions of pulmonary hypertension. Am J Pathol *144*, 275-285.

Tuder, R.M., Marecki, J.C., Richter, A., Fijalkowska, I., and Flores, S. (2007). Pathology of pulmonary hypertension. Clin Chest Med *28*, 23-42, vii.

Tzima, E., Irani-Tehrani, M., Kiosses, W.B., Dejana, E., Schultz, D.A., Engelhardt, B., Cao, G., DeLisser, H., and Schwartz, M.A. (2005). A mechanosensory complex that mediates the endothelial cell response to fluid shear stress. Nature *437*, 426-431.

Umar, S., Ruffenach, G., Moazeni, S., Vaillancourt, M., Hong, J., Cunningham, C., Cao, N., Navab, S., Sarji, S., Li, M., *et al.* (2020). Involvement of Low-Density Lipoprotein Receptor in the Pathogenesis of Pulmonary Hypertension. J Am Heart Assoc *9*, e012063.

Van Damme, T., Gardeitchik, T., Mohamed, M., Guerrero-Castillo, S., Freisinger, P., Guillemyn, B., Kariminejad, A., Dalloyaux, D., van Kraaij, S., Lefeber, D.J., *et al.* (2017). Mutations in ATP6V1E1 or ATP6V1A Cause Autosomal-Recessive Cutis Laxa. Am J Hum Genet *100*, 216-227.

Vockley, J., Dobrowolski, S.F., Arnold, G.L., Guerrero, R.B., Derks, T.G.J., and Weinstein, D.A. (2019). Complex patterns of inheritance, including synergistic heterozygosity, in inborn errors of metabolism: Implications for precision medicine driven diagnosis and treatment. Mol Genet Metab *128*, 1-9.

Vockley, J., Rinaldo, P., Bennett, M.J., Matern, D., and Vladutiu, G.D. (2000). Synergistic heterozygosity: disease resulting from multiple partial defects in one or more metabolic pathways. Mol Genet Metab *71*, 10-18.

Wang, J., Rousseau, J., Kim, E., Ehresmann, S., Cheng, Y.T., Duraine, L., Zuo, Z., Park, Y.J., Li-Kroeger, D., Bi, W., *et al.* (2019). Loss of Oxidation Resistance 1, OXR1, Is Associated with an Autosomal-Recessive Neurological Disease with Cerebellar Atrophy and Lysosomal Dysfunction. Am J Hum Genet *105*, 1237-1253.

Wang, L., Yang, T., and Wang, C. (2017). Are statins beneficial for the treatment of pulmonary hypertension? Chronic Dis Transl Med *3*, 213-220.

Wang, Z., Berkey, C.D., and Watnick, P.I. (2012). The Drosophila protein mustard tailors the innate immune response activated by the immune deficiency pathway. J Immunol *188*, 3993-4000.

Warburg, O. (1956). On the origin of cancer cells. Science *123*, 309-314.

Ward, J.P., and McMurtry, I.F. (2009). Mechanisms of hypoxic pulmonary vasoconstriction and their roles in pulmonary hypertension: new findings for an old problem. Curr Opin Pharmacol *9*, 287-296.

Watrous, J.D., Niiranen, T.J., Lagerborg, K.A., Henglin, M., Xu, Y.J., Rong, J., Sharma, S., Vasan, R.S., Larson, M.G., Armando, A., *et al.* (2019). Directed Non-targeted Mass Spectrometry and Chemical Networking for Discovery of Eicosanoids and Related Oxylipins. Cell Chem Biol *26*, 433-442 e434.

Whetzel, A.M., Sturek, J.M., Nagelin, M.H., Bolick, D.T., Gebre, A.K., Parks, J.S., Bruce, A.C., Skaflen, M.D., and Hedrick, C.C. (2010). ABCG1 deficiency in mice promotes endothelial activation and monocyte-endothelial interactions. Arterioscler Thromb Vasc Biol *30*, 809-817.

Wienerroither, S., Shukla, P., Farlik, M., Majoros, A., Stych, B., Vogl, C., Cheon, H., Stark, G.R., Strobl, B., Muller, M., *et al.* (2015). Cooperative Transcriptional Activation of Antimicrobial Genes by STAT and NF-kappaB Pathways by Concerted Recruitment of the Mediator Complex. Cell Rep *12*, 300-312.

Winkler, M.B.L., Kidmose, R.T., Szomek, M., Thaysen, K., Rawson, S., Muench, S.P., Wustner, D., and Pedersen, B.P. (2019). Structural Insight into Eukaryotic Sterol Transport through Niemann-Pick Type C Proteins. Cell *179*, 485-497 e418.

Xu, J., Dang, Y., Ren, Y.R., and Liu, J.O. (2010). Cholesterol trafficking is required for mTOR activation in endothelial cells. Proc Natl Acad Sci U S A *107*, 4764-4769.

Yang, L., Soonpaa, M.H., Adler, E.D., Roepke, T.K., Kattman, S.J., Kennedy, M., Henckaerts, E., Bonham, K., Abbott, G.W., Linden, R.M., *et al.* (2008). Human cardiovascular progenitor cells develop from a KDR+ embryonic-stem-cell-derived population. Nature *453*, 524-528.

Yoshida, T., and Hayashi, M. (2014). Role of Kruppel-like factor 4 and its binding proteins in vascular disease. J Atheroscler Thromb *21*, 402-413.

Yu, L., Croze, E., Yamaguchi, K.D., Tran, T., Reder, A.T., Litvak, V., and Volkert, M.R. (2015). Induction of a unique isoform of the NCOA7 oxidation resistance gene by interferon beta-1b. J Interferon Cytokine Res *35*, 186-199.

Yu, Q., Tai, Y.Y., Tang, Y., Zhao, J., Negi, V., Culley, M.K., Pilli, J., Sun, W., Brugger, K., Mayr, J., *et al.* (2019). BOLA (BolA Family Member 3) Deficiency Controls Endothelial Metabolism and Glycine Homeostasis in Pulmonary Hypertension. Circulation *139*, 2238-2255.

Zaragoza, C., Marquez, S., and Saura, M. (2012). Endothelial mechanosensors of shear stress as regulators of atherogenesis. Curr Opin Lipidol *23*, 446-452.

Zhang, B., Naik, J.S., Jernigan, N.L., Walker, B.R., and Resta, T.C. (2017). Reduced membrane cholesterol limits pulmonary endothelial Ca(2+) entry after chronic hypoxia. Am J Physiol Heart Circ Physiol *312*, H1176-H1184.

Zhang, B., Naik, J.S., Jernigan, N.L., Walker, B.R., and Resta, T.C. (2018). Reduced membrane cholesterol after chronic hypoxia limits Orai1-mediated pulmonary endothelial Ca(2+) entry. Am J Physiol Heart Circ Physiol *314*, H359-H369.

Zhang, X., Bai, Q., Kakiyama, G., Xu, L., Kim, J.K., Pandak, W.M., Jr., and Ren, S. (2012). Cholesterol metabolite, 5-cholesten-3beta-25-diol-3-sulfate, promotes hepatic proliferation in mice. J Steroid Biochem Mol Biol *132*, 262-270.

Zhao, Y., Peng, J., Lu, C., Hsin, M., Mura, M., Wu, L., Chu, L., Zamel, R., Machuca, T., Waddell, T., *et al.* (2014a). Metabolomic heterogeneity of pulmonary arterial hypertension. PLoS One *9*, e88727.

Zhao, Y.D., Chu, L., Lin, K., Granton, E., Yin, L., Peng, J., Hsin, M., Wu, L., Yu, A., Waddell, T., *et al.* (2015). A Biochemical Approach to Understand the Pathogenesis of Advanced Pulmonary Arterial Hypertension: Metabolomic Profiles of Arginine, Sphingosine-1-Phosphate, and Heme of Human Lung. PLoS One *10*, e0134958.

Zhao, Y.D., Yun, H.Z.H., Peng, J., Yin, L., Chu, L., Wu, L., Michalek, R., Liu, M., Keshavjee, S., Waddell, T., *et al.* (2014b). De novo synthesize of bile acids in pulmonary arterial hypertension lung. Metabolomics *10*, 1169-1175.

Zheng, G.X., Terry, J.M., Belgrader, P., Ryvkin, P., Bent, Z.W., Wilson, R., Ziraldo, S.B., Wheeler, T.D., McDermott, G.P., Zhu, J., *et al.* (2017). Massively parallel digital transcriptional profiling of single cells. Nat Commun *8*, 14049.

Zhu, N., Gonzaga-Jauregui, C., Welch, C.L., Ma, L., Qi, H., King, A.K., Krishnan, U., Rosenzweig, E.B., Ivy, D.D., Austin, E.D., *et al.* (2018a). Exome Sequencing in Children With Pulmonary Arterial Hypertension Demonstrates Differences Compared With Adults. Circ Genom Precis Med *11*, e001887.

Zhu, S., Wang, J., Wang, X., and Zhao, J. (2018b). Protection against monocrotaline-induced pulmonary arterial hypertension and caveolin-1 downregulation by fluvastatin in rats. Mol Med Rep *17*, 3944-3950.